Spring 1978

A KINETIC THEORY OF WEAK WAVE-PARTICLE INTERACTIONS IN AN AURORAL PLASMA

PAUL BERTON DUSENBERY

INFORMATION TO USERS

This material was produced from a microfilm copy of the original document. While the most advanced technological means to photograph and reproduce this document have been used, the quality is heavily dependent upon the quality of the original submitted.

The following explanation of techniques is provided to help you understand markings or patterns which may appear on this reproduction.

1. The sign or "target" for pages apparently lacking from the document photographed is "Missing Page(s)". If it was possible to obtain the missing page(s) or section, they are spliced into the film along with adjacent pages. This may have necessitated cutting thru an image and duplicating adjacent pages to insure you complete continuity.

2. When an image on the film is obliterated with a large round black mark, it is an indication that the photographer suspected that the copy may have moved during exposure and thus cause a blurred image. You will find a good image of the page in the adjacent frame.

3. When a map, drawing or chart, etc., was part of the material being photographed the photographer followed a definite method in "sectioning" the material. It is customary to begin photoing at the upper left hand corner of a large sheet and to continue photoing from left to right in equal sections with a small overlap. If necessary, sectioning is continued again — beginning below the first row and continuing on until complete.

4. The majority of users indicate that the textual content is of greatest value, however, a somewhat higher quality reproduction could be made from "photographs" if essential to the understanding of the dissertation. Silver prints of "photographs" may be ordered at additional charge by writing the Order Department, giving the catalog number, title, author and specific pages you wish reproduced.

5. PLEASE NOTE: Some pages may have indistinct print. Filmed as received.

University Microfilms International
300 North Zeeb Road
Ann Arbor, Michigan 48106 USA
St. John's Road, Tyler's Green
High Wycombe, Bucks, England HP10 8HR

A KINETIC THEORY OF WEAK WAVE-PARTICLE INTERACTIONS IN AN AURORAL PLASMA

BY

PAUL DUSENBERY
A.B., Whitman College, 1972
M.S., University of New Hampshire, 1975

A THESIS

Submitted to the University of New Hampshire
in Partial Fulfillment of
the Requirements for the Degree of

Doctor of Philosophy
Graduate School
Department of Physics
May, 1978

This thesis has been examined and approved.

Thesis director, Richard L. Kaufmann
Professor of Physics

Roger L. Arnoldy, Professor of Physics

Edward L. Chupp, Professor of Physics

Lennard Fisk, Associate Professor of Physics

Harvey Shepard, Associate Professor of Physics

4/14/78
Date

Acknowledgments

I would like to express my deepest gratitude to my thesis advisor Professor Richard Kaufmann, for his encouragement and insights throughout the course of this work.

I would like to express special thanks to Drs. Roger Arnoldy and Len Fisk for the many discussions we had on various problems in magnetospheric physics and plasma physics respectively. I would also like to thank Drs. Ed Roelof and Robert Lambert for giving me a good foundation in electromagnetic theory which is the heart of my thesis.

I am indebted to Ben Thomas for his work in computer analysis, to Janet Weinhous for the graphics, and to Cindy Tunberg for typing the various drafts of this work.

I would like to thank specially my teacher, Master Peter Rose, who has taught me the importance of understanding myself and the world around me and the need for sharing this knowledge with others.

Finally, I am most thankful for both the support and understanding that my family has given me over the years. They have all taught me so much.

This work was supported by the Atmospheric Sciences Section of the National Science Foundation under grants DES - 75 - 03012 and ATM - 77- 01014. The sounding rocket flights were supported by NASA under grant NGR - 30 - 002 - 054.

Dedication

To Verne Dusenbery

I dedicate this thesis, the first of my works, to my grandfather, whose beliefs and life are a constant inspiration to me. He has taught me that knowledge is sacred. In the words of J. Bronowski in his "Ascent of Man":

> Science is a very human form of knowledge. We are always at the brink of the known, we always feel forward for what is to be hoped. Every judgment in science stands on the edge of error, and is personal. Science is a tribute to what we can know although we are fallible.....
>
> I owe it as a scientist to my friend Leo Szilard, I owe it as a human being to the many members of my family who died at Auschwitz, to stand here by the pond as a survivor and a witness. We have to cure ourselves of the itch for absolute knowledge and power. We have to close the distance between the push-button order and the human act. We have to touch people."

TABLE OF CONTENTS

List of Tables

List of Illustrations

ABSTRACT

A KINETIC THEORY OF WEAK WAVE-PARTICLE
INTERACTIONS IN AN AURORAL PLASMA

by

PAUL DUSENBERY

Experimental measurements of the electron distribution function are used to model the auroral plasma at an altitude of 250 km. A kinetic theory of weak wave-particle interactions in such a plasma is formulated when the waves are electrostatic in nature. The dispersion of these waves in k-space is found. The observed plasma is shown to be stable to electrostatic waves that propagate exactly parallel or perpendicular to the earth's magnetic field. The measured distribution function has a secondary peak, but this peak is either too small or too limited in extent to drive parallel or perpendicular instabilities. A methodology is developed to look at the stability of oblique electrostatic waves that are coupled to the measured distribution function.

CHAPTER I

INTRODUCTION

On March 16, 1973 flight 18:152 was launched from Poker Flats, Alaska (Arnoldy et al., 1974). An auroral band observed at Fort Yukon started to move north and broaden at 1038UT. At 1042UT the band divided in two, the southern band proceeding south. It was this structure that the rocket passed through at about 1043UT. For most of the flight (190-310s) the rocket was above this form. Rocket borne detectors made some of the most complete experimental measurements of a highly non-Maxwellian electron distribution function that are currently available.

The auroral arc the rocket passed through occurred during an auroral substorm, which is a time of increased auroral activity. However auroras have been measured frequently in the auroral oval when substorm conditions were absent. The arcs, in the absence of a substorm, are generally rather quiescent structures. We would like to understand the physical processes which produce an auroral substorm. This understanding may better clarify how the magnetosphere and ionosphere couple. With a knowledge of the particle distribution function as a starting point, it is the purpose of this thesis to understand how the auroral plasma interacts with any waves which may be present. Such an interaction may shed some light on the dynamic process we call an auroral substorm.

Because the occurence of an auroral substorm is intimately related to changes which occur many earth radii away, the understanding of the substorm is linked to understanding the changes which occur in what is known as the terrestrial magnetosphere (Akasofu, 1977). The term "magnetosphere" was first introduced by Gold (1959) who used it to mean

that region above the ionosphere in which the earth's magnetic field has a dominant influence over the motions of the charged particles that are present. Due to the interaction of the solar wind with the earth's magnetic field, magnetic field lines which emanate from the polar region of the earth are linked to the magnetic field lines of the solar wind (see figure 1.1a). This results in an open magnetosphere. Because of the relative motion between the solar wind and the magnetosphere, energy may be generated by converting particle kinetic energy into electromagnetic energy. A portion of this energy is fed into the magnetotail circuit while the rest is used to power the large scale convection of magnetospheric plasma. A strong coupling exists between the magnetosphere and the ionosphere. A potential drop across the magnetotail will map down to a potential drop across the ionosphere. As long as the resistance along the magnetic field lines is zero the drops will be the same in both cases. The resulting current systems within the ionosphere are very complicated. However if the field lines become resistive then the potential across the ionosphere will be reduced due to the potential drop along the field line caused by field aligned currents. This potential may accelerate some portion of the field aligned currents resulting in the types of distributions which are commonly observed in the auroral oval. It is because of this coupling that the energy stored in the currents is dissipated by Joule heating in the ionosphere and by the injection of accelerated auroral particles. Where do these accelerated particles come from?

To give a reasonable answer to the above question, one must understand an event called the magnetospheric substorm. It should be noted that the substorm is the time when energy dissipation (which takes

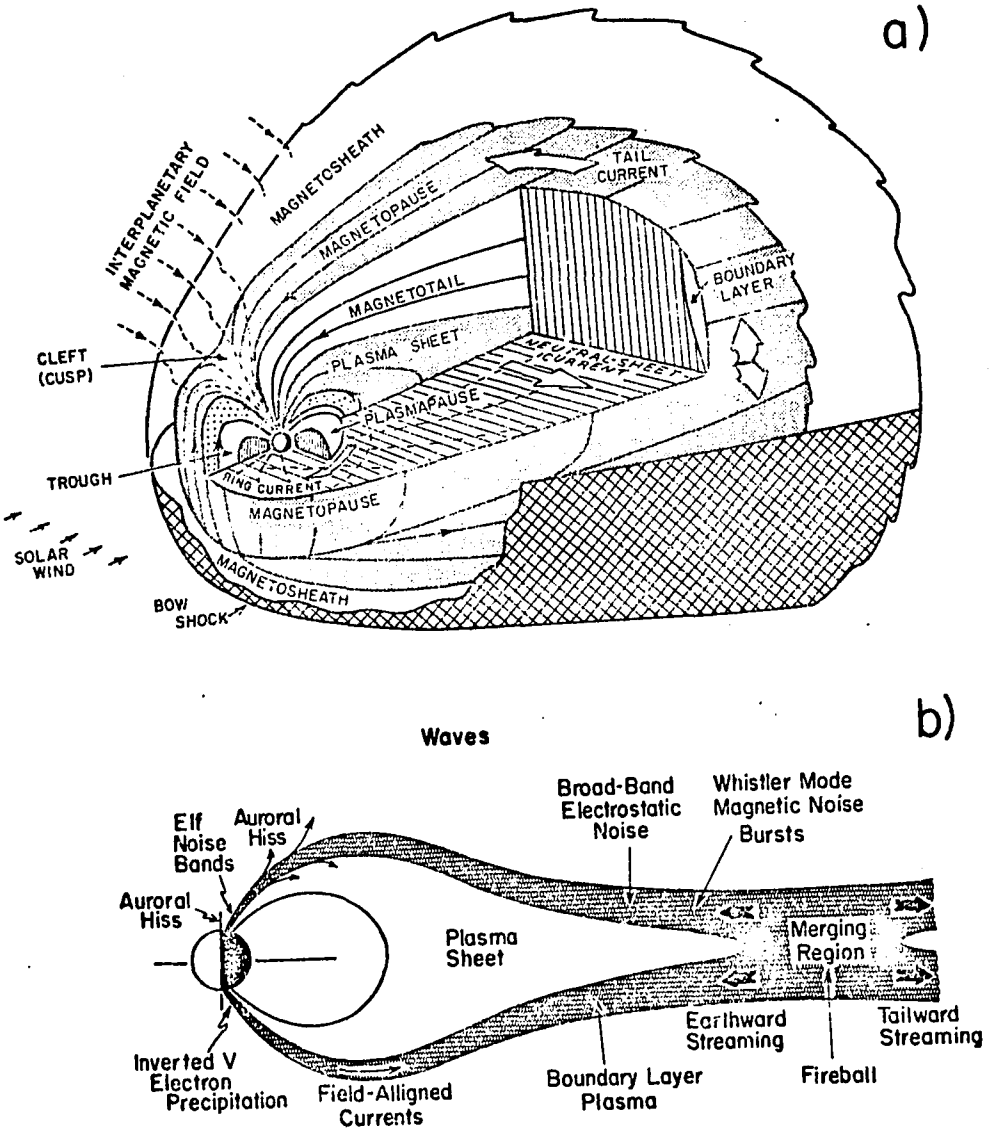

Figure 1.1

a) A three dimensional schematic drawing of the magnetosphere (Courtesy of W. Heikkila)

b) A cross section of the magnetosphere showing the various kinds of turbulence possible along the auroral field lines (Courtesy of L. Frank and D. Gurnett).

place all the time) is most intense. A reasonable model for the occurence of a substorm is present in the following discussion. Other theories which consider the merging of magnetic field lines as most important have also been considered. However definite supporting evidence for these theories has been lacking.

Because the solar wind is a time-dependent phenomena, the magnetic field fluctuates, especially in the magnetotail. This fluctuation or modulation causes accumulation of magnetic energy in the magnetotail which may be released intermittently. A possible explanation for this release in terms of a current interruption has been suggested by Alfven and Carlqvist (1967) and Kan and Akasofu (1977). It is possible that a current instability is responsible for this interruption, the consequences of which will be a large voltage drop across the tail. The inductive electric field will cause a high speed $\underline{E} \times \underline{B}$ drift of plasma toward the earth. A possible consequence of this field aligned plasma may be to induce a potential structure which could accelerate auroral electrons. These electrons travel in on field lines that originate within the tail and are near the boundary between the open and closed field lines (near the boundary of the plasma sheet).

The two most important mechanisms which have been proposed for inducing this acceleration region are anomalous resistivity (Kindel and Kennel, 1971; Papadoupoulos, 1977, Swift, 1965) and the formation of double layers (Block, 1972; Carlqvist, 1972). It is currently believed that the acceleration region is in the top-side ionosphere at a distance of 5,000 to 10,000 km. above the earth (Mizera et al., 1976; Whipple, 1977). Supporting evidence for this comes from a number of rocket measurements of auroral electron distribution functions (Whalen and

McDiarmid, 1972; Maehlum and Moestue, 1973; Reasoner and Chappell, 1973; Arnoldy et al., 1974; Kaufmann et al., 1977). In most of these studies observations of peaked spectra and field aligned pitch angle distributions can only be accounted for by a local parallel electric field region.

Even though the rocket does not make measurements within a highly unstable acceleration region, a stability analysis at rocket altitude provides some information about the acceleration process. For example, if any wave is found to be marginally stable at the rocket then it is likely to have been the last unstable wave at higher altitude. On future flights we hope to compare predictions of wave growth which are based on measured electron distribution functions with on-board measurements of wave intensities. Such an analysis will provide a very sensitive test of several aspects of linear stability theory and will bring us one step closer to using the magnetosphere as a plasma physics laboratory.

Let us detail the areas we wish to investigate in this thesis. We must first develop a kinetic theory which incorporates wave-particle interactions. We shall find that the distribution function plays a central role in our kinetic theory. We will use the measured distribution function with a realistic model background plasma (of ionospheric origin) to model the auroral plasma at rocket altitude. To understand the wave-particle interaction we must know which waves are really present in the plasma. The second area is devoted to deriving the dispersion characteristics of a class of waves known as elestrostatic (ES) waves. The third area is devoted to an understanding of the morphology of the measured distribution function. This is vital to our overall objective because any free energy in the measured distribution may be fed into the waves allowing them to grow. This last possibility is the subject of the forth

and last area we shall consider. Let us begin our study by developing the required kinetic theory we need in order to understand weak wave-particle interactions in an auroral plasma.

CHAPTER II

KINETIC THEORY

2.1 An Introduction

To be able to fully understand the nature of a many body system, it is in principle necessary to know what each individual member is doing in that system. Such knowledge is of course impossible in practice. The role of a kinetic theory is to develop equations which not only allow for the discreteness of the members but are solvable as well. Because the members of our system are charged we expect that they can interact with any electromagnetic fields which happen to be present. The function which dictates how the members will interact with each other (collisions) and with any wave spectrum present is the distribution function. It is the time evolution of this function along with the equations that describe how the fields vary which kinetic theory attempts to solve.

A description which details the phase space distribution of particles is commonly referred to as a microscopic description. A less detailed description is the macroscopic or fluid approach which is based on describing the properties of the system in terms of average quantities. If one is interested in the interaction between the particles and any existing waves or for that matter any process requiring that the particles be treated as discrete (e.g. radiation) then the fluid approach is inadequate. Because we are interested in the above interaction, we shall dispense with a fluid model, even though it is easier to treat and develop a kinetic theory. Before we begin to develop the equations which describe

the behavior of our system, a word about the kind of system we are talking about will be useful.

The system we are studying is called a plasma (see Chen, 1974 page 3). A plasma is a quasi-neutral gas of charged and neutral particles (taken to be points) which exhibits collective behavior, i.e. behavior which depends not only on local conditions but on conditions in remote regions as well. It is found that if the characteristic dimension, L, of our system is much larger than λ_D, the Debye length, then whenever local concentrations of charge are induced or external potentials are present these are shielded out in a distance small compared to L ($\geq \lambda_D$). Thus if we are to admit the existence of collective motions then the number of particles in a Debye sphere must be quite large. Furthermore, if we are to assume that the collective motion has an effect on the particles then its frequency must be much larger than the collision frequency (collisions randomize collective behavior). Bearing these important criteria in mind, let us develop a kinetic theory for a plasma.

2.2 The Klimontovich-Dupree Description

The approach we shall use in developing a kinetic theory of a plasma is the Klimontovich-Dupree description (Klimontovich, 1967). Consider a fully ionized gas made up of positive and negative charges such that the plasma as a whole is electrically neutral. If $\overline{N_\gamma}$ represents the total number of identical particles of the γ^{th} species then the above condition may be written as

$$\sum_\gamma q_\gamma \overline{N_\gamma} = 0 .$$

In a 6-dimensional phase space $(\underline{x}, \underline{v})$ called μ-space, we may define

a function, χ_γ, which locates all N_γ particles. We shall refer to this function as the Klimontovich function.

$$2.1) \qquad \chi_\gamma(\underline{X}, t) = \sum_{i=1}^{N_\gamma} \delta(\underline{X} - \underline{X}_{\gamma i}(t))$$

where,

$$\underline{X} = (\underline{x}, \underline{v}) \quad .$$

In principle the $\underline{X}_{\gamma i}(t)$ are found from solving the Hamiltonian equations of motion. Integrating equation 2.1 over all μ-space must give the total number of particles of the γ^{th} species i.e.

$$2.2) \qquad N_\gamma = \int \chi_\gamma(\underline{X}, t)\, d\underline{X} \quad .$$

At each point in our system there exist electric and magnetic microfields $(\underline{E}^m, \underline{B}^m)$ which include not only the induced fields but also any external fields which may be present. The equations which describe how the particles act as the source for the fields and alternatively how the fields effect the motion of the particles are the set of Maxwell's equations. To write these equations down we need to know the charge and current densities ($\rho(\underline{x},t)$ and $\underline{j}(\underline{x},t)$ respectively).

$$\rho_\gamma(\underline{x},t) = q_\gamma \sum_{i=1}^{N_\gamma} \delta(\underline{x} - \underline{x}_{\gamma i}(t))$$

$$= q_\gamma \int \chi_\gamma(\underline{X}, t)\, d\underline{v}$$

and $$\underline{j}_\gamma(\underline{x},t) = q_\gamma \sum_{i=1}^{N_\gamma} \underline{v}_{\gamma i}\, \delta(\underline{x} - \underline{x}_{\gamma i}(t))$$

$$= q_\gamma \int \underline{v}\, \chi_\gamma(\underline{X},t)\, d\underline{v} \quad .$$

Therefore,

I $$\begin{cases} \nabla\cdot\underline{E}^m = 4\pi \sum_\gamma \rho_\gamma + 4\pi \rho^{ext} \\ \qquad = 4\pi \sum_\gamma q_\gamma \int \chi_\gamma(\underline{X},t)\, d\underline{v} + 4\pi\rho^{ext} \\ \nabla\cdot\underline{B}^m = 0 \\ \nabla\times\underline{E}^m + \frac{1}{c}\partial_t \underline{B}^m = \underline{0} \\ \nabla\times\underline{B}^m - \frac{1}{c}\partial_t \underline{E}^m = \frac{4\pi}{c}\sum_\gamma \underline{j}_\gamma + \frac{4\pi}{c}\underline{j}^{ext} \\ \qquad = \frac{4\pi}{c}\sum_\gamma q_\gamma \int \underline{v}\,\chi_\gamma(\underline{X},t)\,d\underline{v} \\ \qquad\qquad + \frac{4\pi}{c}\underline{j}^{ext} \end{cases}$$

If we assume that the average spacing of the particles is much larger than a DeBroglie wavelength then we may treat these particles as classical point masses. If we further assume that the velocity of all the particles satisfies $|\underline{v}| << c$, then we may dispense with the relativistic corrections we would otherwise need. Therefore, the equations of motion for each particle which close the field-particle interaction are

$$\frac{d\underline{x}_{\gamma i}}{dt} = \underline{v}_{\gamma i}$$

$$\frac{d\underline{v}_{\gamma i}}{dt} = \frac{q_\gamma}{m_\gamma}\left\{\underline{E}^m(\underline{x}_{\gamma i},t) + \frac{\underline{v}_{\gamma i}\times\underline{B}^m(\underline{x}_{\gamma i},t)}{c}\right\}.$$

Because the total number of particles of the γ^{th} species is constant in time we see that $\mathcal{X}_\gamma$ must satisfy the following equation:

$$\frac{d\overline{N}_\gamma}{dt} = \int \frac{d\mathcal{X}_\gamma}{dt}\, d\underline{X} = 0$$

Therefore:

$$\frac{d\mathcal{X}_\gamma(\underline{X},t)}{dt} = \frac{\partial \mathcal{X}_\gamma}{\partial t} + \dot{\underline{X}} \cdot \frac{\partial \mathcal{X}_\gamma}{\partial \underline{X}} = 0$$

i.e.

$$\frac{\partial \mathcal{X}_\gamma}{\partial t} + \underline{v} \cdot \frac{\partial \mathcal{X}_\gamma}{\partial \underline{x}} + \dot{\underline{v}} \cdot \frac{\partial \mathcal{X}_\gamma}{\partial \underline{v}} = 0 \qquad 2.3)$$

where

$$\dot{\underline{v}} = \frac{q_\gamma}{m_\gamma}\left\{ \underline{E}^m + \frac{\underline{v} \times \underline{B}^m}{c} \right\}$$

Equation 2.3 expresses a continuity equation for $\mathcal{X}_\gamma$ in μ-space. With the Maxwell equations defined in set I and equation 2.3, we have all the equations we need to analyze how the particles interact with each other and with any waves which may exist. This self-consistent interaction will be referred to as the interaction event. To understand this event better let us expand the microfields into two parts; the first part includes only the contribution from the external sources while the second includes the induced fields $(\underline{e}, \underline{b})$ produced by the fine-grained distribution of charges. Let

$$\underline{E}^m = \underline{E}_{ext} + \underline{e}$$
$$\underline{B}^m = \underline{B}_{ext} + \underline{b} \quad .$$

Therefore set I transforms into

II.
$$\begin{cases} \nabla \cdot \underline{e} = 4\pi \sum_\gamma q_\gamma \int \chi_\gamma(\underline{X}, t)\, d\underline{v} \\ \nabla \cdot \underline{b} = 0 \\ \nabla \times \underline{e} + \frac{1}{c}\, \partial_t\, \underline{b} = \underline{0} \\ \nabla \times \underline{b} - \frac{1}{c}\, \partial_t\, \underline{e} = \frac{4\pi}{c} \sum_\gamma q_\gamma \int_{\underline{v}} \chi_\gamma(\underline{X}, t)\, d\underline{v} \end{cases}$$

We must emphasize a very important fact about set II, namely that at a point $\underline{X}$ in our system there does not exist any ρ^{ext} or $\underline{j}^{ext}$, which are the sources for $\underline{E}_{ext}$ and $\underline{B}_{ext}$. However this is not to say that $\underline{E}_{ext}$ and $\underline{B}_{ext}$ do not exist at point $\underline{X}$. It merely implies that we are concerned with the interactions within an isolated system. For example, the earth's field is considered an external field in the auroral plasma. The fields may be represented in terms of the potentials $\underline{A}^m$ and ϕ^m as follows:

2.4) $$\underline{b} = \nabla \times \underline{A}^m$$

2.5) $$\underline{e} = -\nabla \phi^m - \frac{1}{c}\, \partial_t\, \underline{A}^m$$

We may simplify calculating the fields from these potentials by exploiting the inherent arbitrariness in the definition of the vector

potential, $\underline{A}^m$. One such condition we may use is called the Coulomb gauge:

$$\nabla \cdot \underline{A}^m = \underline{0} \quad .$$

In this gauge, equation 2.5 gives

$$\nabla \cdot \underline{e} = -\nabla^2 \underline{\phi}^m = 4\pi \sum_\gamma \rho_\gamma \quad .$$

From the above expression $\underline{\phi}^m$ is given by

$$\underline{\phi}^m(\underline{x}, t) = \sum_\gamma \int \frac{\rho_\gamma(\underline{x}', t)}{|\underline{x} - \underline{x}'|} \, d\underline{x}'$$

2.6)

$$= \sum_\gamma q_\gamma \int \frac{\chi_\gamma(\underline{x}', \underline{v}', t)}{|\underline{x} - \underline{x}'|} \, d\underline{x}' \, d\underline{v}' \quad .$$

For a non-relativistic plasma electromagnetic interactions are often negligible as compared to electrostatic interactions ($\underline{b} = \underline{0}$). In the auroral plasma such an approximation will be shown to be valid. However, for now we shall adopt this condition for the sake of clarity. Magnetic effects will be introduced at the end of our calculations for completeness. Using this assumption,

$$\underline{e}(\underline{x}, t) = -\partial_x \underline{\phi}^m(\underline{x}, t)$$

$$\underline{b}(\underline{x}, t) = \underline{0} \quad .$$

Substituting the above expressions into equation 2.3 gives

2.7)

$$\left[\partial_t + \mathcal{L}_\gamma(\underline{X}) - \sum_\sigma \int d\underline{X}' V_{\sigma\gamma}(\underline{X}, \underline{X}') \chi_\sigma(\underline{X}', t) \right] *$$

$$* \chi_\gamma(\underline{X}, t) = 0.$$

$\mathcal{L}_\gamma$ is a single-particle operator defined by

$$\mathcal{L}_\gamma(\underline{X}) = \underline{v}\cdot\partial_{\underline{x}} + \frac{q_\gamma}{m_\gamma}\left\{\underline{E}_{ext} + \frac{\underline{v}\times\underline{B}_{ext}}{c}\right\}\cdot\partial_{\underline{v}}$$

and $V_{\sigma\gamma}(\underline{X},\underline{X}')$ is a two-particle operator which is defined as

$$V_{\sigma\gamma}(\underline{X},\underline{X}') = \frac{q_\sigma q_\gamma}{m_\gamma}\left[\partial_{\underline{x}}\ \frac{1}{|\underline{x}-\underline{x}'|}\right]\cdot\partial_{\underline{v}}$$

Equation 2.7 describes how the Klimontovich function evolves in space-time. In principle we could solve equation 2.7 which would give us knowledge of the complete interaction event in μ-space. This would require knowledge of what each member of our system was doing. If we are not interested in such a detailed description how can we develop a statistical formulation which reduces the difficulty of solving the interaction event in toto but one which still retains some information about the physical evolution of our system?

We begin a statistical description by defining a probability density F_N such that

$$F_N(\underline{X}_{all})\, d\underline{X}_{all}$$

is the probability that at time t the coordinates and velocity of the particles have the values $\underline{X}_{all}$ in the range $d\underline{X}_{all}$ where

$$\underline{X}_{all} = \underline{X}_{11}, \cdots, \underline{X}_{1N_1}, \underline{X}_{21}, \cdots, \underline{X}_{2N_2}, \cdots .$$

If our system were in thermodynamic equilibrium then

$$F_N = D$$

where D is the Gibbs distribution. In general F_N is not equal to D. We shall be interested in understanding how systems which are not initially in thermodynamic equilibrium evolve to an equilibrium state.

Because F_N is a probability density its normalization is given by

2.8) $$\int F_N (\underline{X}_{all}) \, d\underline{X}_{all} = 1 \quad .$$

We may define reduced distributions which contain less information but which are easier to use. The one-particle distribution function is defined as

2.9) $$f_\gamma (\underline{X}_{\gamma 1}, t) = V \int F_N \, d\underline{X}_{\gamma 2} \cdots d\underline{X}_{\gamma N_\gamma} \, d\underline{X}_{all \neq \gamma}$$

where V is the volumn of the system. From equation 2.8

$$\frac{1}{V} \; f_\gamma (\underline{X}_{\gamma 1}, t) \, d\underline{X}_{\gamma 1}$$

gives the probability of finding a single particle at $\underline{X}_{\gamma 1}$ in the range $d\underline{X}_{\gamma 1}$. This distribution is the most highly reduced of all the distribution functions. Obviously, the probability of finding a member of our system at a point $\underline{X}$ is altered by the presence of another member at a point $\underline{X}'$ where $\underline{X} \approx \underline{X}'$. The influence of a near neighbor on the one-particle distribution function is contained in the two-particle distribution,

$$f_{\alpha\beta} (\underline{X}_{\alpha 1}, \underline{X}'_{\beta 1}, t)$$

2.10) $$V^2 \int F_N \, d\underline{X}_{\alpha 2} \cdots d\underline{X}_{\alpha N_\alpha} \, d\underline{X}_{\beta 2} \cdots$$

$$d\underline{X}_{\beta N_\beta} \, d\underline{X}_{all \neq \alpha, \beta} \quad .$$

If the members of our system are non-interacting then

$$f_{\alpha\beta} = f_\alpha \, f_\beta$$

otherwise $f_{\alpha\beta}$ will depend in general on the three-particle distribution function etc.

We have done nothing to simplify our problem, for instead of a single function of $6\bar{N}$ variables we now have $\bar{N}$ functions all chained together. The modus operandi of kinetic theory is to find ways to cut this chain. We shall return to this problem later in the chapter.

Because $F_{\bar{N}}$ is a probability density we may define averages over it. We shall define the phase-space average of any phase function $\psi(\underline{X}; \underline{X}_{\alpha\,11})$ as follows:

$$\langle \psi(\underline{X}, t) \rangle = \int F_{\bar{N}}(\underline{X}_{\alpha\,11})\, \psi(\underline{X}; \underline{X}_{\alpha\,11})\, d\underline{X}_{\alpha\,11} \quad .$$

The particular phase function we have been concerned with is the Klimontovich function. Therefore,

$$\begin{aligned} \langle \mathcal{N}_\gamma(\underline{X}, t) \rangle &= \int F_{\bar{N}}\, \mathcal{N}_\gamma(\underline{X}; \underline{X}_{\alpha\,11})\, d\underline{X}_{\alpha\,11} \\ &= \int F_{\bar{N}} \sum_{i=1}^{\bar{N}_\gamma} \delta(\underline{X} - \underline{X}_{\gamma i}(t))\, d\underline{X}_{\alpha\,11} \\ &= \bar{N}_\gamma \int F_{\bar{N}}\, \delta(\underline{X} - \underline{X}_{\gamma 1})\, d\underline{X}_{\alpha\,11} \\ &= \bar{n}_\gamma\, f_\gamma(\underline{X}, t) \quad . \end{aligned} \tag{2.11}$$

In the above derivation, we have assumed that all the members of the γ^{th} species are identical. Similarly it can be shown (Klimontovich, 1967) that

$$\begin{aligned} \langle \mathcal{N}_\alpha(\underline{X}, t)\, \mathcal{N}_\beta(\underline{X}', t) \rangle &= \bar{n}_\alpha \bar{n}_\beta\, f_{\alpha\beta}(\underline{X}, \underline{X}', t) \\ &\quad + \delta_{\alpha\beta}\, \bar{n}_\alpha\, \delta(\underline{X} - \underline{X}')\, f_\alpha(\underline{X}, t). \end{aligned} \tag{2.12}$$

With the above moments we can average equation 2.7. We shall follow the lead of Ichimaru (1973) and simplify our notation by replacing the $\underline{X}$, $\underline{X}'$ etc. in the above equations by the numerals 1,2, etc. Therefore equation 2.7 reads

$$\{\partial_t + \mathcal{L}_\gamma(1)\}\chi_\gamma(1,t) = \sum_\sigma \int V_{\sigma\gamma}(1,2)\chi_\sigma(2,t)\chi_\gamma(1,t)\,d2 .$$

Averaging the above expression gives

$$\{\partial_t + \mathcal{L}_\gamma(1)\}\bar{n}_\gamma f_\gamma(1,t) = \sum_\sigma \int V_{\sigma\gamma}(1,2)\left[n_\sigma n_\gamma f_{\sigma\gamma}(1,2,t) + \delta_{\sigma\gamma} n_\gamma \delta(1-2) f_\gamma(1,t)\right] d2 .$$

For an arbitrary function ϕ (1, 2, ..., t) one can show that

$$\int V(1,2)\,\delta(1-2)\,\phi(1,2,\cdots,t)\,d2 = 0 . \tag{2.14}$$

Therefore the above equation reduces to

$$\{\partial_t + \mathcal{L}_\gamma(1)\} f_\gamma(1,t) = \sum_\sigma \bar{n}_\sigma \int V_{\sigma\gamma}(1,2) f_{\sigma\gamma}(1,2,t)\,d2 . \tag{2.15}$$

To solve equation 2.15 we need to be able to find $f_{\sigma\gamma}$. The equation which the two-particle distribution function satisfies may be found from averaging

$$\{\partial_t + \mathcal{L}_\alpha(1) + \mathcal{L}_\beta(2)\}\, \mathcal{K}_\alpha(1,t)\, \mathcal{K}_\beta(2,t)$$

$$= \sum_\sigma \int d3 \left[\Gamma_{\sigma\alpha}(1,3) + \Gamma_{\sigma\beta}(2,3) \right] *$$

$$* \mathcal{K}_\sigma(3,t)\, \mathcal{K}_\alpha(1,t)\, \mathcal{K}_\beta(2,t)$$

The result is

$$\{\partial_t + \mathcal{L}_\alpha(1) + \mathcal{L}_\beta(2) - [\Gamma_{\alpha\beta}(2,1) + \Gamma_{\beta\alpha}(1,2)]\} *$$

2.16) $$* f_{\alpha\beta}(1,2,t) = \sum_\sigma \overline{n}_\sigma \int d3 \left[\Gamma_{\sigma\alpha}(1,3) + \Gamma_{\sigma\beta}(2,3) \right] *$$

$$* f_{\alpha\beta\sigma}(1,2,3,t) .$$

In general we may consider a Klimontovich equation for an arbitrary number of Klimontovich functions and carry out a statistical average of that equation. The chain of equations which results from such an averaging is called the BBGKY hierarchy.

2.3 Cutting the Chain

A convenient way of writing the higher order distribution functions is along lines similar to the Mayer cluster expansion (Mayer, 1960). We shall expand our functions into parts which are uncorrelated and parts which are fully correlated. That is, let

$$f_{\alpha\beta}(1,2) = f_\alpha(1)\, f_\beta(2) + g_{\alpha\beta}(1,2)$$

$$f_{\alpha\beta\gamma}(1,2,3) = f_\alpha(1)\, f_\beta(2)\, f_\gamma(3)$$

$$+ f_\alpha(1)\, g_{\beta\gamma}(2,3) + f_\beta(2)\, g_{\alpha\gamma}(1,3)$$

$$+ f_\gamma(3)\, g_{\alpha\beta}(1,2) + g_{\alpha\beta\gamma}(1,2,3)$$

etc.

If the members of our system are statistically independent then

$$g_{\alpha\beta} = g_{\alpha\beta\gamma} = \cdots g_{\alpha\beta\gamma\cdots} = 0 \quad .$$

To be able to terminate the BBGKY hierarchy let us assume that the correlation functions ($g_{\alpha\beta}$ etc.) can be systematically ordered according to a parameter called the plasma parameter, g .

$$g = \frac{1}{\bar{n}\,\lambda_D^3} \ll 1 \quad .$$

The inequality arises from the fact that the number of particles in a Debye sphere is assumed large compared to one. For a plasma near thermodynamic equilibrium we may adopt the following ordering:

$$\begin{aligned} f_\alpha &\sim \Theta(1) \\ g_{\alpha\beta} &\sim \Theta(g) \\ g_{\alpha\beta\gamma} &\sim \Theta(g^2) \quad . \\ &\vdots \end{aligned}$$

Although these are the assumptions commonly adopted for a kinetic theory of a plasma near an equilibrium state, short range correlations cannot be handled as easily for $g_{\alpha\beta}(1,2)$ tends to become of the same order as the product, $f_\alpha(1)\, f_\beta(2)$ A similar violation occurs in the theory of a turbulent plasma in which wave-particle interactions act to enhance the fluctuations in the local electromagnetic field well above the equilibrium level. These fluctuations will therefore enhance the correlations.

One terminates the BBGKY hierarchy by neglecting correlations higher than the chosen order. For the zeroth order in g the BBGKY hierarchy reduces to

$$\{\partial_t + \mathcal{L}_r(1) - \sum_\sigma \bar{n}_\sigma \int V_{\sigma r}(1,2) f_\sigma(2,t)\, d2\} * f_r(1,t) = 0 \quad .$$

i.e.

$$\{\partial_t + \mathcal{L}_r(1) + \frac{q_r}{m_r} \langle \underline{e} \rangle \cdot \nabla_{\underline{v}}\} f_r(1,t) = 0 \tag{2.17}$$

where,

$$\langle \underline{e} \rangle = -\partial_{\underline{x}} \sum_r q_r \bar{n}_r \int \frac{f_r(\underline{x}', \underline{v}', t)\, d\underline{x}'\, d\underline{v}'}{|\underline{x} - \underline{x}'|}$$

Equation 2.17 is commonly referred to as the Vlasov equation. Because the Vlasov equation does not include two-particle correlations, it is unable to describe an approach of the system to thermodynamic equilibrium. However, the equation can describe how the distribution function relaxes under a weak wave-particle interaction. This is the subject of quasi-linear theory which we shall briefly describe in chapter three.

If we retain terms in the BBGKY hierarchy up to first order in g then

$$\{\partial_t + \mathcal{L}_r(1) + \frac{q_r}{m_r} \langle \underline{e} \rangle \cdot \nabla_{\underline{v}}\} f_r(1,t) = \sum_\sigma \bar{n}_\sigma \int V_{\sigma r}(1,2)\, g_{\sigma r}(1,2,t)\, d2 \quad . \tag{2.18}$$

When we include the equation for $g_{\alpha\beta}$, neglecting all three-particle correlations, the resulting solution is called the Balescu-Lenard

equation.

How fast a particular correlation function relaxes determines in large part how a particular system evolves in time. One often finds that there exists a well-defined hierarchy of the characteristic time scales. Such a hierarchy of time scales is called Bogolibov's hierarchy. Let us define the following characteristic times:

$$\tau_0 \sim L/c_s$$

$$\tau_1 \sim \ell/\langle v\rangle \quad \text{and}$$

$$\tau_2 \sim \lambda_0/\langle v\rangle$$

where, L is a macroscopic distance, c_s the sound speed, ℓ the mean free path and $\langle v\rangle$, the mean speed of the particles. The time τ_0 is associated with a hydrodynamic quantity and τ_1 is the characteristic time for the one-particle distribution function to relax. Because $c_s \sim \langle v\rangle$ for slowly varying disturbances ($L >> \ell$),

$$\tau_0 >> \tau_1 \quad .$$

τ_2 is the characteristic time for a two-particle correlation function. It is the average time for a particle to travel over a correlation distance (on the order of a Debye length). Because $\frac{1}{\tau_1} \sim \nu_c$ and $\frac{1}{\tau_2} \sim \omega_p$ where ν_c is the collision frequency and ω_p is the plasma frequency we see that

$$\tau_1 >> \tau_2 \quad (\omega_p >> \nu_c) \quad .$$

The above inequality implies that the two-particle correlation functions relax much faster than the one-particle distribution functions. (See Table 2.1) We therefore see that processes which occur on a short time scale with respect to τ_1 may significantly modify the single-particle distributions before they have relaxed to their equilibrium

Parameters Characterizing Typical Plasmas

	$\bar{n}$	T	B_o	λ_D	L	ℓ	$\langle v \rangle$	C_s	τ_o	τ_1	τ_2
Intergalactic plasma	10^{-5}	10^3	10^{-8}	10^5	10^{23}	10^{15}	10^7	5×10^5	10^{17}	10^8	10^{-2}
An interstellar plasma	1	10^4	10^{-6}	10^3	10^{18}	10^{12}	10^9	10^6	10^{12}	10^3	10^{-5}
The ionosphere of earth	10^5	10^3	0.5	0.5	10^6	10^4	10^7	10^5	10^1	10^{-3}	10^{-7}
A fusion plasma	10^{16}	10^8	10^5	10^{-3}	10^3	10^4	10^{11}	10^8	10^{-5}	10^{-7}	10^{-13}
A stellar plasma	10^{24}	10^8	10^6	10^{-6}	10^{11}	10^{-2}	10^{11}	10^8	10^3	10^{-13}	10^{-17}
	cm^{-3}	°K	G	cm	cm	cm	cm/sec	cm/sec	sec	sec	sec

TABLE 2.1

value.

Let us adopt the assumption that $q \to 0$ for our system. This implies that we may use the Vlasov equation to describe the evolution of the one-particle distribution function. We may generalize our results to include magnetic effects as follows.

III

$$\left\{ \partial_t + \underline{v} \cdot \nabla + \frac{q_r}{m_r} \left(\underline{E} + \frac{\underline{v} \times \underline{B}}{c} \right) \cdot \nabla_{\underline{v}} \right\} f_r(\underline{x}, \underline{v}, t) = 0$$

$$\nabla \cdot \underline{E} = 4\pi \sum_r \bar{n}_r q_r \int f_r \, d\underline{v} + 4\pi \rho^{ext}$$

$$\nabla \cdot \underline{B} = 0$$

$$\nabla \times \underline{E} + \frac{1}{c} \partial_t \underline{B} = \underline{0}$$

$$\nabla \times \underline{B} - \frac{1}{c} \partial_t \underline{E} = \frac{4\pi}{c} \sum_r \bar{n}_r q_r \int \underline{v} f_r \, d\underline{v} + \frac{4\pi}{c} \underline{j}^{ext}$$

where $\rho^{ext} = 0$ and $\underline{j}^{ext} = 0$ in the auroral plasma. The system of equations in set III describe fully the electromagnetic interactions of a Vlasov plasma. Before we solve the above set self consistently, we must understand the meaning of a response function.

2.4 The Response Function

Because our system is composed of charged particles, it responds to any electromagnetic fields which may be present. We may imagine that at a time $t = 0$, a perturbing field is turned on or arises either from an external source or from an induced field. The induced fields exist from statistical fluctuations in the particle motion giving rise to a non-zero charge and current density.

The response of our system in time may be decomposed into two parts. The first part is the transient response while the second part is the steady state response. The transients depend upon the initial

conditions. If we wait sufficiently long (the asymptotic state of the system) then the response is given solely by the steady state solution because the transient solution will have died out. We will assume in the foregoing that we are in such a state.

The nature of the response of a charged system to the turning on of an electric field can only be of two types. One, the value of the field becomes smaller because the particles move to such positions as to shield out electric potentials. We shall call this smaller field the equivalent displacement field, $\underline{D}(\underline{x}, t)$. Two, an induced current density arises as a consequence of Ohm's law. We shall represent the displacement field and the induced current density in terms of a space-time tensor propagator. The reason for studying how our system responds to an electric field is that from such an analysis we shall find the normal oscillations of our system. This may be compared with finding the oscillations of a string by plucking it. Before we discuss the consequences of this formalism let us return to set III and make the following important assumption.

We will find that a simplification exists if we use a perturbation expansion for all the fields and sources. The weak turbulence approximation is that we may truncate the expansion after the first order. Therefore let

$$\underline{E} = \underline{E}_o^e + \underline{E}_o^i + \underline{E}_1^i$$

$$\underline{B} = \underline{B}_o^e + \underline{B}_o^i + \underline{B}_1^i$$

$$\rho = \rho_o^e + \rho_o^i + \rho_1^i$$

$$\underline{j} = \underline{j}_o^e + \underline{j}_o^i + \underline{j}_1^i$$

where e refers to the external fields and sources and i refers to the induced fields and sources. Substituting the above expressions into set III gives,

$$2a.\quad \begin{cases} \nabla \cdot \underline{E}_o^e = 4\pi \rho_o^e \\ \nabla \cdot \underline{B}_o^e = 0 \\ \nabla \times \underline{E}_o^e + \frac{1}{c}\partial_t \underline{B}_o^e = \underline{0} \\ \nabla \times \underline{B}_o^e - \frac{1}{c}\partial_t \underline{E}_o^e = \frac{4\pi}{c}\underline{j}_o^e \end{cases}$$

$$2b.\quad \begin{cases} \nabla \cdot \underline{E}_o^i = 4\pi \rho_o^i \\ \nabla \cdot \underline{B}_o^i = 0 \\ \nabla \times \underline{E}_o^i + \frac{1}{c}\partial_t \underline{B}_o^i = \underline{0} \\ \nabla \times \underline{B}_o^i - \frac{1}{c}\partial_t \underline{E}_o^i = \frac{4\pi}{c}\underline{j}_o^i \end{cases}$$

$$2c.\quad \begin{cases} \nabla \cdot \underline{E}_1^i = 4\pi \rho_1^i \\ \nabla \cdot \underline{B}_1^i = 0 \\ \nabla \times \underline{E}_1^i + \frac{1}{c}\partial_t \underline{B}_1^i = \underline{0} \\ \nabla \times \underline{B}_1^i - \frac{1}{c}\partial_t \underline{E}_1^i = \frac{4\pi}{c}\underline{j}_1^i \end{cases}$$

Because the auroral plasma is isolated, $\underline{E}_o^e = \underline{0}$ and $\underline{B}_o^e$ is a constant vector in space-time (this external magnetic field is induced by complex motions within the earth). Therefore in the aurora, $\rho_o^e = 0$ and $\underline{j}_o^e = \underline{0}$. If we assume that there does not exist any zero order streaming then, in the auroral plasma which is quasi-neutral, there cannot exist any zero order induced fields. That is $\underline{E}_o^i = \underline{B}_o^i = \underline{0}$. This implies $\rho_o^i = 0$ and $\underline{j}_o^i = \underline{0}$. The actual situation obtaining in the auroral plasma may be far more complicated than is assumed above due

to charge build up at the boundaries of the auroral arc, the possibility of zero order streaming, and the fact that the earth's magnetic field varies in space, albeit only over many kilometers. As a first approximation we shall assume the above conditions may be neglected. If $\underline{B}_o^e = \underline{B}_o$, the above results imply that in the auroral plasma

$$\underline{E} = \underline{E}_1^i$$
$$\underline{B} = \underline{B}_o + \underline{B}_1^i$$
$$\rho = \rho_1^i$$
$$\underline{j} = \underline{j}_1^i$$

Because we are interested in how our system oscillates, we will Fourier and Laplace transform the unknowns according to

$$2.19) \quad Q(\underline{x},t) = \frac{1}{2\pi V} \sum_{\underline{k}} \int_C d\omega\, Q(\underline{k},\omega) e^{i(\underline{k}\cdot\underline{x} - \omega t)}$$

where Q is an arbitrary unknown. The contour C is so chosen as to enclose all the singularities of $Q(\underline{k},\omega)$. For an infinite plasma the discrete sum over wave vectors goes over to a continuous sum, i.e.

$$\frac{1}{V} \sum_{\underline{k}} \longrightarrow \frac{1}{(2\pi)^3} \int d\underline{k} \quad .$$

With this assumption for our system equation 2.19 becomes,

$$2.20) \quad Q(\underline{x},t) = \frac{1}{(2\pi)^4} \int d\underline{k} \int_C d\omega\, Q(\underline{k},\omega) e^{i(\underline{k}\cdot\underline{x} - \omega t)}$$

To make our problem easier to solve, let us first define $\underline{D}(x,t)$ then transform Maxwell's equations from the $\underline{E}$ to the $\underline{D}$ representation.

After we have represented $\underline{\mathcal{D}}$ and $\underline{j}$ in the correct response function formalism, we may then Fourier and Laplace transform the resulting set of equations to end up with an expression which describes how a given frequency depends on the wavelength.

Let $\underline{\mathcal{D}}(\underline{x}, t)$ be defined as,

2.21) $$\partial_t \underline{\mathcal{D}}(\underline{x},t) = \partial_t \underline{E}^{i} + 4\pi \underline{j}^{i}$$

Using the continuity equation for ρ^{i} and $\underline{j}^{i}$ we see that

2d.
$$\begin{cases} \nabla \cdot \underline{\mathcal{D}} = 0 \\ \nabla \cdot \underline{B}^{i} = 0 \\ \nabla \times \underline{E}^{i} + \frac{1}{c} \partial_t \underline{B}^{i} = \underline{0} \\ \nabla \times \underline{B}^{i} - \frac{1}{c} \partial_t \underline{\mathcal{D}} = \underline{0} \end{cases}$$

Using equation 2.20 for $\mathcal{D}(x,t)$ we may transform set 2d. The result is

2e.
$$\begin{cases} \underline{k} \cdot \underline{\mathcal{D}}(\underline{k},\omega) = 0 \\ \underline{k} \cdot \underline{B}^{i}(\underline{k},\omega) = 0 \\ \underline{k} \times \underline{E}^{i}(\underline{k},\omega) - \frac{i\omega}{c} \underline{B}^{i}(\underline{k},\omega) = \underline{0} \\ \underline{k} \times \underline{B}^{i}(\underline{k},\omega) + \frac{i\omega}{c} \underline{\mathcal{D}}(\underline{k},\omega) = \underline{0} \end{cases}$$

To find the relation between $\underline{\mathcal{D}}(\underline{k},\omega)$ and $\underline{E}^{i}(\underline{k},\omega)$ let us define $\underline{\mathcal{D}}(\underline{k},\omega)$ in terms of a response function.

As a first approximation we may assume that the electrical response of our system at a specific space-time point is determined solely by the past history of the perturbing field, independent of the spatial position of the field. However, if the external field varies appreciably over distances characterizing the medium's properties, then the above assumption must fail. This is due primarily to the fact that the response of our system is determined not only by the value of the

field at the specific point in space but also in the region surrounding it.

If the properties of the medium do not depend upon the specific observation point $\underline{x}$, but only on the difference between the applied disturbance at $\underline{x}'$ and the observation point then we call such a system translationally invariant in space. The response function for such a system depends only on $\underline{x} - \underline{x}'$. Similarly, if the mean charged particle concentration does not vary appreciably with time then the response function may be assumed to vary only as $t - t'$.

As a summary of the above discussion, let $\underline{\underline{K}}$ be a general response function of a system to perturbing field, $\underline{F}$, which induces a response $\underline{Q}$ in the system. If our system is translationally invariant in space-time then

$$\underline{Q}(\underline{x}, t) = \int d\underline{x}' \int_0^t dt' \; \underline{\underline{K}}(\underline{x} - \underline{x}', t - t') \cdot \underline{F}(\underline{x}', t') + \underline{Q}_0$$

where $\underline{Q}_0$ is the transient response. We have assumed in the above expression that the system is linear in the perturbing field, $\underline{F}$. The case of a non-linear behavior will not be dealt with in this work.

Let us write $\underline{D}(\underline{x}, t)$, assuming we are in the asymptotic state of our system, as

$$\underline{D}(\underline{x}, t) = \underline{E}_i(\underline{x}, t) + \int d\underline{x}' \int_0^t dt' \, \underline{\underline{\mathcal{G}}}(\underline{x} - \underline{x}', t - t') \cdot \underline{E}_i(\underline{x}', t') \tag{2.22}$$

Fourier and Laplace transforming the above equation and using the convolution theorem for Laplace transforms we see that

$$\underline{\underline{D}}(\underline{k},\omega) = \left(\underline{\underline{1}} + \underline{\underline{\chi}}(\underline{k},\omega)\right) \cdot \underline{E}_1^i(\underline{k},\omega)$$
$$= \underline{\underline{\varepsilon}}(\underline{k},\omega) \cdot \underline{E}_1^i(\underline{k},\omega) \quad .$$

We may find an expression for $\underline{\underline{\varepsilon}}$ by transforming equation 2.21 where we shall write $\underline{j}_1^i$ as,

$$\underline{j}_1^i(\underline{x},t) = \int d\underline{x}' \int_0^t dt' \, \underline{\underline{\sigma}}(\underline{x}-\underline{x}',\, t-t') \cdot \underline{E}_1^i(\underline{x}',t') \, .$$

The result is

$$\underline{\underline{D}}(\underline{k},\omega) = \left(\underline{\underline{1}} + \frac{4\pi i}{\omega} \underline{\underline{\sigma}}(\underline{k},\omega)\right) \cdot \underline{E}_1^i(\underline{k},\omega) \, .$$

Therefore,

2.23) $$\underline{\underline{\varepsilon}}(\underline{k},\omega) = \underline{\underline{1}} + \frac{4\pi i}{\omega} \underline{\underline{\sigma}}(\underline{k},\omega) \, .$$

In principle we know $\underline{\underline{\varepsilon}}$ because $\underline{\underline{\sigma}}$ may be found from

2.24) $$\underline{\underline{\sigma}}(\underline{k},\omega) \cdot \underline{E}_1^i(\underline{k},\omega) = \sum_\gamma q_\gamma n_\gamma \int d\underline{v} \, \underline{v} \, f_{\gamma 1}(\underline{k},\underline{v},\omega)$$

once $f_{\gamma 1}$ is known. We shall find $f_{\gamma 1}$ in the following chapter from the method of the unperturbed orbit. We may now return to set 2c. It is trivial to show that

$$\underline{k} \times (\underline{k} \times \underline{E}_1^i) + \frac{\omega^2}{c^2} \underline{\underline{\varepsilon}} \cdot \underline{E}_1^i \quad \underline{0} \quad .$$

Therefore,

2.25) $$\left\{ \underline{\underline{\varepsilon}} - \frac{k^2 c^2}{\omega^2} \left(\underline{\underline{1}} - \frac{\underline{k}\,\underline{k}}{k^2} \right) \right\} \cdot \underline{E}_1^i = \underline{0} .$$

Let

$$\underline{\underline{1}} - \frac{\underline{k}\,\underline{k}}{k^2} = \underline{\underline{\hat{I}}}$$

where

$$\underline{\underline{\hat{I}}} \cdot \underline{k} = \underline{0}$$

and let

$$\underline{\underline{\Delta}} = \underline{\underline{\varepsilon}} - \frac{k^2 c^2}{\omega^2} \underline{\underline{\hat{I}}} .$$

Therefore equation 2.25 is

2.26) $$\underline{\underline{\Delta}}(\underline{k}, \omega) \cdot \underline{E}_1^i(\underline{k}, \omega) = \underline{0} .$$

$\underline{\underline{\Delta}}$ is the dispersion tensor. The above equation can only have a non-trivial solution if

$$\det | \underline{\underline{\Delta}} | = 0 .$$

The above equation gives all possible waves that can exist in our system. Because we are interested in the subset of all waves which are purely electrostatic (ES) we see from Appendix A that

$$\varepsilon_L(\underline{k}, \omega) = \frac{\underline{k} \cdot \underline{\underline{\varepsilon}} \cdot \underline{k}}{k^2} = 0$$

gives all possible waves which are ES. $\underline{\underline{\varepsilon}}$ is called the dielectric tensor and ε_L is the longitudinal dielectric function (l.d.f.).

We will focus our attention on the properties and behavior of

the above function in the remaining chapters of this thesis. At this point, I think it worthwhile to reflect for a moment on how far we have actually come in the understanding of a many-body, charged system. From a consideration of the $\overline{N}$ -body distribution function we were led to the equations which describe the wave-particle interaction event self-consistently. By assuming that the time scale of the processes we were interested in was much shorter than the period between collisions we could utilize the Vlasov formalism. This eventually led us to the function which describes how our system oscillates electrostatically (i.e. $\mathcal{E}_{\ell}$). It is important for the reader to bear in mind the many assumptions and approximations we had to make to find $\mathcal{E}_{\ell}$. The difference between theory and reality will be in how accurate our theory is in describing the waves which are really present. To find these waves we must solve $\mathcal{E}_{\ell}$ as a function of the distribution of particles. This is the topic of the following chapter.

CHAPTER III

WEAK ELECTROSTATIC TURBULENCE

3.1 An Introduction

The electric field fluctuations in a weakly turbulent plasma (the linear and quasi-linear regime) may be represented as a superposition of independent Fourier waves (plasmons). As we derived in the previous chapter the dispersion of these waves comes from transforming the wave equation of Maxwell. The members of the kernel of the dispersion tensor are specific frequencies that are functions of $\underline{k}$.

When strong turbulence is present, the fluctuation spectrum becomes smeared and the individual waves which existed under weak turbulence lose their individual identity. This smearing tends to broaden the wave spectrum and at the same time makes it appear continuous. Under weak turbulence the individual waves were completely independent. This is no longer true under strong turbulence where the fluctuations at a particular wave vector and frequency depend strongly on fluctuations at other wave vectors and frequencies. Such an interaction is called a wave-wave interaction. In this situation there cannot possibly exist a dispersion relation of the form

$$\omega = \omega(\underline{k})$$

which embodies the fact that not only are the plasmons independent but that they exist only in the time asymptotic state of our system. A plasmon which satisfies the above conditions is called normal. If a particular wave is either heavily damped or rapidly growing it is <u>not</u>

a normal oscillation and one cannot use a normal oscillation dispersion relation to describe it. In the damped case above even though the wave is independent it exists in the transient state of the system not the asymptotic state. In the growing case, the wave will strongly couple to other waves through wave-wave interactions thereby losing its independence.

We may make an analogy to fluid turbulence by equating eddies with plasmons. In an ordinary fluid if one includes the mutual interaction between the eddies they will spread out in space-time with some relative velocity. If this relative velocity is small then each eddy can interact with its neighbors for a considerable time resulting in strong interactions. The fluid in this state is strongly turbulent. If on the other hand, the eddies are excited and separate from one another over large distances then the interactions will be weak. The fluid in this state is weakly turbulent.

One would not expect strong turbulence to exist for long in an isolated plasma. This is because the excited plasmons generally propagate which precludes high order correlations from forming. In addition, plasmons can couple only to a limited free energy source. In the auroral plasma we are studying the above conditions obtain. We may therefore view our weakly turbulent plasma as an ensemble of particles and small amplitude waves (Kennel and Petschek, 1966) whose properties are determined from linear theory.

Dissipation in a plasma in any state is generally of three kinds. One, particle-particle interactions, two, wave-wave interactions and three, wave-particle interactions. We have explicitely neglected the first interaction in the Vlasov formalism. We may neglect the second interaction which causes a loss of coherence of the plasmons through

binary wave collisions because the density of plasmons is low in our system. The third interaction is present in the linear regime since wave growth or damping depends upon velocity gradients in the one-particle distribution function. The non-linear effect is the change which the plasmons make in the particle distribution function. This change is proportional to the plasmon energy density. Let us now solve the longitudinal dielectric function for a plasma in a weakly turbulent state in the linear regime. We will then consider a quasi-linear change in the distribution function under a linear wave perturbation.

3.2 Linear Theory

We begin our analysis by expanding f_γ to first order,

$$f_\gamma = f_{\gamma 0} + f_{\gamma 1}$$

where $f_{\gamma 0}$ is the unperturbed distribution function which is independent of space and time. $f_{\gamma 0}$ may be any function as long as it satisfies the zero-order Vlasov equation:

$$\frac{q_\gamma}{m_\gamma c} \left(\underline{v} \times \underline{B}_0^e \right) \cdot \nabla_{\underline{v}} f_{\gamma 0}(\underline{v}) = 0 \quad .$$

The corresponding equation for $f_{\gamma 1}$ is

$$3.1) \quad \left\{ \partial_t + \underline{v} \cdot \nabla + \frac{q_\gamma}{m_\gamma c} (\underline{v} \times \underline{B}_0^e) \cdot \nabla_{\underline{v}} \right\} f_{\gamma 1} = - \frac{q_\gamma}{m_\gamma} \left\{ \underline{E}_1^i + \frac{\underline{v} \times \underline{B}_1^i}{c} \right\} \cdot \nabla_{\underline{v}} f_{\gamma 0}$$

where we have assumed that $\underline{E}_0^e = \underline{E}_0^i = \underline{0}$. In order to find ϵ_L we need to know $f_{\gamma 1}$. Can we find $f_{\gamma 1}$ once $f_{\gamma 0}$ is known?

The Snapshot

The particles of our plasma are all moving around in complicated orbits especially if there exists $\underline{E}_o^e$ and $\underline{B}_o^e$ fields. Let us take a snapshot of this plasma at a time we shall designate as $t > 0$. We could in principle compute the positions and velocities of all the particles thereby finding the value of $f_{\gamma,}(\underline{x}, \underline{v}, t)$. Is there an easier method to use? If we assume that we know $f_{\gamma,}$ at an earlier time t' and if from that time the trajectory of each particle followed the unperturbed orbit given solely by the zero order fields, then the evolution of $f_{\gamma,}(\underline{x}', \underline{v}', t')$ to $f_{\gamma,}(\underline{x}, \underline{v}, t)$ may be deduced as follows.

The Method of the Unperturbed Orbit

Let

$$\frac{d\underline{x}'}{dt'} = \underline{v}' \tag{3.2}$$

$$\frac{d\underline{v}'}{dt'} = \frac{q_\gamma}{m_\gamma}\left\{\underline{E}_o^e(\underline{x}', t') + \frac{\underline{v}' \times \underline{B}_o^e(\underline{x}', t')}{c}\right\} \tag{3.3}$$

with the boundary conditions

$$\underline{x}'(t' = t) = \underline{x}(t) \quad , \text{ and}$$
$$\underline{v}'(t' = t) = \underline{v}(t) \quad .$$

Therefore

$$\frac{df'_{\gamma,}}{dt'} = \frac{d}{dt'} f_{\gamma,}(\underline{x}', \underline{v}', t')$$

$$= \left\{\partial_{t'} + \underline{v}' \cdot \nabla' + \frac{d\underline{v}'}{dt'} \cdot \nabla_{\underline{v}'}\right\} f'_{\gamma,} \tag{3.4}$$

$$= -\frac{q_r}{m_r}\left\{\underline{E}_i^{i\prime} + \frac{\underline{v}'\times \underline{B}_i^{i\prime}}{c}\right\}\cdot\nabla_{\underline{v}'} f_{r0}'$$

$$= \rho_r(\underline{x}', \underline{v}', t')$$

where we have used equation 3.1 in the above expression. Integrating along the unperturbed orbit gives

$$\int_0^t dt' \frac{df_{r1}'}{dt'} = f_{r1}(\underline{x}, \underline{v}, t) - f_{r1}(\underline{x}_0, \underline{v}_0, 0)$$

$$= \int_0^t dt' \rho(\underline{x}', \underline{v}', t') .$$

Because $\underline{E}_i^i(\underline{x}', t') = \underline{B}_i^i(\underline{x}', t') = 0$ for $t' < 0$ we may extend the limit of $t' = 0$ to $t \to -\infty$ without affecting the above integral. Therefore

$$f_{r1}(\underline{x}, \underline{v}, t) = f_{r1}(\underline{x}_0, \underline{v}_0, 0) + \int_{-\infty}^t dt' \rho(\underline{x}', \underline{v}', t') .$$

Let f_{r1}, $\underline{E}_i^i$ and $\underline{B}_i^i \sim e^{i(\underline{k}\cdot\underline{x} - \omega t)}$. Therefore

$$f_{r1}(\underline{k}, \underline{v}, \omega) = f_{r1}(\underline{x}_0, \underline{v}_0, 0) e^{-i(\underline{k}\cdot\underline{x} - \omega t)}$$

$$- \frac{q_r}{m_r}\int_{-\infty}^t dt' \left\{\underline{E}_i^i(\underline{k}, \omega) + \frac{\underline{v}'\times \underline{B}_i^i(\underline{k}, \omega)}{c}\right\}\cdot\nabla_{\underline{v}'} f_{r0}' *$$

$$* e^{i[\underline{k}\cdot(\underline{x}' - \underline{x}) - \omega(t' - t)]} .$$

If we let ω have a real and imaginary part and further assume that $\omega_I > 0$ then the transient solution will die out in the asymptotic state of the system. For notational purposes let

$$\underline{X} = \underline{x}' - \underline{x}$$
$$\tau = t' - t \quad .$$

Therefore,

$$3.5) \qquad f_{r1}(\underline{k}, \underline{v}, \omega) = -\frac{q_r}{m_r} \int_{-\infty}^{0} d\tau \left\{ \underline{E}_1^{\,i} + \frac{\underline{v}' \times \underline{B}_1^{\,i}}{c} \right\} \cdot$$
$$\cdot \nabla_{\underline{v}'} f_{r0}(\underline{v}') e^{i(\underline{k}\cdot\underline{X} - \omega\tau)} \quad .$$

As long as we may describe the trajectories of all our particles in terms of the unperturbed orbit defined in equations 3.2 and 3.3, then equation 3.5 is the correct solution for the perturbed one-particle distribution function. With its solution we have solved the problem of finding ε_L in terms of the equilibrium distribution function, f_{r0} . Let us indicate the steps we shall use to find this function:

1. find $f_{r1}(\underline{k}, \underline{v}, \omega)$ from equation 3.5
2. find $\underline{\sigma}(\underline{k}, \omega)$ from equation 2.24
3. find $\underline{\underline{\varepsilon}}$ from
$$\underline{\underline{\varepsilon}} = \underline{\underline{1}} + \frac{4\pi i}{\omega} \underline{\underline{\sigma}}$$
4. find ε_L from
$$\varepsilon_L = \frac{\underline{k} \cdot \underline{\underline{\varepsilon}} \cdot \underline{k}}{k^2}$$

1. Let us orient the axis of our coordinate system along the zero order magnetic field direction. i.e. $\underline{B}_o^{e'} = \hat{z} B_o$. Furthermore let $\underline{E}_o^{e'} = \underline{0}$ (see section 2.4). Equation 3.3 may be rewritten as

3.6) $$\frac{d\underline{v}'}{d\tau} = \frac{q_r B_o}{m_r c} (\underline{v}' \times \hat{z}) = \omega_{cr} (\underline{v}' \times \hat{z})$$

where $$\underline{v}'(\tau = 0) = \underline{v} \quad .$$

3.7) $$\frac{d\underline{x}'}{d\tau} = \underline{v}'$$

where

$$\underline{x}'(\tau = 0) = \underline{x} \quad .$$

The solution of equation 3.6, after transforming from Cartesian to cyclindrical coordinates (see figure 3.1a), is

$$v_x' = v_\perp \cos(\phi - \omega_{cr}\tau)$$
$$v_y' = v_\perp \sin(\phi - \omega_{cr}\tau)$$
$$v_z' = v_\parallel \quad .$$

From equation 3.7 we see that

$$\Delta x = x' - x = \frac{v_\perp}{\omega_{cr}} \sin\phi - \frac{v_\perp}{\omega_{cr}} \sin(\phi - \omega_{cr}\tau)$$

$$\Delta y = y' - y = -\frac{v_\perp}{\omega_{cr}} \cos\phi + \frac{v_\perp}{\omega_{cr}} \cos(\phi - \omega_{cr}\tau)$$

$$\Delta z = z' - z = v_\parallel \tau \quad .$$

Because we are in the electric field representation let us express $\underline{B}_1^i(\underline{k},\omega)$ in terms of $\underline{E}_1^i(\underline{k},\omega)$ using Maxwell's equations. The result is

$$\underline{E}_1^i + \frac{\underline{v}' \times \underline{B}_1^i}{c} = \frac{1}{\omega}\left\{(\omega - \underline{k}\cdot\underline{v}')\,\underline{E}_1^i + (\underline{v}'\cdot\underline{E}_1^i)\,\underline{k}\right\} .$$

The other terms in equation 3.5 may be expressed as follows,

$$\nabla_{\underline{v}'} f_{r0}(\underline{v}') = \hat{v}_\perp \partial_{v_\perp} f_{r0} + \hat{v}_z \partial_{v_\parallel} f_{r0}$$

because the equilibrium distribution function is assumed to be azimuthally symmetric about the v_z axis. We may choose $\underline{k}$ to be

$$\underline{k} = \hat{x}\, k_\perp + \hat{z}\, k_\parallel$$

without too much loss of generality (see figure 3.1b).

$$\underline{X} = \hat{x}\,\Delta x + \hat{y}\,\Delta y + \hat{z}\,\Delta z .$$

Therefore

$$I \equiv e^{i(\underline{k}\cdot\underline{X} - \omega\tau)}$$

$$= e^{i(k_\parallel v_\parallel - \omega)\tau}\, e^{i\frac{k_\perp v_\perp}{\omega_{cr}}\sin\phi} * e^{-i\frac{k_\perp v_\perp}{\omega_{cr}}\sin(\phi - \omega_{cr}\tau)} .$$

We may express the latter two exponentials in terms of a Jacobi expansion (Watson, 1966) i.e.

$$e^{i a_r \sin\phi} = \sum_{n=-\infty}^{+\infty} J_n(a_r)\, e^{in\phi}$$

$$e^{-i a_r \sin(\phi - \omega_{cr}\tau)} = \sum_{l=-\infty}^{+\infty} J_l(a_r) * e^{-il(\phi - \omega_{cr}\tau)} .$$

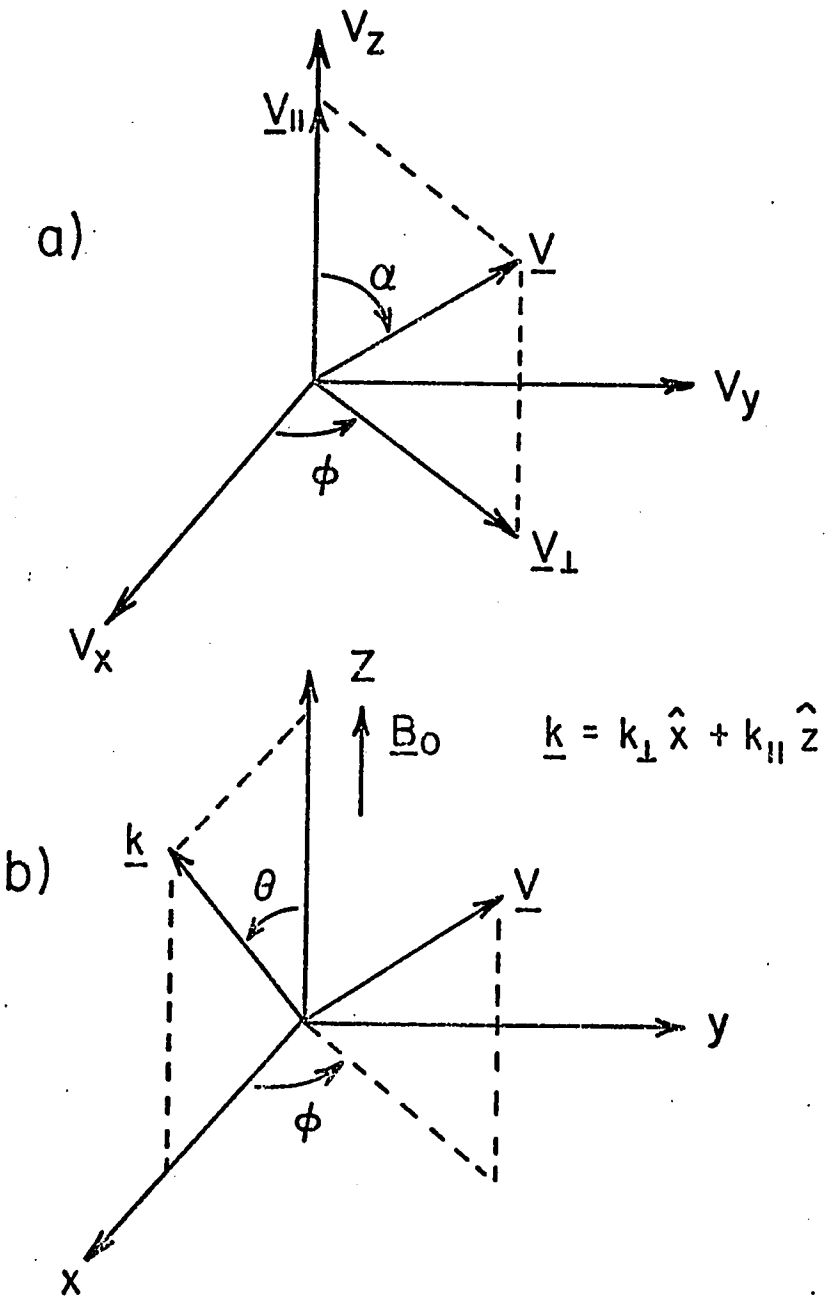

Figure 3.1

The two important spaces used in kinetic theory: a) velocity space where α is the pitch angle and b) real space or configuration space where θ is the angle of wave propagation.

we find that

3.9) $$\frac{4\pi i}{\omega}\,\underline{\underline{\sigma}}(\underline{k},\omega) = -\sum_{\gamma}\frac{\omega_{p\gamma}^2}{\omega^2}\left\{\underline{\underline{1}} + \int d\underline{v}\sum_{n}\frac{\mathcal{L}_v f_{\gamma 0}}{(k_{\parallel}v_{\parallel} + n\omega_{c\gamma} - \omega)}\,\underline{\underline{\Pi}}_{\gamma}\right.$$

where,

$$\mathcal{L}_v = \frac{n\omega_{c\gamma}}{v_{\perp}}\partial_{v_{\perp}} + k_{\parallel}\partial_{v_{\parallel}},$$

$$\underline{\underline{\Pi}}_{\gamma} = \begin{bmatrix} (\chi_{\gamma})^2 J_n^2 & i v_{\perp}\chi_{\gamma} J_n J_n' & v_{\parallel}\chi_{\gamma} J_n^2 \\ -i v_{\perp}\chi_{\gamma} J_n J_n' & v_{\perp}^2 (J_n')^2 & -i v_{\parallel} v_{\perp} J_n J_n' \\ v_{\parallel}\chi_{\gamma} J_n^2 & i v_{\parallel} v_{\perp} J_n J_n' & v_{\parallel}^2 J_n^2 \end{bmatrix}$$

$$\chi_{\gamma} = \frac{n\omega_{c\gamma}}{k_{\perp}}.$$

3. The dielectric tensor, $\underline{\underline{\varepsilon}}$ can now be found because

$$\underline{\underline{\varepsilon}} = \underline{\underline{1}} + \frac{4\pi i}{\omega}\,\underline{\underline{\sigma}}$$

4. We are now in a position to find an expression for the longitudinal dielectric function (l.d.f.).

$$\varepsilon_L = \frac{\underline{k}\cdot\underline{\underline{\varepsilon}}\cdot\underline{k}}{k^2}$$

3.11)
$$= 1 + \sum_{n,\gamma}\frac{\omega_{p\gamma}^2}{k^2}\int d\underline{v}\,\frac{J_n^2(a_{\gamma})}{(\omega - k_{\parallel}v_{\parallel} - n\omega_{c\gamma})} * \left\{\frac{n\omega_{c\gamma}}{v_{\perp}}\partial_{v_{\perp}} f_{\gamma 0} + k_{\parallel}\partial_{v_{\parallel}} f_{\gamma 0}\right\}.$$

The above expression is often referred to as the Harris dispersion relation.

Let us turn now to a quasi-linear theory of the change which f_{v0} must undergo in time when a weakly turbulent spectrum is excited. We will then return to a detailed study of some fascinating properties of the l.d.f. defined by equation 3.11.

3.3 Quasi-Linear Theory

This theory describes the initial interaction between the waves and the particles. The term "quasi-linear" refers to the fact that the waves are deduced from the linear theory whereas the time change in the equilibrium distribution, due to these linear waves, is quadratic in the wave energy and therefore inherently non-linear. There may exist a problem with time scales (Montgomery and Tidman, 1964) because the normal modes exist only in the asymptotic state of our system ($t \rightarrow \infty$) whereas the changes in f_{v0} begin at time $t = 0$, the initial state. I have not seen an adequate resolution of this problem that specifies under what conditions the theory becomes inaccurate. We shall therefore assume on faith either the transients in the response functions die out quickly or that the transients have little effect on the normal oscillation that we may develop the following theory.

Consider a spatially uniform plasma. The space average of a function f is defined as

$$\langle f \rangle = \lim_{V \to \infty} \frac{1}{V} \int f \, d\underline{x} \quad .$$

Let us define the following averages.

$$f_{r0}(\underline{v},t) = \langle f_r \rangle = \frac{1}{V} \int f_r(\underline{x},\underline{v},t)\, d\underline{x}$$

$$\underline{E}_0 = \langle \underline{E} \rangle = \underline{0}$$

$$\underline{B}_0 = \langle \underline{B} \rangle \quad .$$

The Vlasov equation is

$$\left\{ \partial_t + \underline{v}\cdot\nabla + \frac{q_r}{m_r}\left[\underline{E} + \frac{\underline{v}\times\underline{B}}{c}\right]\cdot\nabla_{\underline{v}} \right\} f_r = 0 \quad .$$

Averaging the above equation gives

3.12)
$$\partial_t f_{r0} = -\frac{q_r}{m_r}\nabla_{\underline{v}}\cdot\langle \underline{E}, f_{r1}\rangle$$

where we have assumed in deriving equation 3.12

1. A perturbation approach i.e.

$$f_r = f_{r0} + f_{r1}$$

$$\underline{E} = \underline{E}_0 + \underline{E}_1 = \underline{E}_1$$

$$\underline{B} = \underline{B}_0 + \underline{B}_1$$

2. the wave spectrum is electrostatic ($\underline{B}_1 = \underline{0}$).
3. $\frac{q_r}{m_r}\frac{(\underline{v}\times\underline{B}_0)}{c}\cdot\nabla_{\underline{v}} f_{r0} = 0$ (from the linear theory).

Note that

$$\langle \underline{E}, f_{r1}\rangle = \frac{1}{V}\int \underline{E}, f_{r1}\, d\underline{x}$$

$$= \frac{1}{V}\int \frac{d\underline{k}}{(2\pi)^3}\, \underline{E}_1(-\underline{k},t)\, f_{r1}(\underline{k},\underline{v},t) \quad .$$

If we assume an electrostatic (ES) perturbation, $\underline{E}_1 = -\nabla \Phi_1$, then

$$f_{r1}(\underline{k}, \underline{v}, \omega) = -\frac{q_r}{m_r} \sum_{n,\ell} \left[\frac{\ell \omega_{cr}}{v_\perp} \partial_{v_\perp} f_{r0} + k_\parallel \partial_{v_\parallel} f_{r0} \right] * \frac{J_\ell J_n e^{i\phi(n-\ell)}}{(\omega - \ell\omega_{cr} - k_\parallel v_\parallel)} \Phi_1(\underline{k}, \omega) \quad .$$

As we shall see in Chapter IV, only a discrete spectrum of ES waves is excited in k-space, therefore let

$$\Phi_1(\underline{k}, \omega) = A(\underline{k}, \omega^\alpha)\, \delta(\omega - \omega^\alpha)$$

where $\alpha(\underline{k})$ is the set of all possible waves at a specific point in k-space. Each wave is a member of a specific branch (see Chapter IV). We may now inverse Laplace transform the above function and average over ϕ. The result is

$$\frac{1}{2\pi} \int_0^{2\pi} d\phi\, f_{r1}(\underline{k}, \underline{v}, t) = \sum_\alpha \sum_n -\frac{q_r}{m_r} J_n^2(a_r) [\,] \frac{A(\underline{k}, \omega^\alpha) e^{-i\omega^\alpha t}}{\omega^\alpha - n\omega_{cr} - k_\parallel v_\parallel}$$

where

$$[\,] = \mathcal{L}_v f_{r0} \quad .$$

Because f_{r0} is independent of ϕ we find that equation 3.12 may be written as

$$\partial_t f_{r0}(\underline{v}, t) = 8\pi \left(\frac{q_r}{m_r}\right)^2 \sum_n \int d\underline{k} \sum_{\alpha(\underline{k})} \frac{\mathcal{E}_\alpha(\underline{k}, t)}{k^2} * \mathcal{L}_v \left\{ \frac{J_n^2(a_r)}{i(k_\parallel v_\parallel + n\omega_{cr} - \omega^\alpha)} \mathcal{L}_v f_{r0}(\underline{v}, t) \right\} \tag{3.13}$$

where,

$$\mathcal{E}_\alpha(\underline{k},t) = \frac{1}{V}\frac{1}{(2\pi)^5}\frac{k^2}{8\pi} A(\underline{k},\omega^\alpha) A(-\underline{k},\omega^\alpha) * e^{2\omega_I^\alpha t}$$

implying

$$\partial_t \mathcal{E}_\alpha = 2\omega_I^\alpha \mathcal{E}_\alpha \quad .$$

In the above expressions we have assumed that we may expand the frequency, ω^α, into real and imaginary parts i.e.,

$$\omega^\alpha = \omega_R^\alpha + i\,\omega_I^\alpha \qquad [\,\omega(-\underline{k}) = -\omega^*(\underline{k})\,] \quad .$$

We will explore the consequences of the fact that ω can be complex in the following section. To derive equation 3.13 we have further assumed that because

$$\underline{E}_1(\underline{k},t) = -i\,\underline{k}\frac{1}{2\pi}\sum_\alpha A(\underline{k},\omega^\alpha)\, e^{-i\omega^\alpha t}$$

$$\underline{E}_1(-\underline{k},t) = i\,\underline{k}\frac{1}{2\pi}\sum_\beta A(-\underline{k},\omega^\beta)\, e^{-i\omega^\beta t}$$

then $\underline{E}_1(\underline{k},t)\cdot\underline{E}_1(-\underline{k},t)$ is large only when $\alpha = \beta$. We may define a spectral wave energy density as

$$\mathcal{E}(\underline{k},t) = \sum_{\alpha(\underline{k})} \mathcal{E}_\alpha(\underline{k},t) \quad .$$

This is due to the fact that

$$\langle W_E \rangle = \left\langle \frac{E_1^2}{8\pi} \right\rangle = \int \mathcal{E}(\underline{k},t)\, d\underline{k}$$

where W_E is the ES wave energy density. (See Davidson, 1972; Krall and Trivelpiece, 1972; Hasegawa, 1975, for further details).

Let us briefly describe what occurs when a zero order distribution function has sufficient free energy to excite a growing wave spectrum at time t = 0. Generally there will only be a small number of particles which possess the necessary free energy. These particles are called the resonant particles. As the wave's grow they take energy away from the resonant particles thereby changing the form of the distribution function (see figure 3.2). Under this interaction the particles diffuse in velocity space. The morphology of the measured distribution function at rocket altitude is consistent with wave-particle diffusion of a Maxwellian plasma which has passed through a parallel electric field. Let us now return to the solution of equation 3.11, the longitudinal dielectric function.

3.4 The Solution

Let us rewrite equation 3.11 here to facilitate our analysis of its solution.

$$3.14)\quad \varepsilon_L(\underline{k},\omega) = 1 + \sum_{n,\gamma} \frac{\omega_{p\gamma}^2}{k^2} \int d\underline{v} \frac{J_n^2(a_\gamma)}{(\omega - k_{\parallel}v_{\parallel} - n\omega_{c\gamma})} * \left\{ \frac{n\omega_{c\gamma}}{v_\perp} \partial_{v_\perp} f_{\gamma 0} + k_{\parallel} \partial_{v_{\parallel}} f_{\gamma 0} \right\} .$$

The symbols in the above expression have been defined previously and are listed in appendix D for easy reference. In the previous section you may recall that we assumed ω to be a complex function given by

$$3.15)\quad \omega = \omega_R + i\omega_I$$

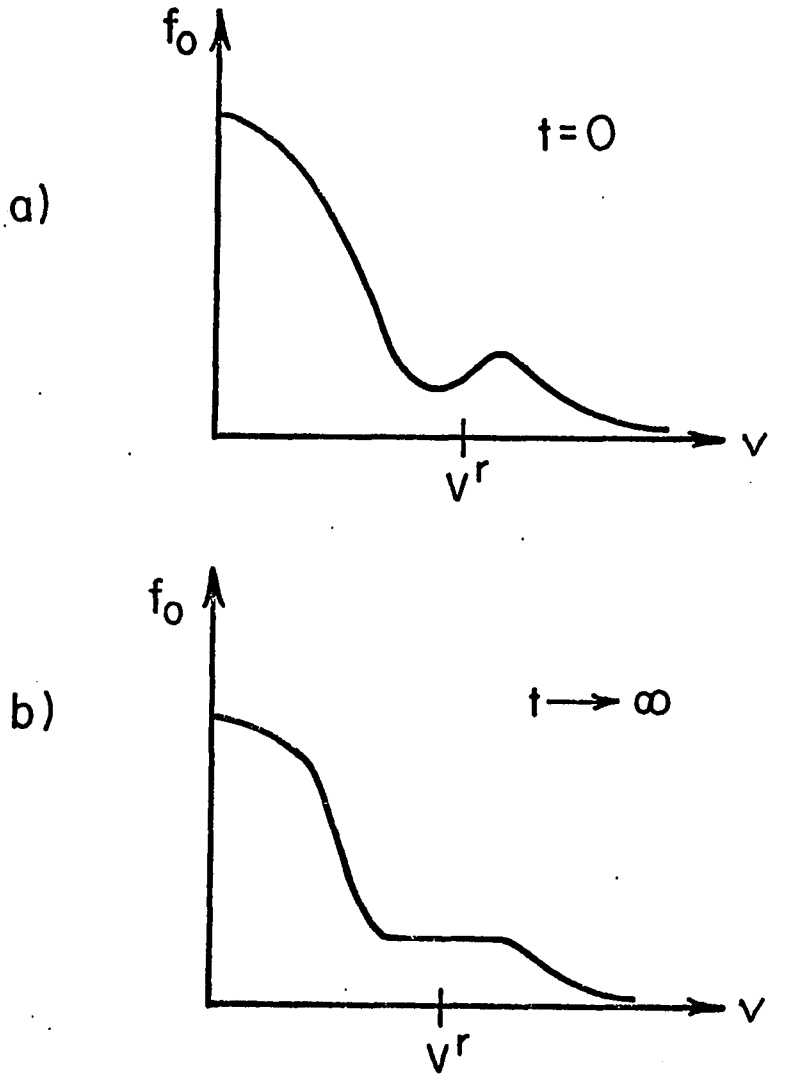

Figure 3.2

The quasi-linear change in a distribution function, f_o . The bump-in-the-tail at t = 0 evolves to a plateau at $t \longrightarrow \infty$.

We shall see that we can find ω_R and ω_I explicitly only if $\underline{k}$ is assumed real. This is not a serious limitation on our theory for we could just as easily expand $\underline{k}$ into real and imaginary parts and assume ω to be real. Because we are interested only in temporal effects as opposed to spatial effects we shall expand ω according to equation 3.15. Because ω is complex this implies that ε_L must be a complex function. The solution of this complex function rests upon our ability to handle the pole in the integrand of equation 3.14.

Because we are in the weak turbulent regime it seems reasonable to assume that

$$\mathcal{K} = \frac{|\omega_I|}{\omega_R} << 1 .$$

The above inequality suggests that we expand $\varepsilon_L(\omega)$ in a Taylor series. If we know $\varepsilon_L(\omega_R)$ the question is can we find $\varepsilon_L(\omega)$? The answer to this very important question can be found in Appendix B. From equation B.4 and equation B.5 we see that to first order

3.16) $$\varepsilon_R(\underline{k}, \omega_R) = 0$$

3.17) $$\omega_I(\omega_R) = - \frac{\varepsilon_I(\underline{k}, \omega_R)}{\partial \varepsilon_R / \partial \omega_R}$$

where

$$\varepsilon_L(\underline{k}, \omega_R) = \varepsilon_R(\underline{k}, \omega_R) + i\,\varepsilon_I(\underline{k}, \omega_R).$$

The above equations form the foundation for our remaining work. ω_I can be either positive or negative. In the previous section we saw that the spectral wave energy density is proportional to $e^{2\omega_I^{\alpha} t}$ where α defined a particular branch (see Chapter IV for a classification

of these branches). Therefore if ω_I is positive, the waves increase in energy and if ω_I is negative the waves lose energy. The wave is referred to as damped in the latter case and amplified in the former case. It is convenient that to first order the equations, which we use to find ω_R and ω_I, are uncoupled. Unfortunately such is not the case when we include the higher order terms in the expansion. We may think of the expansion of ε_L in terms of $\mathcal{N}$ defined above. We have as yet not found the radius of convergence (R) for this function. From Appendix B it is evident that $R < \infty$ but its actual value is unknown. What the above discussion implies is that for a given $\mathcal{N}$ we may be unable to find $\varepsilon_L(\omega)$ from a knowledge of $\varepsilon_L(\omega_R)$ using a Taylor series. This is not to say that one cannot find an ω which makes $\varepsilon_L(\omega) = 0$ for any value of $\mathcal{N}$. In Appendix C we develop the W-function (Ichimaru, 1973) which is closely related to the plasma dispersion function of Fried and Conte (Fried and Conte, 1960). The plasma dispersion function has been tabulated for large imaginary arguments. But for such a situation the problems still facing us are immense because we still must solve

$$\varepsilon_R(\omega) = 0$$

and

$$\varepsilon_I(\omega) = 0$$

simultaneously to find ω_R and ω_I. The death knell for a general solution of $\varepsilon_L(\omega)$ is that the plasma dispersion function can only be used for plasmas describable by a class of distributions related to the Maxwell-Boltzmann (MB) distribution. No such analysis can easily be undertaken for the general case.

The astute reader has no doubt been thinking that it hardly matters for the following reasons. If $|\omega_I|$ and ω_R are comparable

then one of two situations occurs. Either the wave damps very quickly or it grows very quickly. In the former case the wave never makes it out of the transient state of the system whereas in the latter case it quickly couples to other waves via wave-wave interactions. In neither case is the wave which was first induced in our system present in its' initial form in the asymptotic state. Assuming that our distribution of particles makes it through the transient state without too much diffusion then we are interested, in this work, in those waves which exist in the asmytotic state that can resonantly interact with the particles present. It is these waves which we call normal.

I feel that the above discussion is vital to our modus operandi. It is for the above reasons that we may expand $\varepsilon_L(\omega)$ in a Taylor series and find the normal modes from a knowledge of ε_R and ε_I along the real frequency axis. This is truly a remarkable result. Let us begin our stability analysis of the auroral plasma by stating the model we shall use to describe this plasma.

The model is made up of a population of cool ions and electrons of ionospheric origin and a measured population of hot electrons of magnetospheric origin. The distribution functions for the cool components are all in MB form. Let us solve ε_L for particles describable by

3.18) $$f_{\gamma 0}(\underline{v}) = \sqrt{\frac{m_\gamma}{2\pi K T_{\parallel\gamma}}} \left(\frac{m_\gamma}{2\pi K T_{\perp\gamma}}\right) * $$

$$* e^{-\frac{m_\gamma}{2KT_{\parallel\gamma}}(v_\parallel - u_{o\gamma})^2} e^{-\frac{m_\gamma}{2KT_{\perp\gamma}}v_\perp^2}$$

where

$$\int f_{r0}\, d\underline{v} = 1 \quad .$$

Let $\varepsilon_L = \varepsilon_L^f$, where f is defined in equation 3.18. Substituting 3.18 into equation 3.14 we find after a bit of algebra that

3.19) $$\varepsilon_L^f(\underline{k},\omega) = 1 + \sum_r \frac{1}{k^2 \lambda_{Dr}^2} \left\{ 1 + \sum_n \left[1 + \sigma_r \frac{n\omega_{cr}}{\omega - n\omega_{cr}} \right] \left[W(x_r^n) - 1 \right] \Lambda_n(\lambda_r) \right\}$$

where

$$x_r^n = \frac{\sqrt{\alpha_r}}{k_{\parallel}} \left(\omega - n\omega_{cr} - k_{\parallel} u_{or} \right)$$

$$\lambda_{Dr}^2 = \frac{K T_{\parallel r}}{4\pi \bar{n}_r e^2} \qquad \text{(Debye length)}$$

$$\lambda_r = \frac{K T_{\perp r}}{m_r \omega_{cr}^2} k_{\perp}^2$$

$$\sigma_r = T_{\parallel r} / T_{\perp r}$$

$$\Lambda_n(\lambda_r) = e^{-\lambda_r} I_n(\lambda_r)$$

$$\alpha_r = m_r / K T_{\parallel r}$$

All of the above symbols are defined in Appendix D. Because the W-function has real and imaginary parts we may in turn find the real and imaginary parts for ε_L^f. From Appendix C we see that

3.20) $$W(z) = 1 + z e^{-z^2/2} \int_0^z e^{y^2/2}\, dy + \sqrt{\frac{\pi}{2}}\, z\, e^{-z^2/2} * \begin{cases} i & , k_{\parallel} > 0 \\ -i & , k_{\parallel} < 0 \end{cases}$$

where z is complex and depends on $k_{\parallel}$. We therefore find that

3.21) $$\varepsilon_R^f(\underline{k},\omega_R) = 1 + \sum_\gamma \frac{1}{k^2\lambda_{D\gamma}^2}\left\{1 + \sum_n \left[1 + \sigma_\gamma \frac{n\omega_{c\gamma}}{\omega_R - n\omega_{c\gamma}}\right]\left[W_R(x_\gamma^n) - 1\right]\Lambda_n(\lambda_\gamma)\right\}$$

3.22) $$\varepsilon_I^f(\underline{k},\omega_R) = \frac{1}{k^2|k_\parallel|}\sum_{n,\gamma}\left\{\sqrt{\frac{\pi\alpha_\gamma}{2}}\frac{1}{\lambda_{D\gamma}^2} * \right.$$

$$* \left(1 + \sigma_\gamma \frac{n\omega_{c\gamma}}{\omega_R - n\omega_{c\gamma}}\right)(\omega_R - n\omega_{c\gamma} - k_\parallel u_{o\gamma}) *$$

$$\left. * \Lambda_n(\lambda_\gamma)\, e^{-\frac{\alpha_\gamma}{2}\left(\frac{\omega_R - n\omega_{c\gamma} - k_\parallel u_{o\gamma}}{k_\parallel}\right)^2}\right.$$

where

3.23) $$W_R(x_\gamma^n) = 1 + x_\gamma^n e^{-(x_\gamma^n)^2/2}\int_0^{x_\gamma^n} e^{y^2/2}\,dy$$

and $x_\gamma^n = x_\gamma^n(\omega_R)$, is a real quantity. We shall assume that the hot, measured distribution contributes to ε_I^f but not to ε_R^f . The reason for this is obvious when one considers that the number density for the cool particles in the auroral plasma is approximately $10^5/cm^3$ whereas the number density for the measured particles is about $10/cm^3$. The oscillations are governed by the number of particles whereas the dissipation (i.e. ε_I) is governed by which species' are anisotropic. For the measured distribution only weak free energy sources have been found to possibly couple to the normal oscillations of the background plasma. We shall consider this problem in more detail

where

$$\mathcal{H}^{n}_{\perp e} = -2\pi n |\omega_{ce}| \int dv_\perp \, J_n^2(a_e) \, \partial_{v_\perp} f^h_{eo} \Big|_{v_\parallel^r}$$

$$\mathcal{H}^{n}_{\parallel e} = 2\pi k_\parallel \int dv_\perp \, v_\perp \, J_n^2(a_e) \, \partial_{v_\parallel} f^h_{eo} \Big|_{v_\parallel^r}$$

$$v_\parallel^r = \omega_R + n|\omega_{ce}| / k_\parallel \quad .$$

In the above expressions f^h_{eo} is the measured distribution function. Refer to Chapter V for a comprehensive analysis of it. We may now write the final form for our equations.

---

1. The normal oscillations.

$$\varepsilon^c_R(\underline{k}, \omega_R) = 0$$

where,

3.24)
$$\varepsilon^c_R = 1 + \sum_\gamma \frac{1}{k^2 \lambda^2_{D\gamma}} \left\{ 1 + \sum_n \frac{\omega_R}{\omega_R - n\omega_{c\gamma}} * \right.$$
$$\left. * \left[W_R(x^n_\gamma) - 1 \right] \Lambda_n(\lambda_\gamma) \right\} \quad .$$

---

2. The dissipation.

$$\omega_I = -\varepsilon_I \beta_R$$

3.25)
$$= -\beta_R (\varepsilon^c_I + \varepsilon^h_I)$$
$$= \omega^c_I + \omega^h_I$$

where,

3.26)
$$\beta_R = (\partial \varepsilon^c_R / \partial \omega_R)^{-1}$$

$$3.27)\quad \varepsilon_I^c = \frac{1}{k^2 |k_{||}|} \sum_{n,\nu} \sqrt{\frac{\pi \alpha_\nu}{2}}\, \frac{\omega_R}{\lambda_{D\nu}^2}\, \Lambda_n(\lambda_\nu) * e^{-\frac{\alpha_\nu}{2}\left(\frac{\omega_R - n\omega_{c\nu}}{k_{||}}\right)^2} *,$$

$$3.28)\quad \varepsilon_I^h = -\frac{\pi}{k^2 |k_{||}|} \sum_n \frac{\omega_{pe}^2}{\bar{n}_e} \left(\mathcal{H}_{\perp e}^n + \mathcal{H}_{||e}^n\right).$$

We shall devote the remaining space in this work to an understanding of equations 3.24 - 3.28. In the following chapter, we shall explore the behavior of the analytic form of $\varepsilon_L^c(\underline{k}, \omega_R)$ namely ε_R^c and ε_I^c . This will be done for a variety of possible plasma states including the auroral plasma we are studying. Before we can understand ε_I^h we need to know much more about f_{eo}^h , the measured distribution function. Chapter V is devoted to this understanding. In Chapter VI we shall return to our complete set of stability equations and develop the recipe we shall use to find electrostatic instabilities in an auroral plasma.

With this knowledge of where we are going, let us turn our attention to the understanding of the normal oscillations and weak dissipation of the background plasma, which is describable by an analytic distribution function.

CHAPTER IV

THE OSCILLATIONS OF THE BACKGROUND PLASMA

4.1 The Problem with Waves

One's understanding of the complicated processes which occur in a plasma rests in large part on how that plasma oscillates. Unfortunately the investigator, who first enters this field, is unceremoniously swamped with a cornucopia of waves and names with their respective instabilities. This often confusing situation is complicated by the fact that investigators tend to study the effects of a particular wave only in a very limited region of k-space. While this approach may have decided benefits in terms of a simplification of the equations used, the raison d'etre for its' utilization lies more in the fact that free energy sources in the particle distributions may couple to such waves more effectively. However, in order to make use of such an approach it would seem that a knowledge of the dispersion characteristics of the particular wave of interest throughout k-space would be required. With this knowledge one could then say with reasonable assurance what the coupling between the free energy sources in the particle distribution and the waves in any region of k-space would be.

In this work instead of choosing the region of k-space we shall only choose which cyclotron harmonic we wish our wave to be Doppler shifted down to in order to resonate with particles having a parallel velocity, $v_{\parallel}^{r}$ (see section 3.4). With this kind of constraint

our waves could end up anywhere in k-space (see Chapter VI for a complete discussion of this wave-particle resonance).

We shall devote the whole of this chapter to the study of waves. To be able to bring some amount of order to this study let us classify them according to the following scheme.

A wave is in either an electrostatic mode (ES) or an electromagnetic mode (EM) or a combination of the two (hybrid mode) (see Appendix A). ES waves are often referred to as longitudinal because

$$\underline{k} \times \underline{E}_1^{\iota}(\underline{k}, \omega) = \underline{0}$$

whereas EM waves are referred to as transverse because

$$\underline{k} \cdot \underline{E}_1^{\iota}(\underline{k}, \omega) = 0 \ .$$

Any given mode is made up of distinct branches (designated by $\alpha(\underline{k})$ defined in section 3.3). All the members of a given branch are related to one another as to the particular state of the system which induced the oscillation.

We will refer to a wave as being evanescent (damped) or amplifying (growing) depending on whether the ω_I associated with the wave is negative or positive respectively. As we have mentioned often in this work, $|\omega_I|$ cannot be too large to negate the definition of a normal oscillation (see sections 3.1, 3.4 and Appendix B).

The wave either damps or grows because of its interaction with a particular group of particles. Such an interaction is called a resonance. This interaction may be either a Landau resonance ($n=0$) or a cyclotron resonance ($n\neq 0$) where n, an integer, defines the particular cyclotron harmonic (see equations 3.24 - 3.28).

In a thermal plasma the normal oscillations can propagate. Due to the importance of amplifying waves (wave instabilities) in our system, we shall refer to a wave instability that can propagate as a convective instability. We shall refer to the unique situation where an instability grows at every point in our system with time as an absolute instability. The latter situation requires the system to be coupled to an external resoivoir of free energy (see figure 4.1.1).

It is very important to realize that waves represent the fact that collective phenomena can exist in our system. This is due not to collisions as in a gas or to the fact that our particles are atomically bound as in a drumhead but rather to the fact that our particles are coupled by small fluctuating fields. In what follows we shall find that the presence of a strong magnetic field significantly modifies the nature of the longitudinal collective modes from that found in the absence of the field. In the following section we will look only at the properties of $\varepsilon_L^f(k, \omega_R)$ not only at various points in k-space but also for four representative plasma states. In the final section of this chapter we shall find those zeros of ε_L^f that are normal and plot them over various regions in k-space. Such waves will be referred to as the dispersion waves of a particular branch. We will be able to classify all of the branches of the ES mode by looking at just the four representative plasma states introduced in section 4.2. Let us now turn to the numerical analysis of ε_L^f, the longitudinal dielectric function.

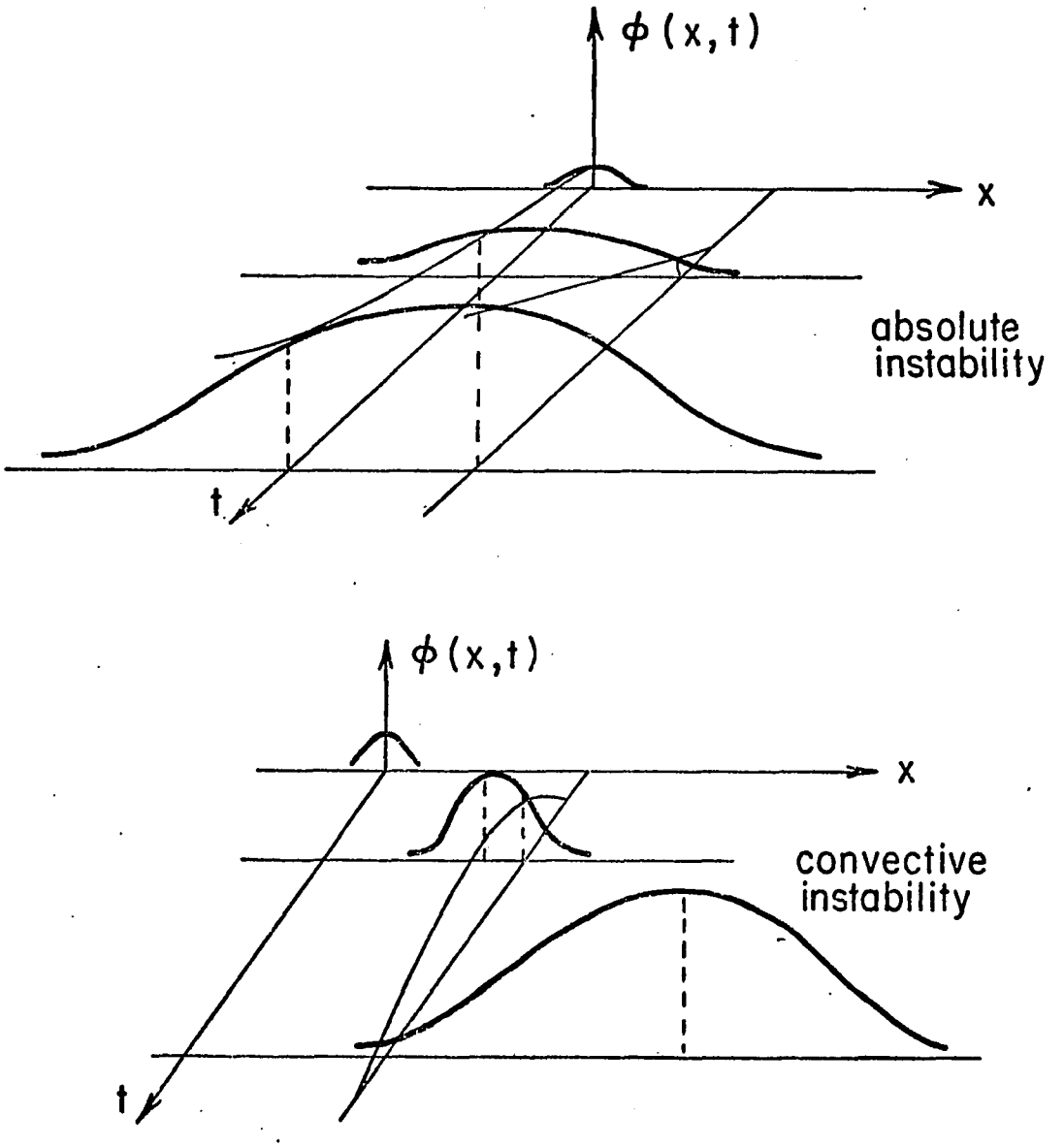

Figure 4.1.1

The possible types of instability.

4.2 The Properties of ε_L^f

We shall begin this section by rewriting equation 3.21 in a form more conducive for computer analysis, i.e.

4.1) $$\varepsilon_R^f(\underline{k}, \omega_R) = F - G$$

where,

$$F = 1 + \sum_\gamma \frac{1}{k^2 \lambda_{D\gamma}^2} W_R(x_\gamma^0) \Lambda_0(\lambda_\gamma) ,$$

$$G = \sum_\gamma \frac{1}{k^2 \lambda_{D\gamma}^2} \left\{ \sum_{p=1}^{p_{m\gamma}} \frac{2\sigma_\gamma \omega_{c\gamma}^2 \Gamma_p(\lambda_\gamma)}{\omega_R^2 - p^2 \omega_{c\gamma}^2} - C_\gamma^p - C_\gamma^{-p} \right\} ,$$

$$C_\gamma^p = \frac{W_R(x_\gamma^p) \Lambda_p(\lambda_\gamma)}{\omega_R - p\omega_{c\gamma}} \left[\omega_R + p(\sigma_\gamma - 1)\omega_{c\gamma}\right] ,$$

$$\Gamma_p(\lambda_\gamma) = p^2 \Lambda_p(\lambda_\gamma) .$$

In rewriting equation 3.21 we have substituted p for n for notational clarity. Instead of keeping all harmonics in $\sum_p$ we have chosen to cut the sum off at $p_{m\gamma}$, which may vary according to the γ^{th} species. The error introduced in ε_R^f by expanding it in terms of a finite sum rather than an infinite sum may easily be computed by calculating the change in ε_R^f when one or more terms are added. We shall discuss this problem in greater depth in the following section when we make plots of the dispersion curves. We may rewrite equation 3.22 as,

$$4.2)\quad \varepsilon_I^f(\underline{k},\omega_R) = \sum_\gamma \frac{1}{k^2\lambda_{D\gamma}^2}\left\{B_\gamma^0 + \sum_{p=1}^{p_{m\gamma}}\left(B_\gamma^p + B_\gamma^{-p}\right)\right\}$$

where

$$B_\gamma^p = \sqrt{\frac{\pi\alpha_\gamma}{2}}\left(1+\sigma_\gamma\frac{p\omega_{c\gamma}}{\omega_R - p\omega_{c\gamma}}\right)\Lambda_p(\lambda_\gamma)\cdot$$

$$\cdot\frac{1}{|k_\parallel|}(\omega_R - p\omega_{c\gamma} - k_\parallel u_{o\gamma})\, e^{-\frac{\alpha_\gamma}{2}\left(\frac{\omega_R - p\omega_{c\gamma} - k_\parallel u_{o\gamma}}{k_\parallel}\right)^2}.$$

Because $\varepsilon_L^f(\omega)$ is an analytic function in and on a circle of radius $R < \infty$ we can expand ε_L^f in a Taylor series about the point $\omega = \omega_R$. To construct this series we need to take derivatives of ε_L^f. For a given problem it may be possible to truncate the series after a given order. For the finite series to accurately represent ε_L^f the error introduced must be negligible. (We are currently working on this problem). If equations 3.24 and 3.25 are correct (i.e. ε_R^f is expanded to zero order and ε_I^f is expanded to first order) then the zeros of $\varepsilon_R^f(\omega_R)$ represent the normal oscillations as long as $\mathcal{K} = \frac{|\omega_I|}{\omega_R} << 1$ (see Appendix B for a discussion of the Taylor series method).

In this section we shall be concerned with the behavior of $\varepsilon_R^f(\omega_R)$ and ε_I^f at various points in k-space and with the changes which occur when we consider various plasma states. An understanding of equations 4.1 and 4.2 requires that we understand the behavior of the functions which make up ε_R^f and ε_I^f. The most important functions are W_R, Λ_p, and $\Gamma_p(Z_o)$ where Z_o is some fixed number. In figures 4.1.2 - 4.3 we plot the above functions. (See Appendix C for a derivation of the asymptotic and power series for W_R). From figure

Figure 4.1.2 The real part of the W-function as a function of real argument. The power and asymptotic forms of the W-function may be found in Appendix C.

Figure 4.2 $\Lambda_n(z)$ vs. z for various harmonics, n. $\Lambda_n(z) = e^{-z} I_n(z)$. This function plays an important role in the behavior of ϵ_R^f and ϵ_I^f

Figure 4.3 $\Gamma_n(x_o)$ vs n for various fixed arguments, a: $x_o = 0.5$, b: $x_o = 1.0$, c: $x_o = 2.0$, d: $x_o = 3.0$, e: $x_o = 4.0$, f: $x_o = 5.0$. As can be seen from the figure, the number of significant harmonics increases with an increasing argument.

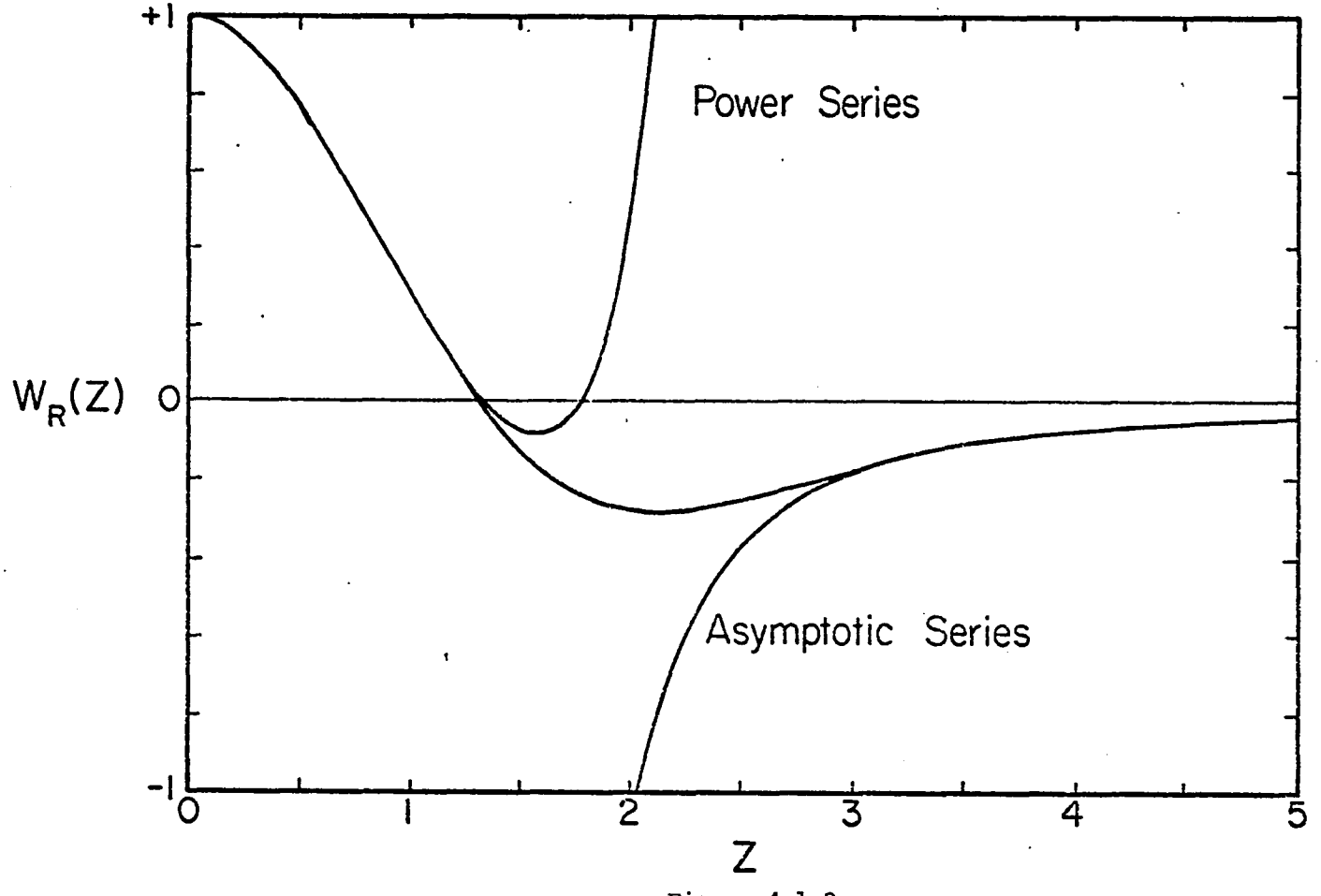

Figure 4.1.2

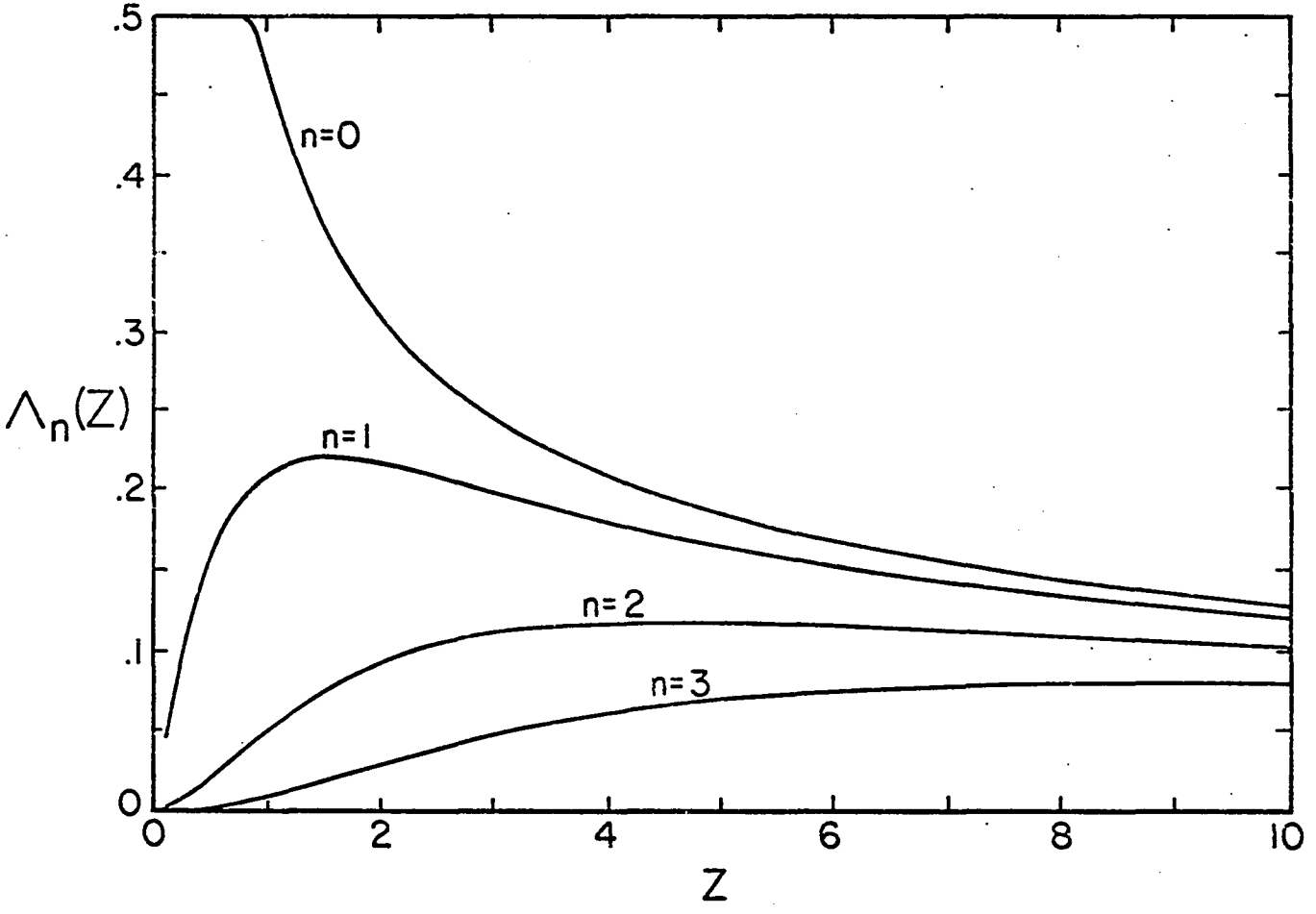

Figure 4.2

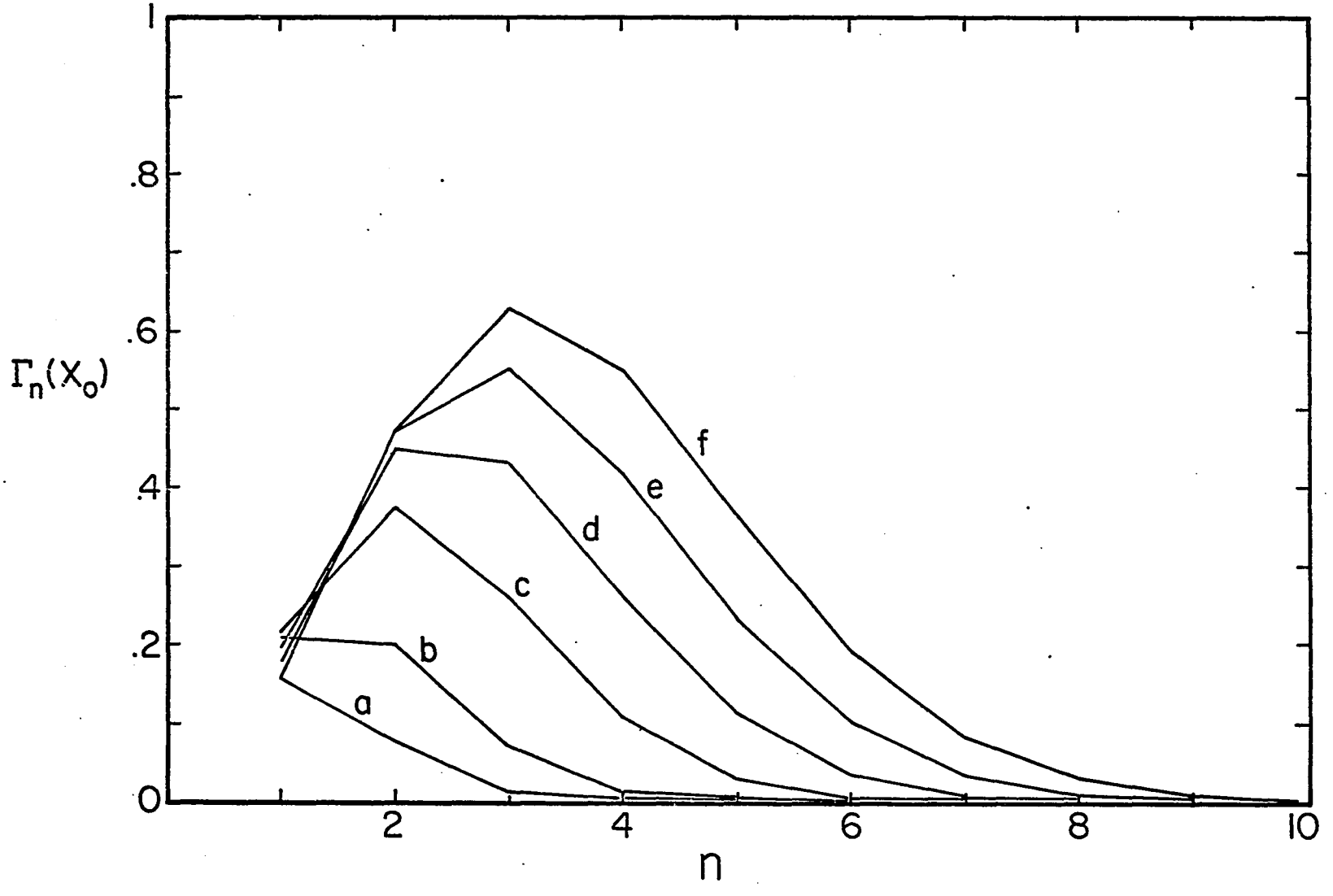

Figure 4.3

4.1.2 we see that over a finite inteval neither series is an adequate approximation. Because of the behavior of W_R (see equation 3.23) we cannot use a trapezoidal rule for integrating W_R (because of the nature of the integrand) rather we must resort to using a cautious adaptive Romberg extrapolation (de Boor, 1971). Let us turn now to a description of the program which plots ε_R^f and ε_I^f and their derivatives. The program is called DISPER.

We find it most convenient to plot all the functions with respect to $X = \frac{\omega_R}{\omega_c}$ where ω_c is the cyclotron frequency of a particular species specified by the user. This program will describe the possible ES branches in a plasma composed of up to ten different species (e^-, O^+, NO^+, N^+, N_2^+, H^+, He^+, O_2^+ and any two user defined species not included in the above list). As we see from equation 3.18 any particular species may be distributed in velocity space as follows:

Equilibrium

a) MB

Non-equilibrium

a) two temperature MB (2T-MB)

b) streaming MB

c) 2T-streaming MB

Streaming is restricted to be along the magnetic field. The user has the option of specifying whether a zero order current is present for any given species. It must be pointed out however that the existence of a

zero order current may negate the existence of ES waves because such waves are induced by density perturbations while EM waves are induced by current perturbations. If no zero order current is desired the program will divide the particular distribution into two equal density but oppositely directed streams (each stream has $\frac{1}{2}$ the total number density). See Kindel and Kennel, (1971) for a discussion of the above situation.

The operator may chose to investigate the following dispersion functions: F, G, ER, EI, DER, DEI, WI, D2R, D2I, TR1, TR2, TI1, TI2, and NYQ where

---

$$DER = \omega_R \frac{\partial \epsilon_R^f}{\partial \omega_R}$$

$$DEI = \omega_R \frac{\partial \epsilon_I^f}{\partial \omega_R}$$

$$WI = \frac{\omega_I}{\omega_R}$$

$$D2R = \omega_R^2 \; \partial^2 \epsilon_R^f / \partial \omega_R^2$$

$$D2I = \omega_R^2 \; \partial^2 \epsilon_I^f / \partial \omega_R^2$$

$$TR1 = -\omega_I \; \partial \epsilon_I^f / \partial \omega_R$$

$$TR2 = -\tfrac{1}{2} \omega_I^2 \; \partial^2 \epsilon_R^f / \partial \omega_R^2$$

$$TI1 = \omega_I \; \partial \epsilon_R^f / \partial \omega_R$$

$$TI2 = -\tfrac{1}{2} \omega_I^2 \; \partial^2 \epsilon_I^f / \partial \omega_R^2$$

$$ER = F - G = \epsilon_R^f$$

$$EI = \epsilon_I^f$$

The T functions are used in the Taylor series expansion of $\varepsilon_{\perp}^{f}(\omega)$ and are developed in Appendix B. NYQ stands for Nyquist plot. It is a method to test whether or not a particular plasma state is unstable to ES waves. See Krall and Trivelpiece, (1973) for a good discussion of this method.

To help in understanding the behavior of these functions the user can plot any of them at a particular x (i.e. frequency) with respect to either temperature or the magnitude of the zero order magnetic field, which are the two most important parameters in the behavior of any magneto-active plasma. To help in debugging and as an aide in setting limits on the ordinate axis the program prints out the value of any function at a particular x.

The plotting options for any function are as follows:

	Abscissa	Ordinate
1.	linear	linear
2.	linear	$\log_{10}$
3.	$\log_{10}$	linear
4.	$\log_{10}$	$\log_{10}$

The flexibility in plotting allows one to either include everything on one plot or to look at just a small frequency region. On all plots the principal frequencies are clearly marked on the abscissa and listed on the terminal. These frequencies are:

1. The plasma frequency of all species, $\omega_{p\gamma}$ (small tick marks)
2. The cyclotron frequency of all species, $\omega_{c\gamma}$ (large tick marks)
3. The upper hybrid frequency, ω_{uH} (large tick mark)
4. The lower hybrid frequency, ω_{LH} (large tick mark)

Because we are interested in the frequency dependence of our dispersion functions at any point in the two dimensional k-space, three options exist to locate one's position in this space. They are

1. (k, θ)
2. $(k_\perp, \theta)$
3. $(k_\parallel, \theta)$

We shall look at the important variations of ε_R^f and ε_I^f over k-space for four representative plasma states when f is a MB distribution.

The final plasma state is the one which most closely models the actual auroral plasma the rocket flew through (see Chapters I and VI). Preceeding the frequency maps for each plasma state will be a list of the important parameters which describe the plasma and the values of the principal frequencies.

Plasma State I

Species: (e^-, O^+)

$T_e = 0°$ K

(the cold plasma)

$T_i = 0°$ K

$n_e = n_i = 10^4$ cm^{-3}

$k = 0.01$ cm^{-1}

$B_o = 0.5$ Gauss

Principal Frequencies (sec^{-1})

$\omega_{pe} = 5.64 \times 10^6$

$\omega_{pi} = 3.29 \times 10^4$

$|\omega_{ce}| = 8.8 \times 10^6$

$\omega_{ci} = 299.44$

$\omega_{LH} = 2.77 \times 10^4$

$\omega_{UH} = 1.045 \times 10^7$

Figure 4.4 The real part of ε_L^f, ε_R^f vs. $x = \frac{\omega_e}{|\omega_{ce}|}$ on a log, log plot for P.S. I (the cold plasma): a) $\theta = 5°$, b) $\theta = 45°$, c) $\theta = 85°$, d) $\theta = 89.9°$. The low frequency ion wave which does not appear on a), b) and c) is really present but is too close to ω_{ci} to show up. For P.S. I there are three ES branches.

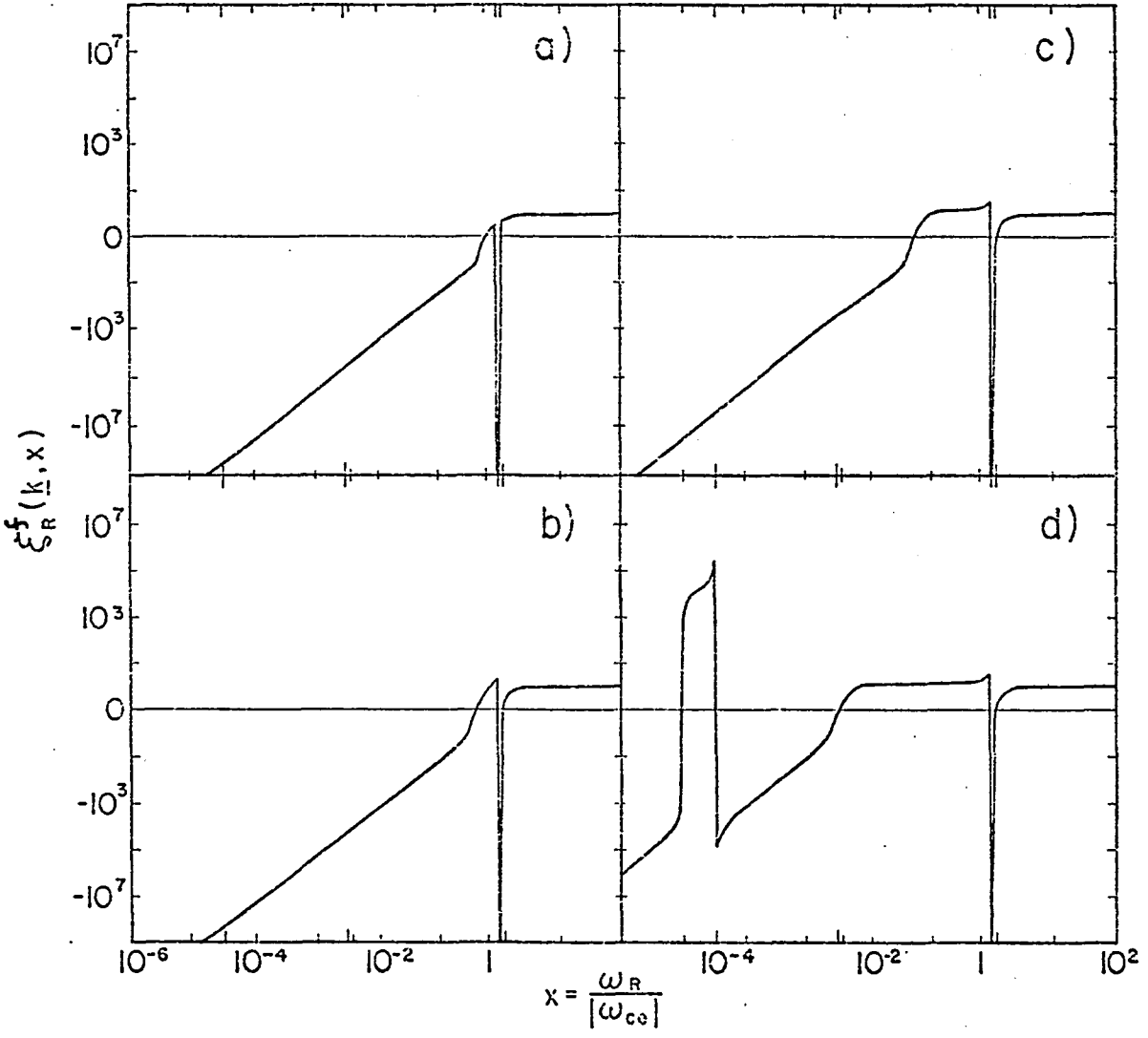
a)
c)
b)
d)
10^7
10^3
0
-10^3
-10^7
10^{-6}
10^{-4}
10^{-2}
1
10^2
$\xi_R^{ff}(\underline{k}, x)$
$x = \frac{\omega_R}{|\omega_{ce}|}$

Figure 4.4

Plasma State II

Species: (e^-, O^+)

$T_e = 1770^\circ$ K

$T_i = 0^\circ$ K

$\bar{n}_e = \bar{n}_i = 10^4 cm^{-3}$

$B_o = 0.5$ Gauss

$k = 0.01 cm^{-1}$

Principle Frequencies (sec^{-1})

Same as in Plasma State I.

Figure 4.5 ε_R^S vs. $x = \frac{\omega_e}{|\omega_{ce}|}$ on a log, log plot for P.S. II: a), b), c) and d) are for the same angles as in figure 4.4. For this plasma state there are four major branches, the maximum number possible. Notice the difference in the angular variation of the lowest frequency, positive sloped, wave in P.S. I and P.S. II.

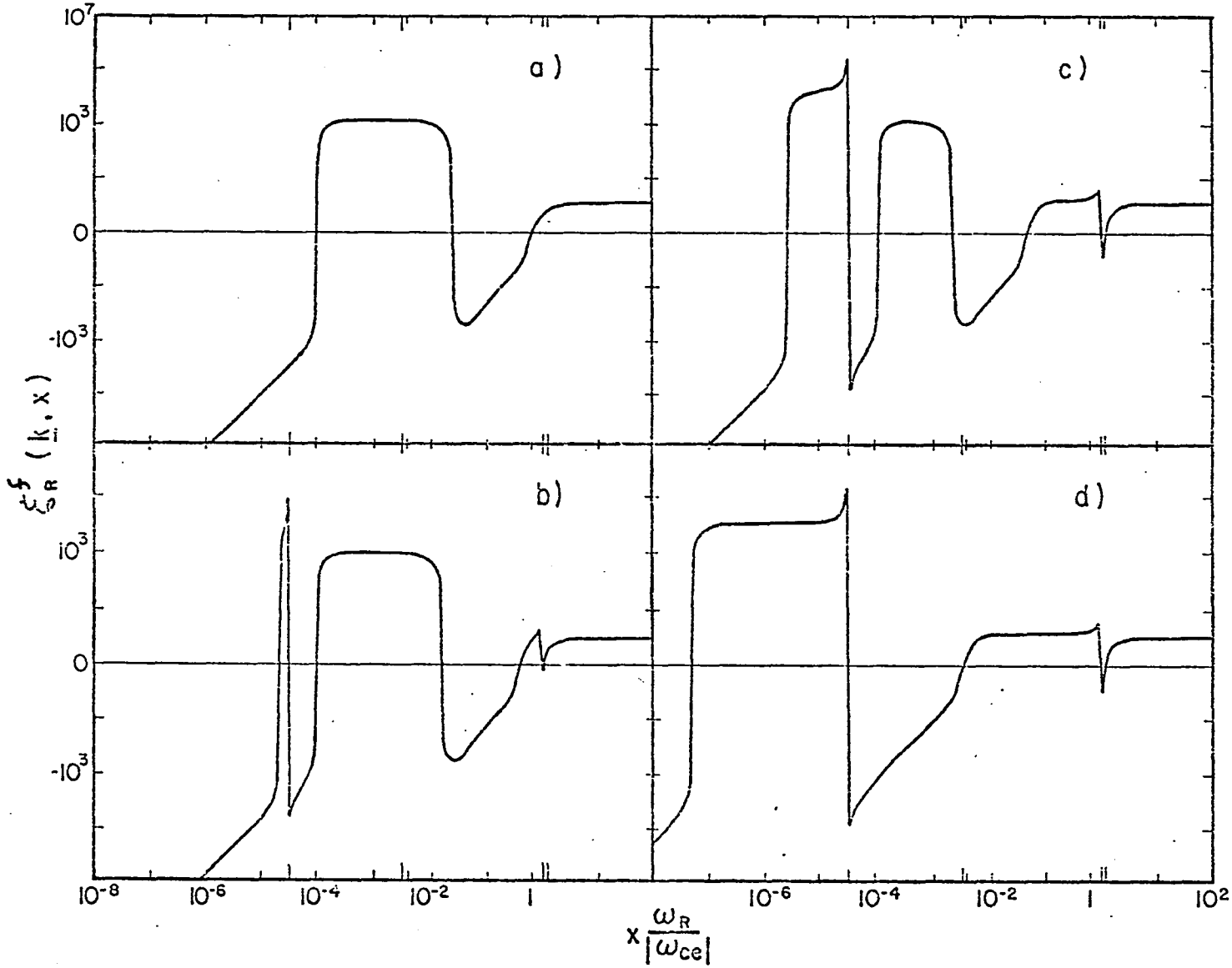
a)
c)
b)
d)
10^7
10^3
0
-10^3
$\xi_R^{-\frac{1}{2}}(k,x)$
10^{-8}
10^{-6}
10^{-4}
10^{-2}
1
10^2
$x\frac{\omega_R}{|\omega_{ce}|}$

Figure 4.5

Plasma State III

Species: (e^-, O^+)

$T_e = 10^4 \cdot K$

$T_i = 500 \cdot K$

$\bar{n}_e = \bar{n}_i = 10^4 cm^{-3}$

$k = 0.01 cm^{-1}$

$B_o = 0.5$ Gauss

Principle Frequencies (sec^{-1})

Same as in Plasma State I.

Figure 4.6 ε_R^5 vs. x on a log, log plot for P.S. III: a), b), c), and d) are for the same angles as in figure 4.4. The ion harmonic waves, at large angles, exist because the ion temperature is non-zero.

Figure 4.7 ε_R^5 vs. $x = \frac{\omega_e}{\omega_{ci}}$ on a log, linear plot. This is a detail of the above figure near the ion cyclotron frequency showing the angular variation of the ion harmonic waves: a) $\theta = 75^\circ$, b) $\theta = 80^\circ$, c) $\theta = 85^\circ$, d) $\theta = 89.5^\circ$.

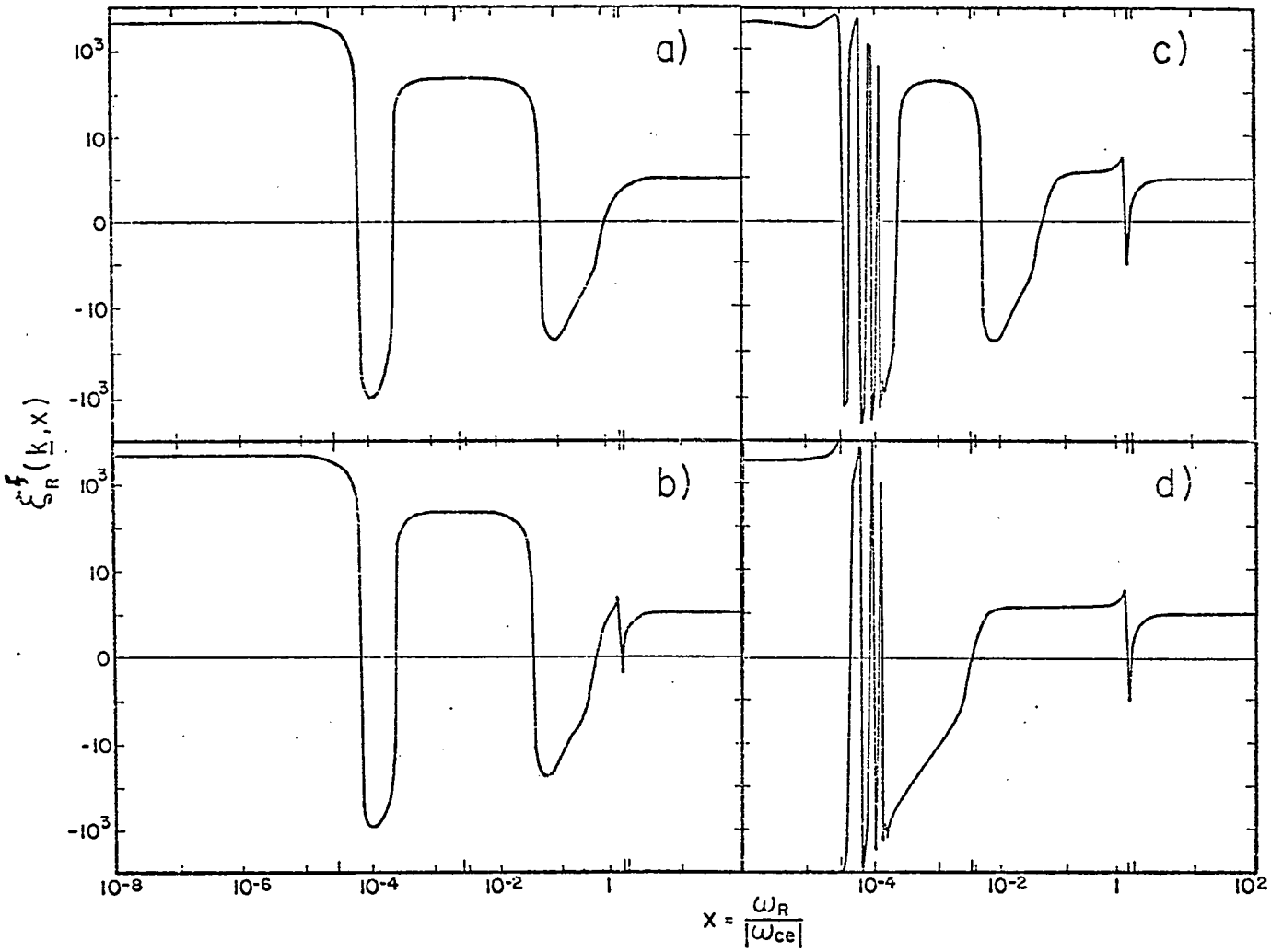
a)
b)
c)
d)
10^3
10
0
-10
-10^3
$\xi_R(\underline{k},x)$
10^{-8}
10^{-6}
10^{-4}
10^{-2}
1
10^2
$X = \frac{\omega_R}{|\omega_{ce}|}$

Figure 4.6

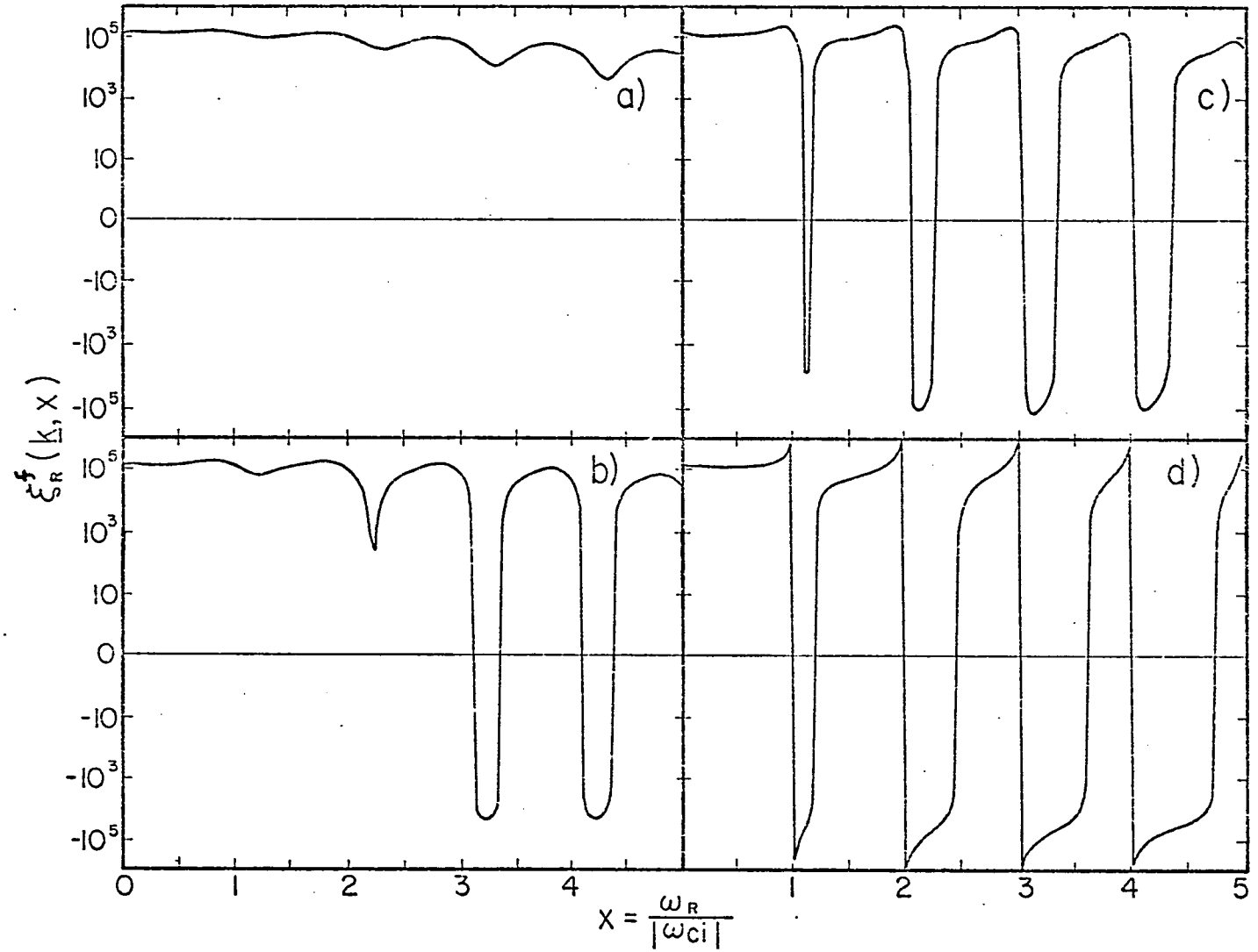
a)
b)
c)
d)
10^5
10^3
10
0
-10
-10^3
-10^5
$\xi_R^f(\underline{k}, X)$
0
1
2
3
4
5
$X = \frac{\omega_R}{|\omega_{ci}|}$

Figure 4.7

Plasma State IV

The Auroral Plasma.

Species: (e^-, O^+)

$T_e = 1770$ K

$T_i = 1023$ K

$\bar{n}_e = \bar{n}_i = 4.419 \times 10^5 cm^{-3}$

$k = 0.01\ cm^{-1}$

$B_o = 0.5$ Gauss

Principle Frequencies (sec^{-1})

Same as in Plasma State I.

Figure 4.8 ε_R^S and ε_I^S vs. $x = \frac{\omega_R}{|\omega_{ci}|}$ on a log, log plot for P.S. IV (the background auroral plasma): a), b), c) and d) are for the same angles as in figure 4.4. Because this plasma is in thermal equilibrium ε_I^S is positive definite. Note that no acoustic wave exists in P.S. IV because $Te \cong Ti$.

Figure 4.9 ε_R^S vs. $x = \frac{\omega_R}{\omega_{ci}}$ on a log, linear plot. This is a detail of the above figure near the ion cyclotron frequency showing the angular variation of the ion harmonic waves: a) $\theta = 84^\circ$, b) $\theta = 86^\circ$, c) $\theta = 88^\circ$, d) $\theta = 89.9^\circ$. Note the differences between these waves and those in figure 4.7.

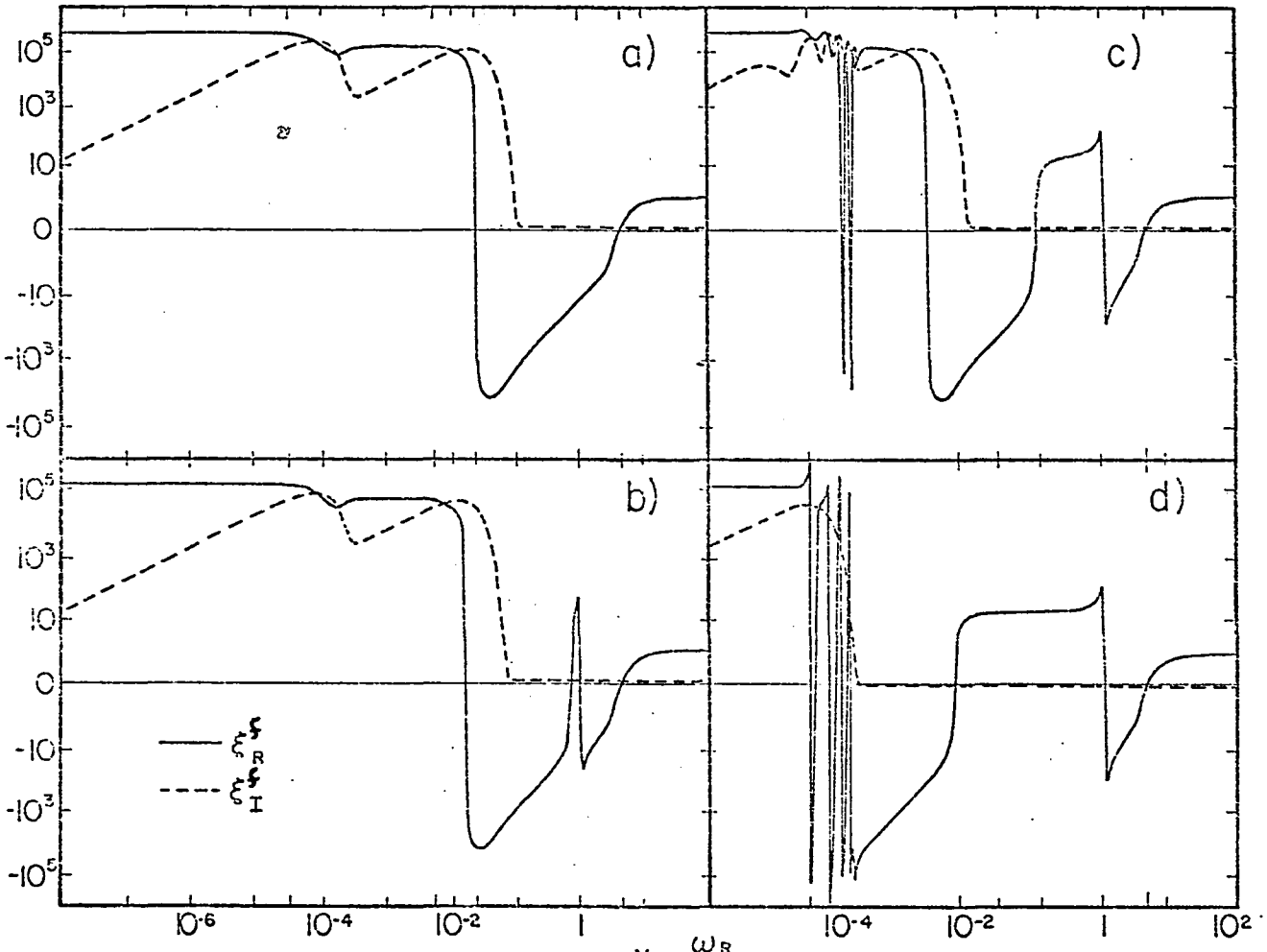
a)
b)
c)
d)
10^5
10^3
10
0
-10
-10^3
-10^5
ξ_R
ξ_I
10^{-6}
10^{-4}
10^{-2}
1
10^2
$X = \frac{\omega_R}{|\omega_{ce}|}$

Figure 4.8

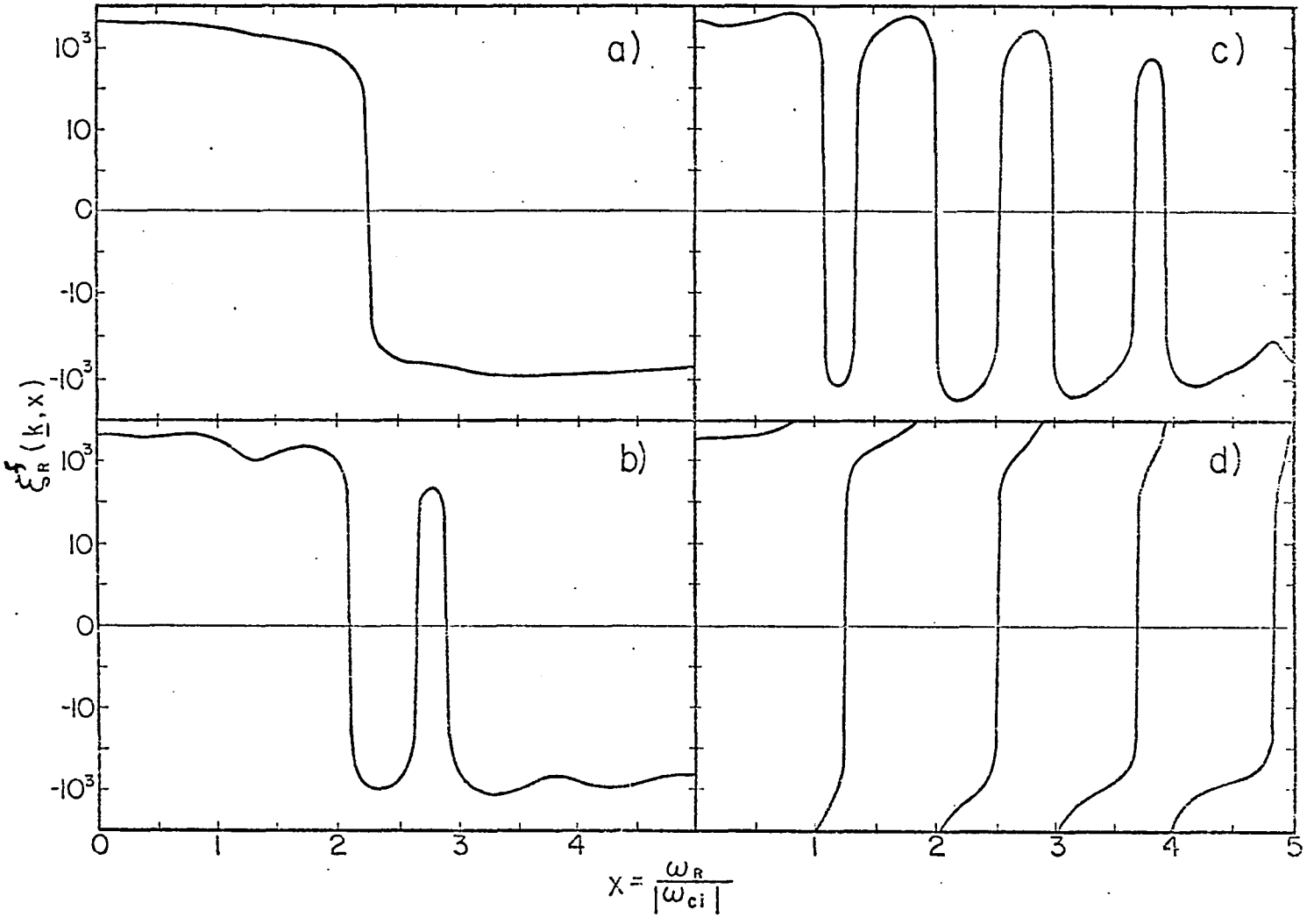

Figure 4.9

In our model of the auroral plasma, the zeros of $\varepsilon_R^f = \varepsilon_R^c$ give the normal ES oscillations of the plasma. However, this is only true when the slope of ε_R^c at a zero is positive. If this was not the case then growing waves would exist in an equilibrium plasma, (ω_I would be greater than zero) obviously an untenable situation. See Krall and Trivelpiece (1973) for a proof that any monotonically decreasing function of velocity is stable to an ES perturbation. The problem we are faced with is how are we to deal with the negative sloped zeros in figures 4.4 - 4.9. The problem is far from trivial. Its' resolution may be found in Appendix B. Our primary goal in understanding the behavior of ε_R^f and ε_I^f is to be able to say something about the normal ES oscillations of our system. In other words what we need is to develop a program which can find those zeros of ε_R^f whose slopes are positive.

4.3 The Dispersion Curves of the Background Plasma

The program we have developed to find a particular zero of ε_R^f is called INTER. To find these zeros we use a Newton-Raphson (N-R) method. The inner workings of this program are very similar to DISPER. We shall list below a summary of the available options.

As in DISPER the ordinate and abscissa may be plotted in terms of either a $\log_{10}$ or a linear scale. We currently have five frequency options:

1. ω_I / ω_R
2. ω_R / ω_c
3. ω_I
4. ω_I / ω_c
5. ω_R

In k-space there are only four possible ways of plotting a particular frequency option, call it y (see figure 4.10). They are:

1. y vs. (θ , $k_{\parallel}$, $k_{\perp}$); $k = k_o$
2. y vs. (k , $k_{\parallel}$, $k_{\perp}$); $\theta = \theta_o$
3. y vs. (k , θ , $k_{\perp}$); $k_{\parallel} = k_{\parallel o}$
4. y vs. (k, θ, $k_{\parallel}$); $k_{\perp} = k_{\perp o}$

Once the fixed variable in k-space is specified the user then specifies which independent variable he wishes y to be plotted against.

To be able to plot one of the frequency options over a region in k-space requires that we know ω_R at a particular point within the region. We may find this information from DISPER. We will summarize the workings of INTER by looking at the various dispersion curves of Plasma State III (P.S. III) over a few regions in k-space. We shall finish up this section with a comparison of the high frequency branches of P.S.I. and P.S. IV. We will make use of this comparison in Chapter VI.

Figure 4.11 is a summary of the ES branches of P.S. III. In this figure UHB stands for upper hybrid branch, WB stands for Whistler branch, AB is the acoustic branch and IC (n) is the ion cyclotron branch where n denotes the harmonic number. The only other ES branches that can exist in a plasma in any state that are absent from figure 4.11 are the EC (n) (i.e. the electron cyclotron branches) which do not appear because they are too close to the electron cyclotron harmonics and the low frequency Alfvén branch which exists in P.S. I and P.S. II (see figures 4.4 and 4.5).

The hole in the UHB for small angles truly exists. It may happen that a failure in the Taylor series expansion has occurred in which case these waves will be more heavily damped than is predicted by the first order theory we are presently using. What this indicates is the fact that

Figure 4.10 The plotting options in k-space: a) for fixed k, b) for fixed θ, c) for fixed $k_\perp$, d) for fixed $k_\parallel$.

Figure 4.11 The angular dispersion of the ES branches of P.S. III: ω_R / ω_{pe} vs. θ. Note the hole in the UHB and the AB. Both holes are explained in the text.

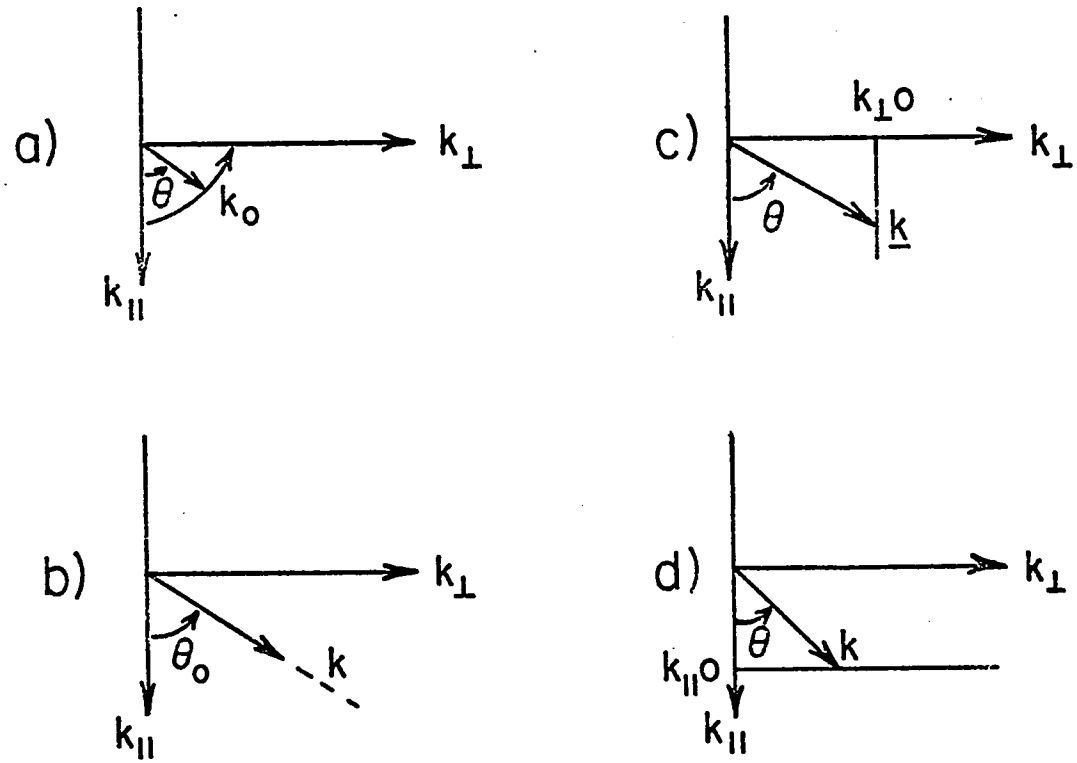
a)
$k_\perp$
θ
k_o
$k_{||}$
c)
$k_\perp o$
$k_\perp$
θ
$\underline{k}$
$k_{||}$
b)
$k_\perp$
θ_o
k
$k_{||}$
d)
$k_\perp$
θ
k
$k_{||}o$
$k_{||}$

Figure 4.10

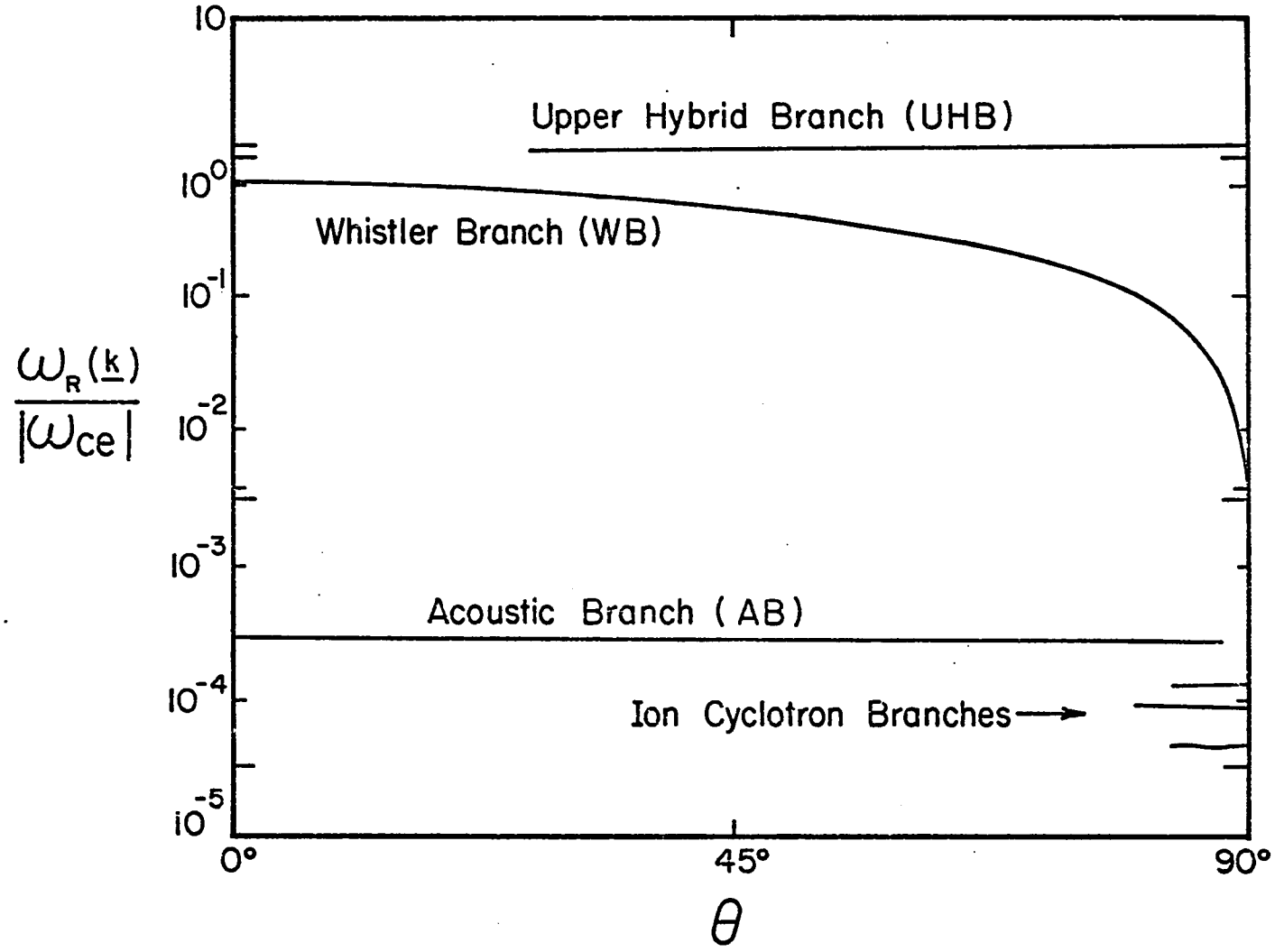
10
10^0
10^{-1}
10^{-2}
10^{-3}
10^{-4}
10^{-5}
$\frac{\omega_R(\underline{k})}{|\omega_{ce}|}$
Upper Hybrid Branch (UHB)
Whistler Branch (WB)
Acoustic Branch (AB)
Ion Cyclotron Branches
0°
45°
90°
θ

Figure 4.11

a non-Maxwellian distribution of particles may add enough damping or growth to the virtual waves to make them appear. We must clearly explore this area in greater detail before we can make any rigorous statements on the appearance of these "virtual waves". It is observed that only the high frequency branch which approaches $|\omega_{ce}|$ at $\theta = 0^\circ$ can have a hole, the existence of which seems to be highly temperature dependent and to a lesser extent k dependent. I did not specify which branch because by changing the number density the WB would approach $|\omega_{ce}|$ at small angles (instead of ω_{pe} as it does in P.S. III).

The above discussion should reinforce the fact that one must be very careful in using approximations for the wave structure of a particular plasma state.

We mentioned at the beginning of the previous section the importance of p_{my}, which specifies the maximum number of harmonic terms we keep in equations 4.1 and 4.2. This importance is illustrated in figures 4.12 and 4.13 for the acoustic branch. In figure 4.12 note that the percentage error in the real frequency is not as significant as in the imaginary frequency. Figure 4.12a demonstrates the important fact that one must be sure to include "enough harmonics" in the series contained in equations 4.1 and 4.2 to fairly represent ε_R^f and ε_I^f. The actual number seems to depend on the relative value of $\Gamma_p(z_o)$ (see figure 4.3), which acts very much like a weighting function. In the region of k-space defined in figure 4.12 when $p_{mi} = 10$ the harmonic series has converged. Such is not the case in figure 4.13. Here we are fixing $k_{//}$ at $0.01 cm^{-1}$ and stepping out along $k_\perp$. The problem that we face is that the argument of Γ_p depends upon $k_\perp^2$. The largest value z_o could attain in figure 4.12 was 2.9. Compare this to 290

Figure 4.12 The angular dispersion of the acoustic branch (AB) for various $\rho_{m\dot{v}}$ for a) the real frequency and b) the imaginary frequency. For $\rho_{m\dot{v}} = 10$ the harmonic series has converged. It is essential to know the correct $\rho_{m\gamma}$ for every branch.

Figure 4.13 ω_R vs. $k_\perp$ for the AB on a linear, log plot ($k_{\prime\prime} = 0.01 cm^{-1}$). For small $k_\perp$ this branch is only weakly dependent on $\rho_{m\dot{v}}$ however for large $k_\perp$ this particular branch is very sensitive to $\rho_{m\dot{v}}$. Near $k_\perp = 0.1 cm^{-1}$ the curve labeled $\rho_{m\dot{v}} = 12$ has not converged.

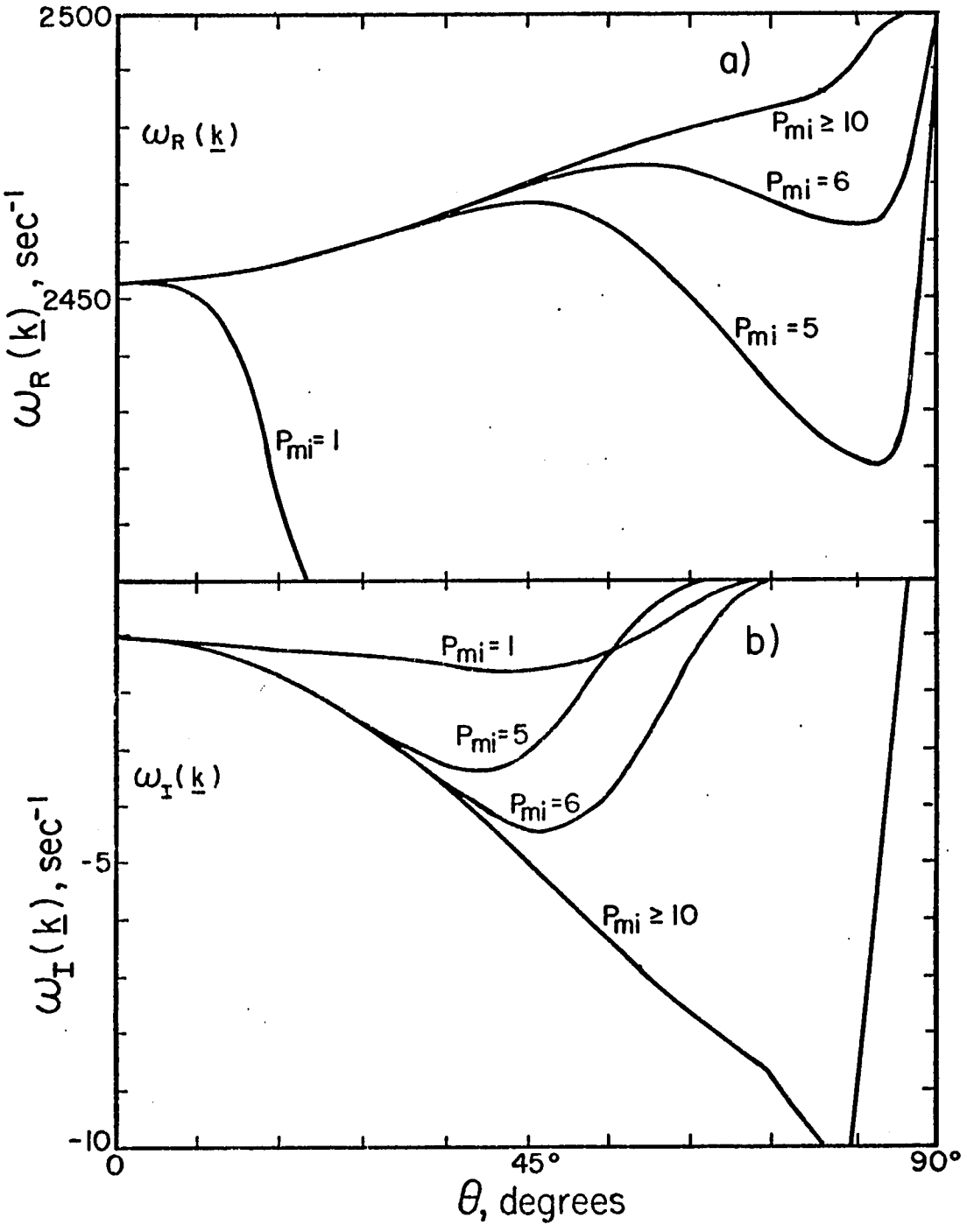
2500
2450
a)
$\omega_R(\underline{k})$
$\omega_R(\underline{k})$, sec^{-1}
$P_{mi} \geq 10$
$P_{mi} = 6$
$P_{mi} = 5$
$P_{mi} = 1$
b)
$P_{mi} = 1$
$P_{mi} = 5$
$P_{mi} = 6$
$P_{mi} \geq 10$
$\omega_I(\underline{k})$
$\omega_I(\underline{k})$, sec^{-1}
-5
-10
0
45°
90°
θ, degrees

Figure 4.12

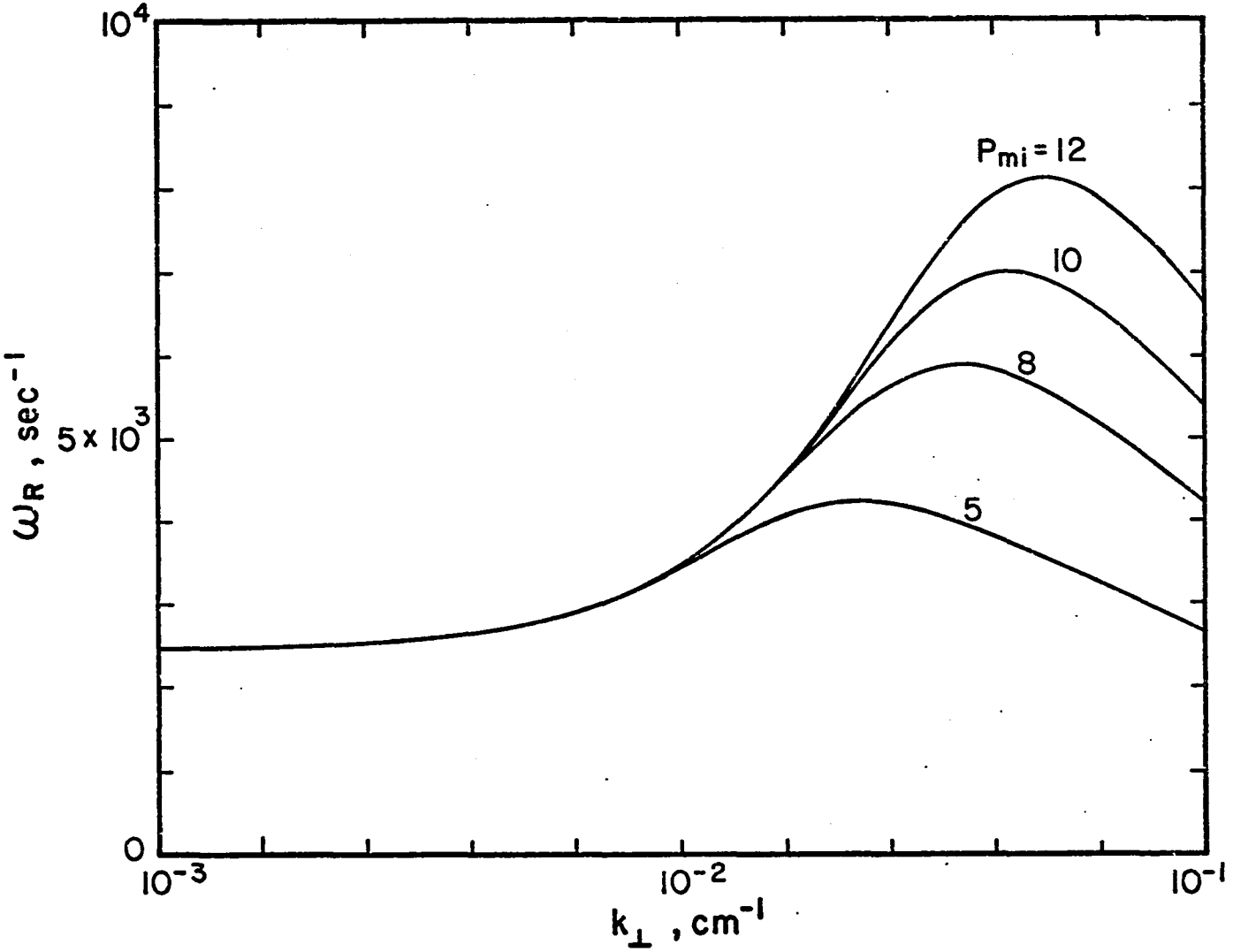

Figure 4.13

when $k_\perp = 0.1 cm^{-1}$. Such a large argument demands that we include many harmonics to represent ε_R^f and ε_I^f. We see from figure 4.13 that the harmonic series has not converged near $k_\perp = 0.1 cm^{-1}$ even when $p_{max} = 12$. From the above discussion one must choose p_{max} very carefully. There are only two remaining features which should be noted about the acoustic branch. One, only for acoustic waves propagating along the magnetic field is the damping small and two the hole at large angles in the acoustic branch is real. The physical reason for this is as follows.

In the presence of a magnetic field, the charged particles move in helical orbits along the magnetic lines of force (see figure 4.14a). Freedom of motion in the perpendicular directions is therefore suppressed substantially. If we pass to the limit of an extremely strong magnetic field then the plasma behaves as if it were a one-dimensional gas. These features must obviously be reflected in the behavior of the collective modes.

The acoustic branch is entirely new from a cold plasma point of view (look at the difference between figures 4.4 and 4.5). The electrons, being more mobile than the ions, perserve charge neutrality but because they have such small Larmor radii, they cannot do this by moving in the x direction (for large θ, this is approximately the direction of $\underline{k}$). If θ is not exactly 90° however, the electrons are still free to move along the magnetic field and carry out the important function of Debye shielding (see figure 4.14b). The hole in the acoustic branch therefore exists because the electrons can no longer provide this shielding. Let us complete this section by looking at the Whistler and upper hybrid branches for P.S. I and P.S. IV.

Figure 4.14

a) The helical orbits of charged particles in a magnetic field.

b) The geometry of an acoustic wave propagating nearly perpendicular to $\underline{B}_o$. The dashed line is the motion of the electron preserving charge neutralily. When $\underline{k}$ is perpendicular to $\underline{B}_o$ the electrons can no longer free-stream in the z direction and therefore there cannot exist an acoustic wave propagating close to 90° .

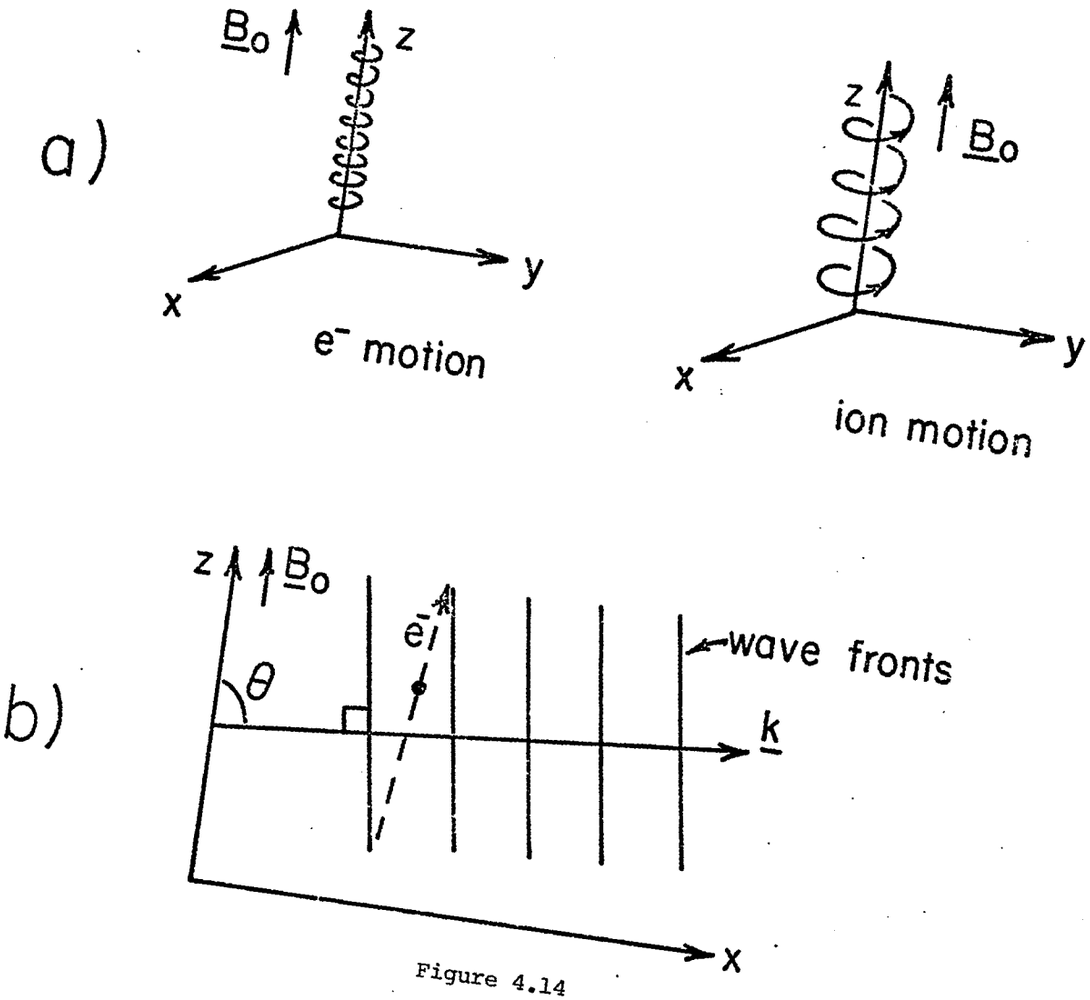

Figure 4.14

Figures 4.15, 4.16 and 4.17 summarize the important variations of these branches in k-space. In figures 4.15 and 4.16 we have mapped the corresponding branches found in P.S. I, the cold plasma. From these figures we see that only in figure 4.15b does P.S. I differ from P.S. IV. This is because the UHB in a warm plasma depends on wave number whereas in a cold plasma it does not. Except for the hole in the UHB in P.S. IV, the cold plasma map is a good approximation for the angular dispersion (see figure 4.15a). For the Whistler branch there is, in essence, no difference (see figure 4.16). In the auroral plasma the background number density may change very quickly. Figure 4.17 shows the remarkable changes which occur when the electron number density is reduced from $4.42 \times 10^5 cm^{-3}$ to $10^4 cm^{-3}$. In Chapter VI we shall refer to this new plasma as P.S. V.

In this chapter we have explored the behavior of the l.d.f. and the resulting ES branches given by those zeros which have a positive slope (see Appendix B). We looked at the ES dispersion in k-space for four different plasma states. From our analysis we concluded that in some regions of k-space we could approximate P.S. IV, which is our model of the background auroral plasma with a cold plasma. As we saw from figure 4.15b this approximation breaks down if k becomes too large. We will now turn our attention to the study of the measured distribution function, f_{eo}^{h}. As we saw in Chapter III this function may play a deciding role in the ES stability of the auroral plasma.

Figure 4.15 The angular and k dispersion of the UHB for P.S. I and P.S. IV: a) $k = 0.01 cm^{-1}$, b) $\theta = 0.1$ and 45°. From the curves in a), P.S. I is a good fit to P. S. IV however from b) we see that P.S. IV is slightly k-dependent. The bottom curves for each angle in b) are the UHB for P.S. I.

Figure 4.16 The angular and k dispersion of the WB for P.S. I and P.S. IV: a) $k = 0.01 cm^{-1}$, b) $\theta = 45^{\circ}$. From these curves we see that P.S. I is a good fit to P.S. IV for this branch. The only real difference is that the WB of P.S. IV has a hole at small angles whereas the WB of P.S. I does not.

Figure 4.17 The angular dispersion of the WB for two different values of k: 0.1 cm^{-1} and 0.01 cm^{-1}; a) P.S. IV, b) P.S. V. This shows the rather remarkable changes in a branch when just number density is changed.

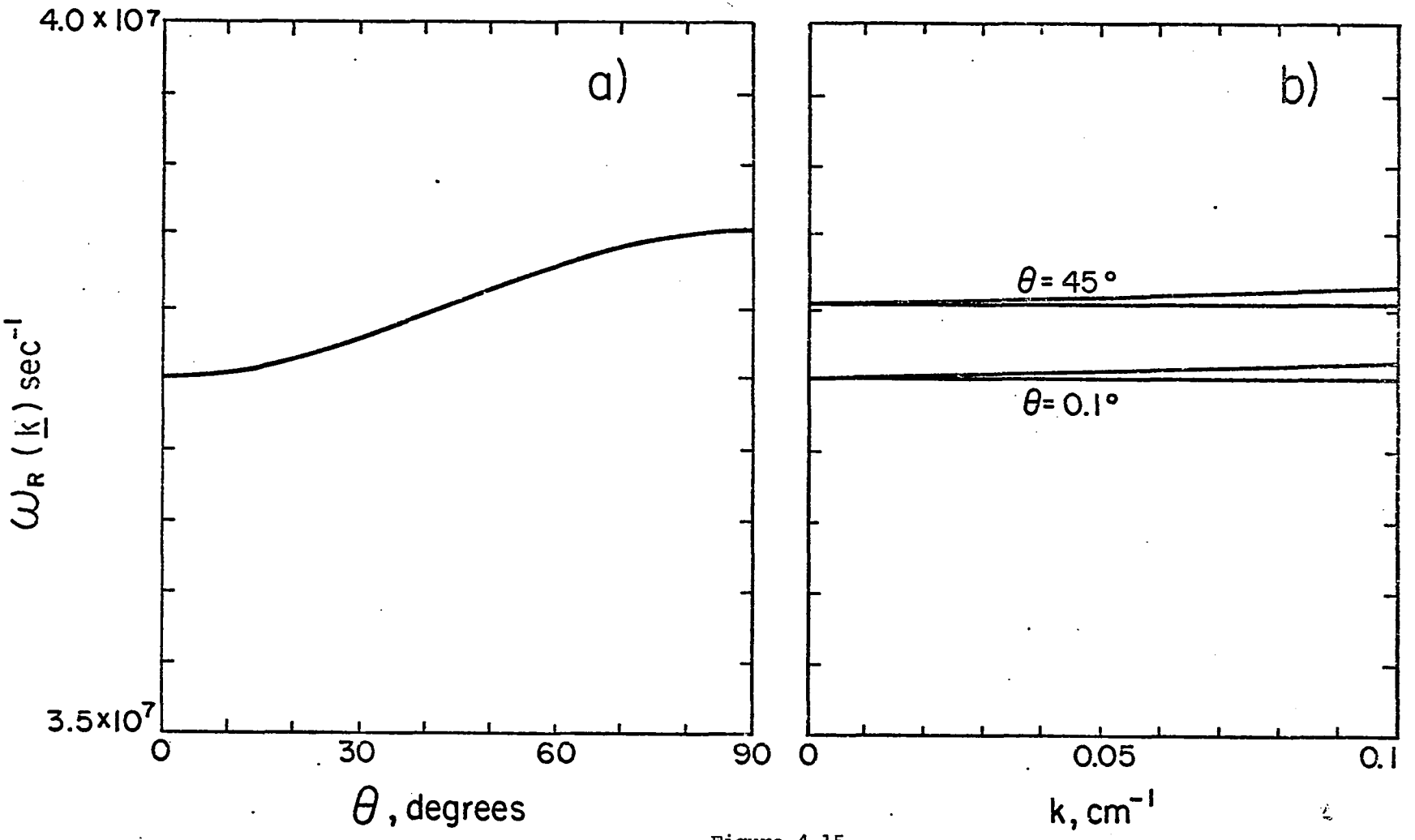
4.0 x 10⁷
3.5x10⁷
a)
b)
θ= 45°
θ= 0.1°
0
30
60
90
0
0.05
0.1
θ, degrees
k, cm⁻¹
ω_R (k) sec⁻¹

Figure 4.15

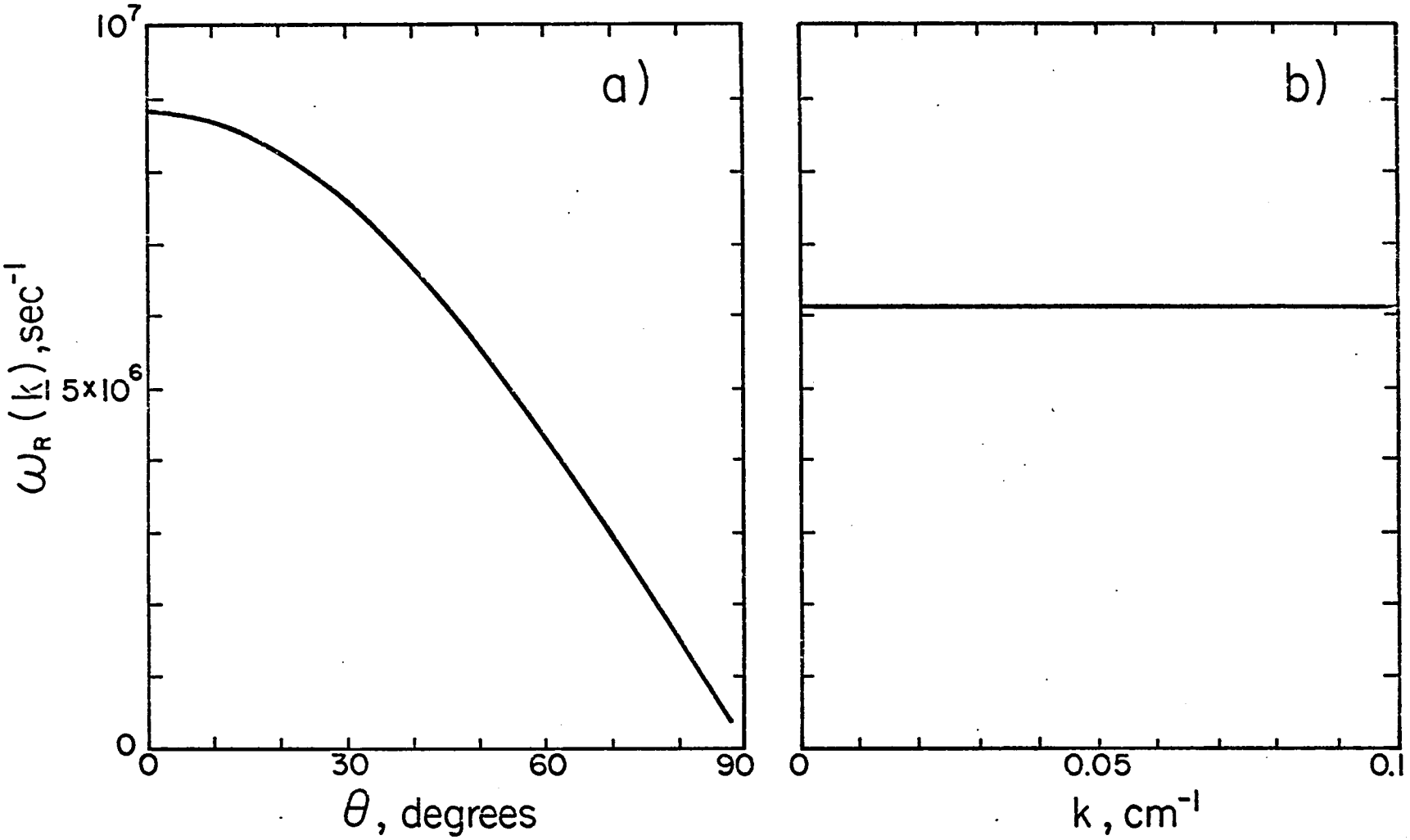
a)
b)
10^7
5×10^6
0
$\omega_R(\underline{k})$, sec^{-1}
0
30
60
90
θ, degrees
0
0.05
0.1
k, cm^{-1}

Figure 4.16

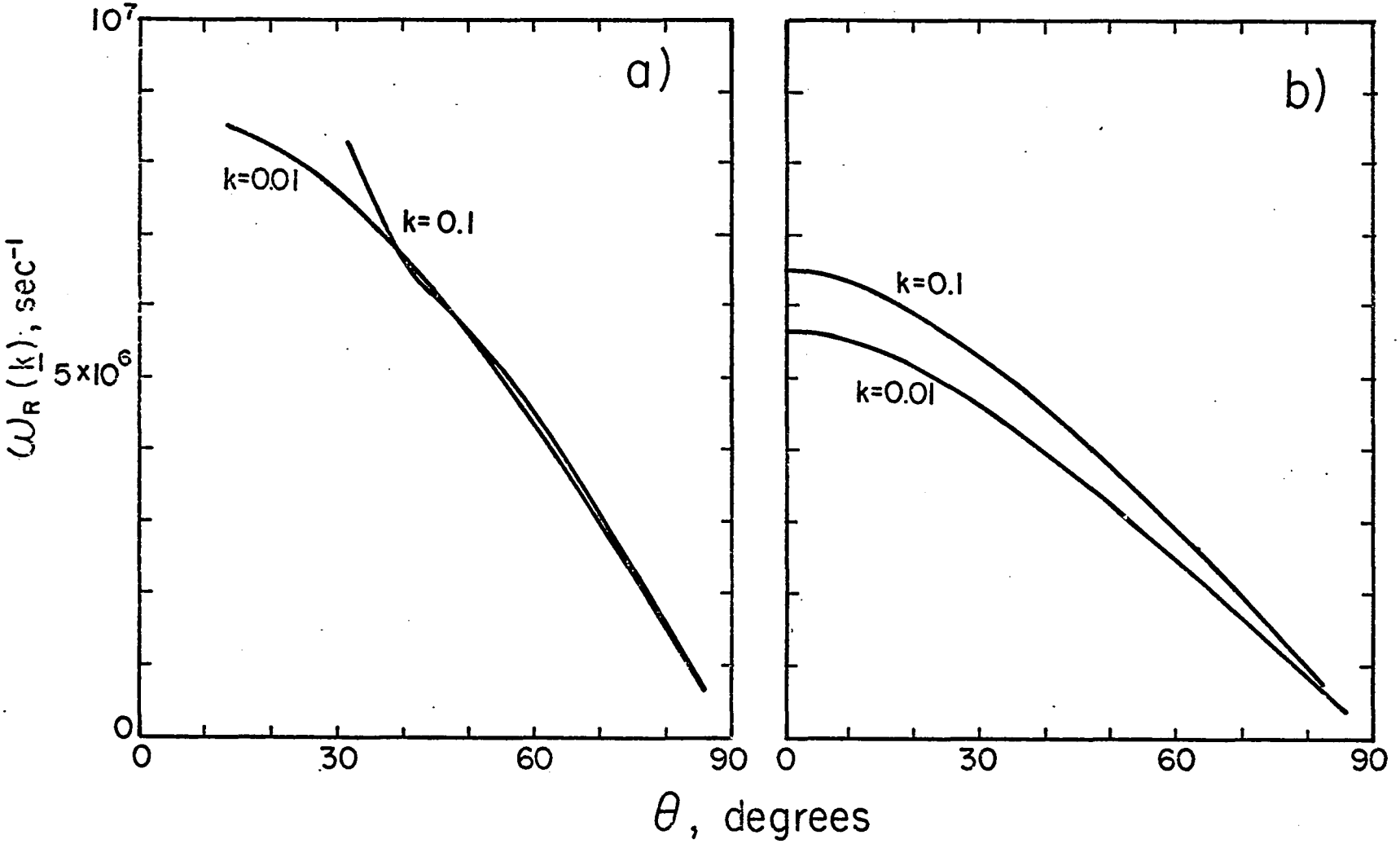
10^7
5×10^6
0
$\omega_R(\underline{k})$, sec^{-1}
a)
b)
k=0.01
k=0.1
k=0.1
k=0.01
0
30
60
90
0
30
60
90
θ, degrees

Figure 4.17

CHAPTER V

THE MEASURED DISTRIBUTION FUNCTION

5.1 Introduction

We saw at the end of Chapter III the importance the measured distribution function may have in determining the coupling between any ES waves present and the particle distributions which induce those waves. Because we have modeled the background plasma of ionospheric origin by a MB distribution for each species, the induced waves can only be damped in such a plasma (see equations 3.25 - 3.28). If amplifying waves are to exist in the auroral plasma then they can only be driven by velocity space anisotropies in the measured distribution function. The anisotropies must be large enough to overcome the damping inherent in the plasma due to either the thermal population of particles or to those particles in the measured distribution which have diffused to a quasi-equilibrium state.

In this chapter we shall examine the changes that are seen in the measured distribution function as a rocket (flight 18:152) passed over several active auroral forms. We will look at the fluid properties of f_{eo}^{h} and end the chapter by proving the necessary condition for ES stability of waves propagating exactly parallel and perpendicular to the earth's magnetic field.

5.2 Auroral Observations

In this section we will present complete plots of the measured electron distribution function in the energy interval 25eV < E < 15keV and correlate the features that can be seen in the plots with features of the optical aurora.

The differential energy flux, j(E) $(cm^{-2} \cdot sec \cdot ster \cdot keV)^{-1}$ has already been plotted for flight 18:152 at several characteristic energies by Arnoldy et al. (1974) and Kintner et al. (1974). These authors showed that the flux was always highest at energies below 100eV and that the upgoing fluxes always decreased monotonically as the energy increased. Downgoing fluxes also declined as the energy increased to several hundred electron volts but usually exhibited one or two peaks in the kilovolt energy range.

Optical auroral activity was monitored during the flight by all-sky cameras and a television camera. All-sky cameras took pictures every 30s and were located near the launch point (College), under apogee (Fort Yukon), and about 500km northeast of the impact point (Inuvik). Figure 5.1 (supplied by S. - I. Akasofu) shows a series of photographs from before launch (1040UT) to after impact (1048 UT). The dots on the Fort Yukon photographs indicate the rocket location projected down magnetic field lines to an altitude of 100km. The rocket was south of the bright auroral forms until 1043. An additional photograph taken at 1043:30 shows that the rocket entered the southernmost bright arc that appears in the 1043 Fort Yukon photograph. Auroral forms near the rocket then moved northward and faded.

It was through the aurora described above that the high energy

electron detectors of the rocket were able to measure the electrons produced in the magnetosphere. Figures 5.2 - 5.6 show contour plots of f^h_{eo} . The lower half of each plot (positive $V_{//}$) corresponds to downcoming electrons. All plots show the same contour levels, and each level is labeled by the common logarithm of f^h_{eo} . The distribution function changes by about a factor of 2 between adjacent levels. Each peak and valley is labeled by a P or V in the contour plots. Three detectors were used to make these measurements. The dashed lines with no contours between them are regions in which no data are available because the set of detectors did not scan all pitch angles (the angle α in figure 4.1a) during each sampling period. About 1000 flux measurements were needed to prepare each contour plot with the SYMAP plotting routine (Laboratory for Computer Graphics, Harvard University).

To aid in visualizing the distribution function, figure 5.7 shows three-dimensional plots of several data segments. The central peaks at $|\underline{v}| = 0$ have smooth rounded tops because only data at $E > 25$ eV were used to produce these plots. Inclusion of the background ionospheric electrons would extend the peaks to much greater heights very near $|\underline{v}| = 0$. Similarly, the flat base planes were introduced at the log $f^h_{eo} = -1.0$ level to aid in visualization. Actual fluxes continue to drop off at higher velocities. Because the morphology of the measured distribution function is of such importance to our study of weak ES turbulence let us analyze figures 5.2 - 5.6 in greater detail.

The upper three plots in figures 5.2 and 5.7a show distributions seen when the rocket was well south of the bright arcs. The rocket altitude was between about 190 and 200 kilometers during the interval shown here. An apogee of 246 kilometers was reached at T=244s. The

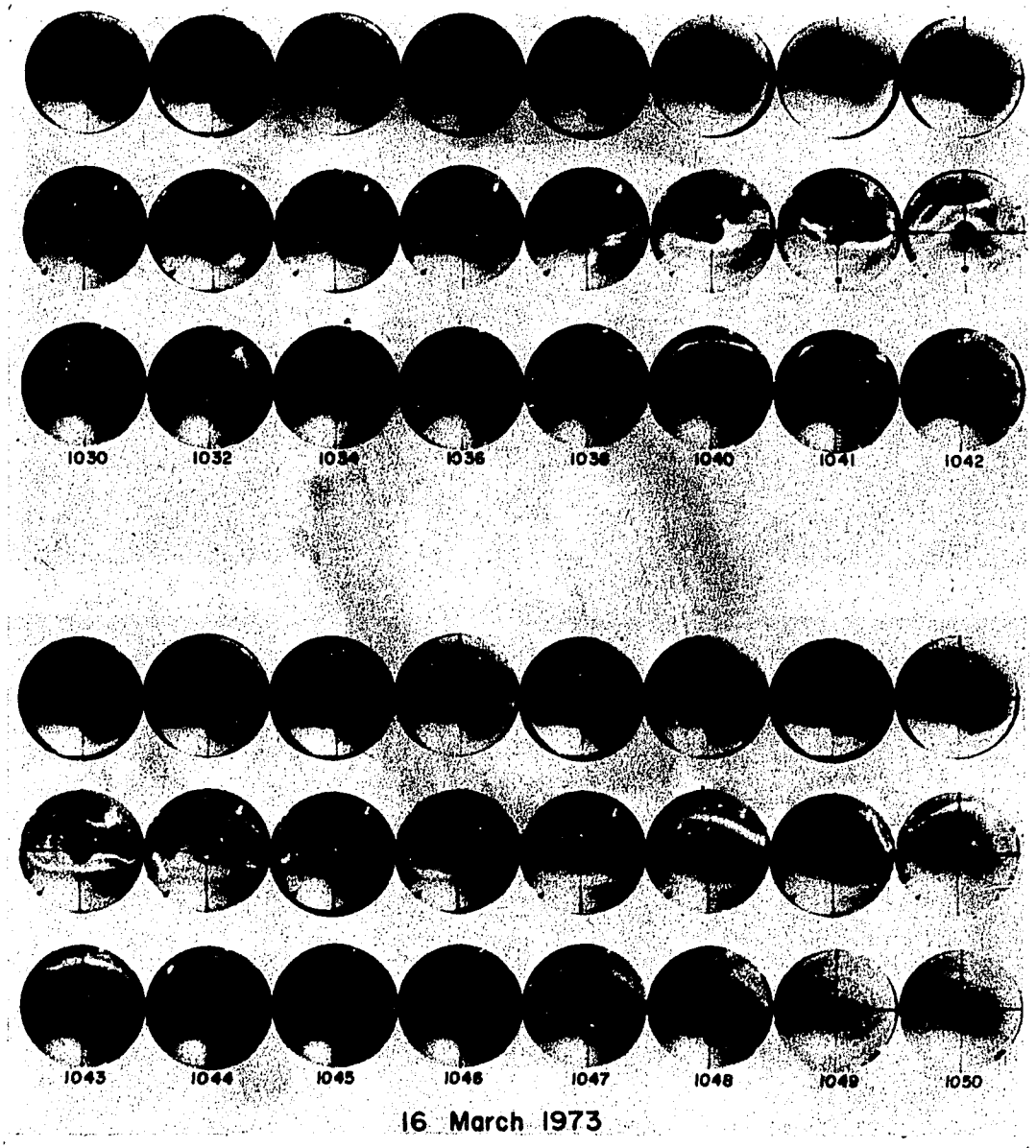

Figure 5.1. All-sky camera photographs. Geomagnetic north is to the top, west to the left. Launch time (T = 0 s) was 1040 UT. Moonlight appears in the lower left of each frame. For a given time the top panel was taken at Inuvik, the middle panel at Fort Yukon and the bottom panel at college. The black or white dots on the Fort Yukon photographs show the rocket position projected down to 100-km altitude.

Figure 5.2 Contour plots of the measured electron distribution function of magnetospheric origin. Downcoming electrons have positive $V_{//}$. Contour levels are labeled by the common logarithm of $f_{eo}(\underline{v})$ in units of sec^3/km^{-6}. Secondary peaks and valleys in the distribution function are marked by the letters P and V. Times shown (T=130 - 144 and 179 - 193) refer to seconds after launch.

Figure 5.3 Similar to figure 5.2 but for T=193 - 220s.

Figure 5.4 Similar to figure 5.2 but for T=220 - 247s.

Figure 5.5 Similar to figure 5.2 but for T=277 - 304s.

Figure 5.6 Similar to figure 5.2 but for T=304 - 331s.

Figure 5.7 Three dimensional plots of several representative electron distribution functions. Each plot is shown as if it were viewed from a position 75° from the positive $V_{//}$ axis and 15° above the flat background plane. Downcoming electrons have positive $V_{//}$, so they produce fluxes on the left half of each figure. The edges of the base planes are at $V_{//} = 60 \times 10^8$ and -60×10^8cm/s and $V_\perp = 0$ and 60×10^8cm/s. The vertical axis is the common logarithm of $f_{eo}(\underline{v})$ and the base plane was introduced at log $f_{eo} = -1.0$ to aid in visualization.

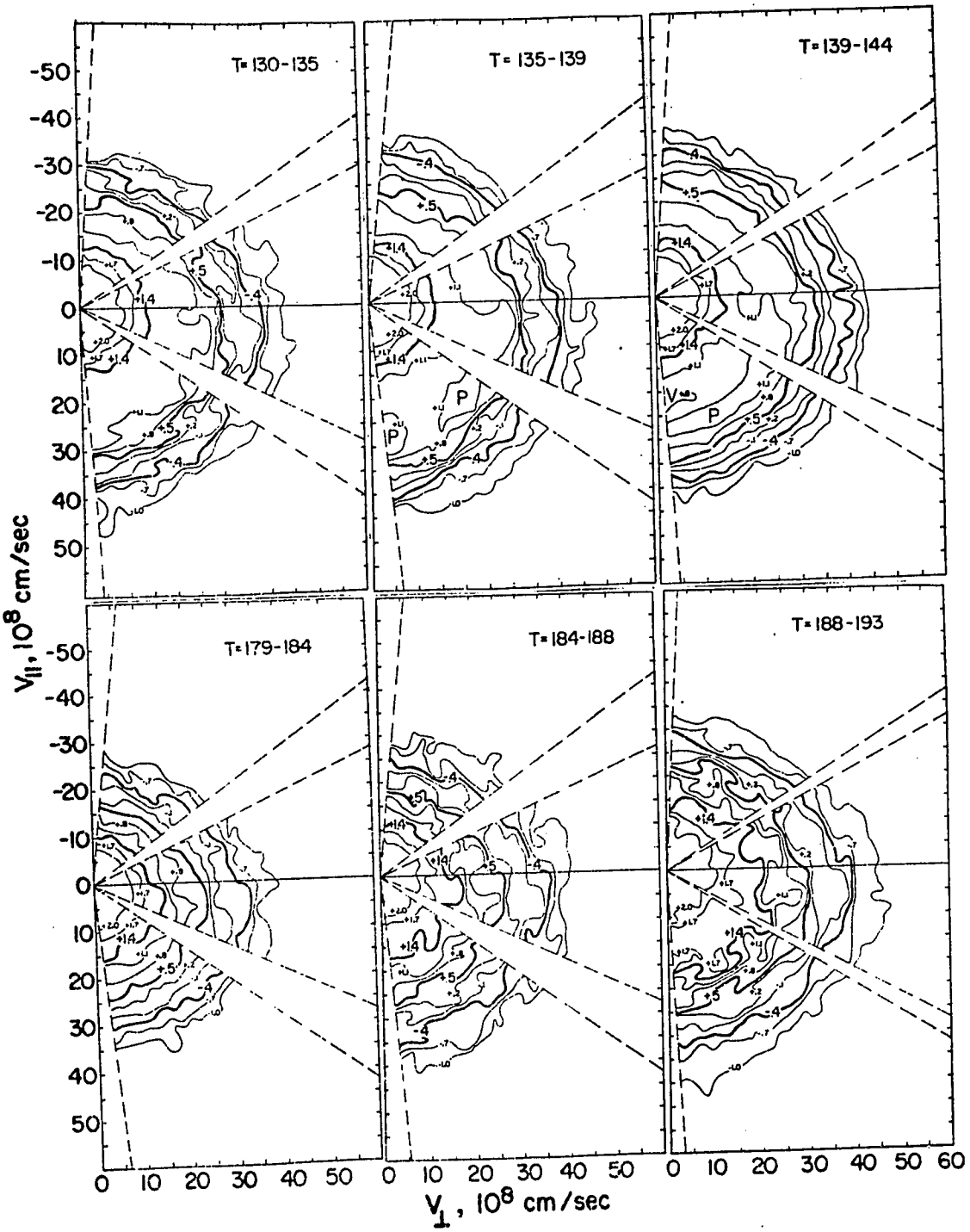
T= 130-135
T= 135-139
T= 139-144
T= 179-184
T= 184-188
T= 188-193
P
$V_{||}$, 10^8 cm/sec
$V_\perp$, 10^8 cm/sec

Figure 5.2

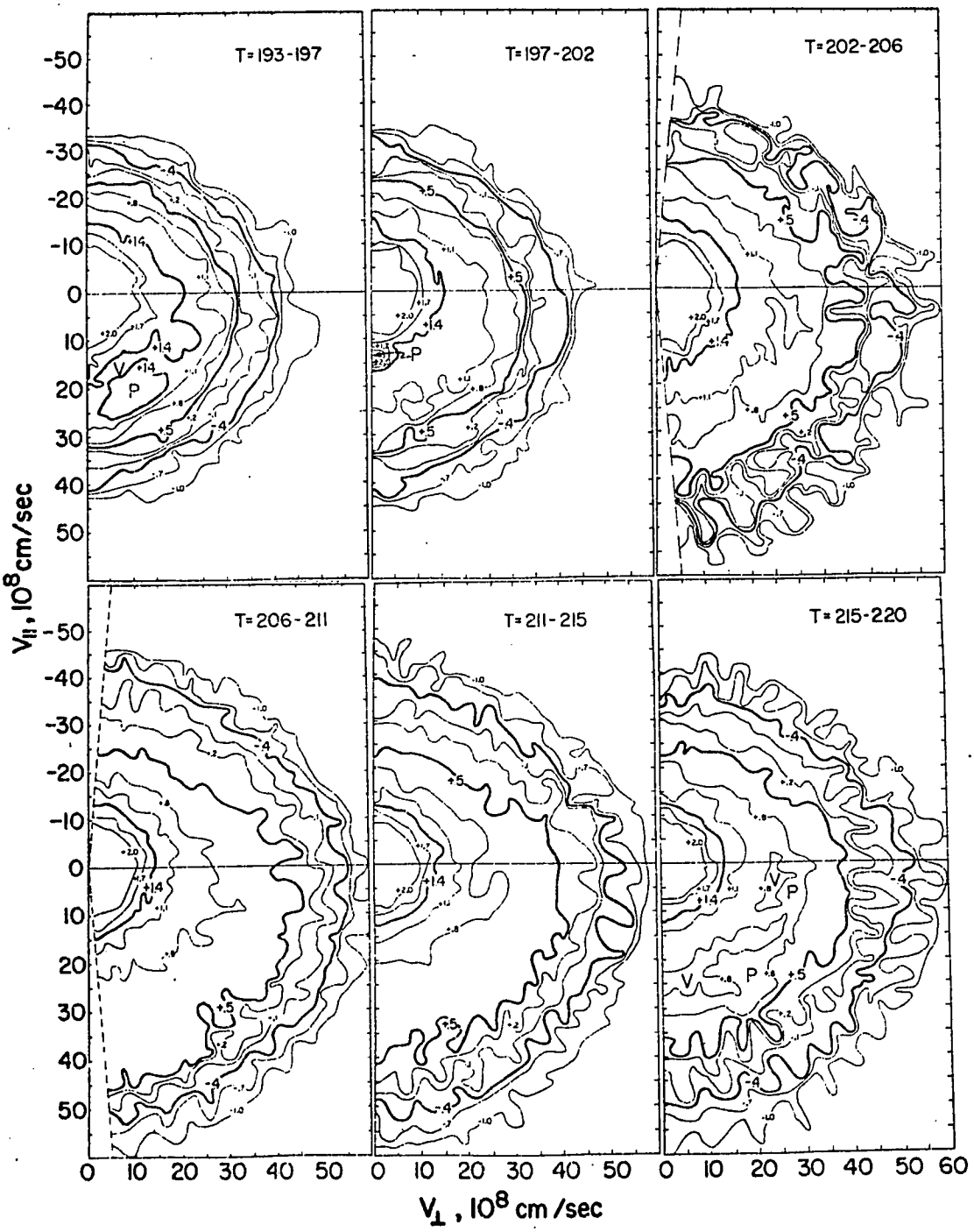
T=193-197
T=197-202
T=202-206
T=206-211
T=211-215
T=215-220
V
P
$V_{||}$, 10^8cm/sec
$V_\perp$, 10^8 cm/sec

Figure 5.3

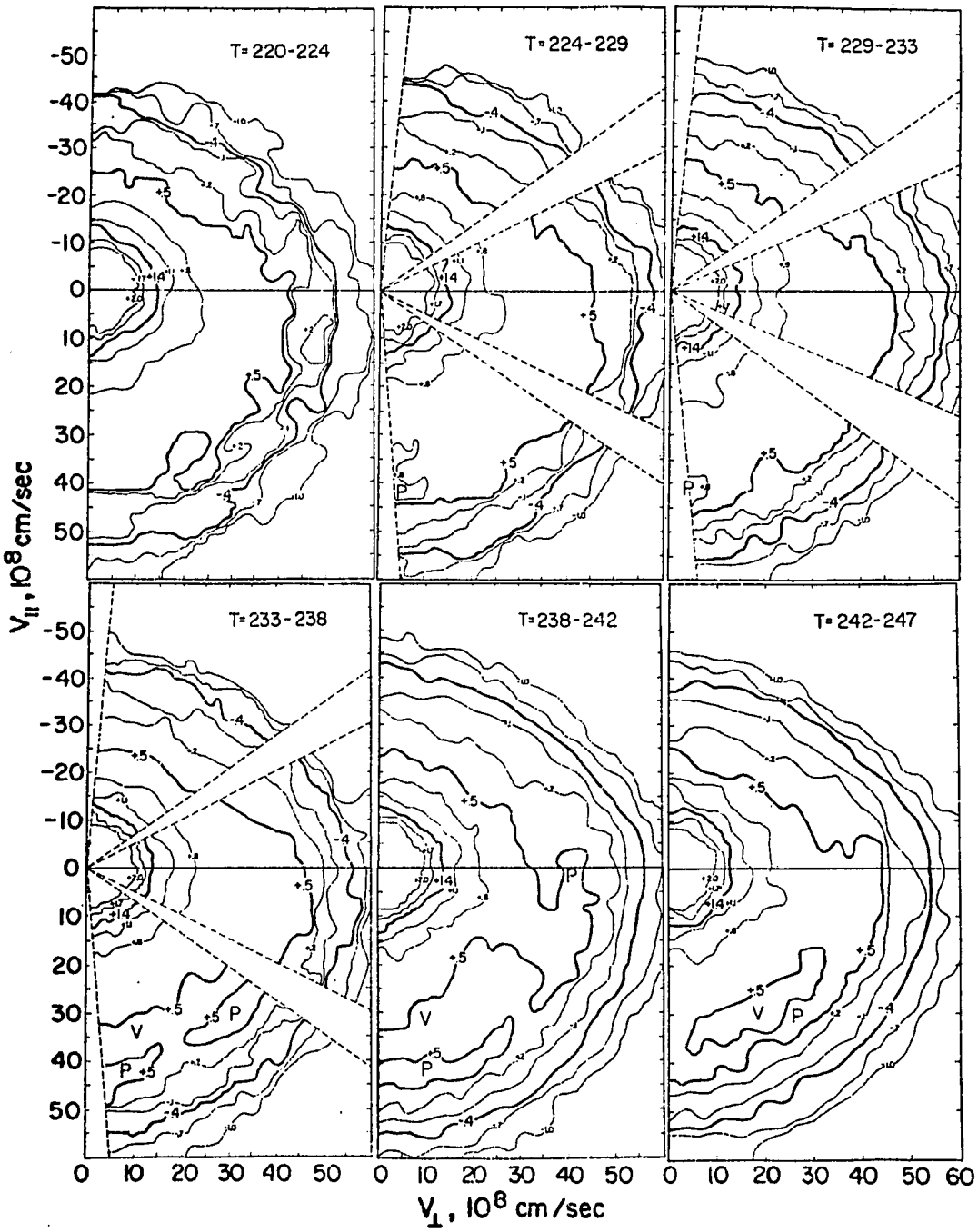
T= 220-224
T= 224-229
T= 229-233
T= 233-238
T= 238-242
T= 242-247
V
P
$V_{\parallel}$, 10^8 cm/sec
$V_{\perp}$, 10^8 cm/sec

Figure 5.4

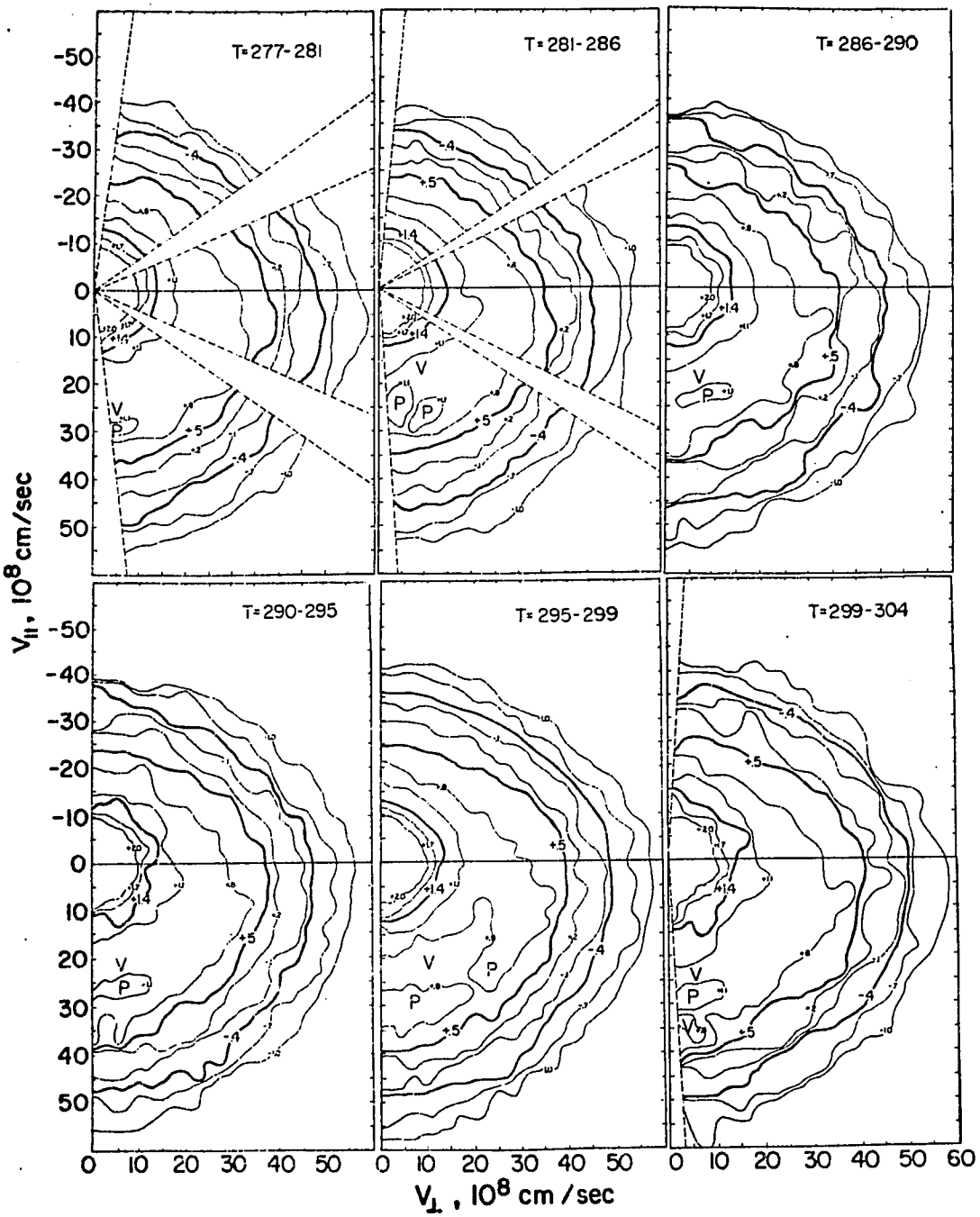
T=277-281
T=281-286
T=286-290
T=290-295
T=295-299
T=299-304
V
P
$V_{\parallel}$, 10^8 cm/sec
$V_{\perp}$, 10^8 cm/sec

Figure 5.5

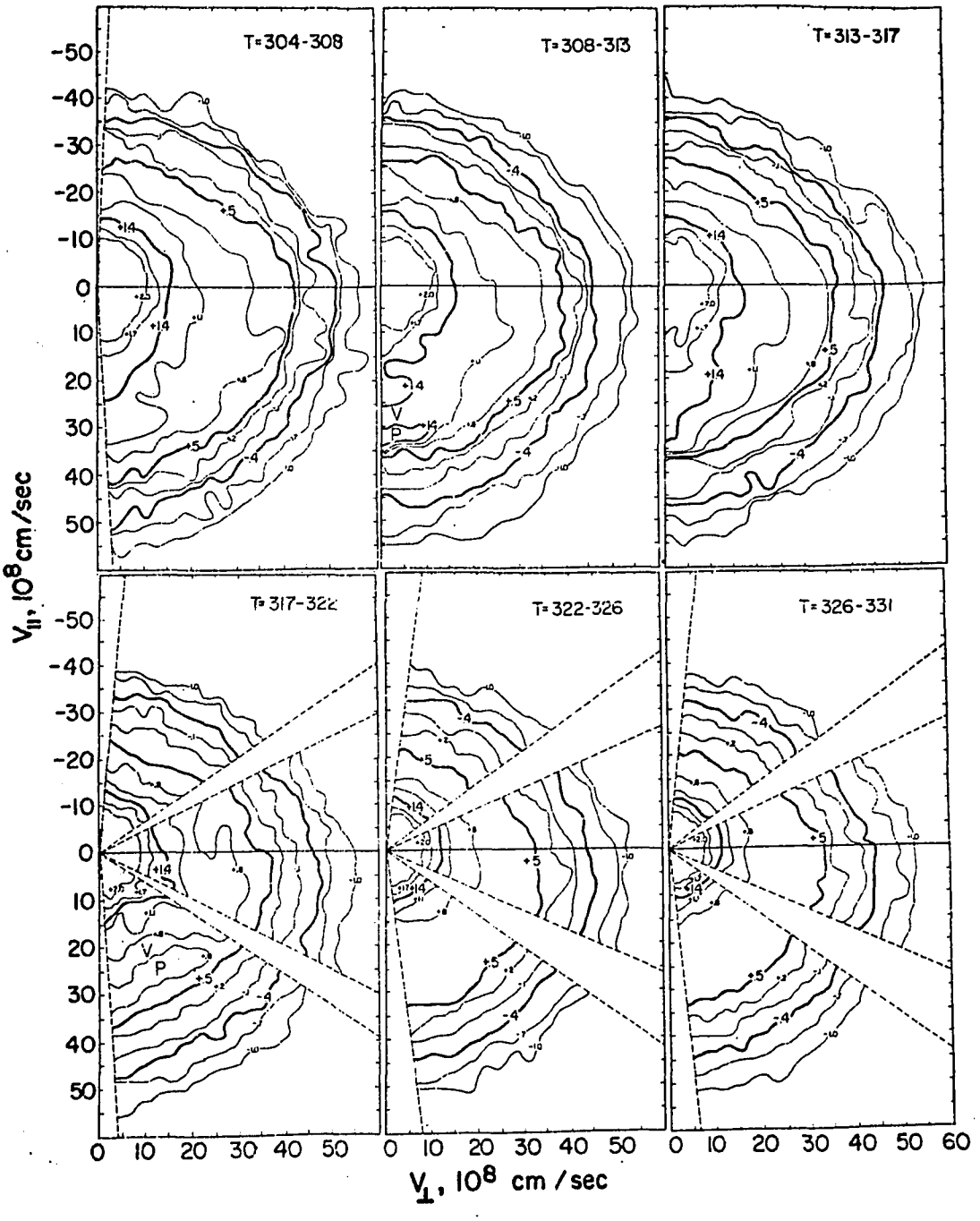
T=304-308
T=308-313
T=313-317
T=317-322
T=322-326
T=326-331
V
P
$V_{||}$, 10^8 cm/sec
$V_\perp$, 10^8 cm/sec

Figure 5.6

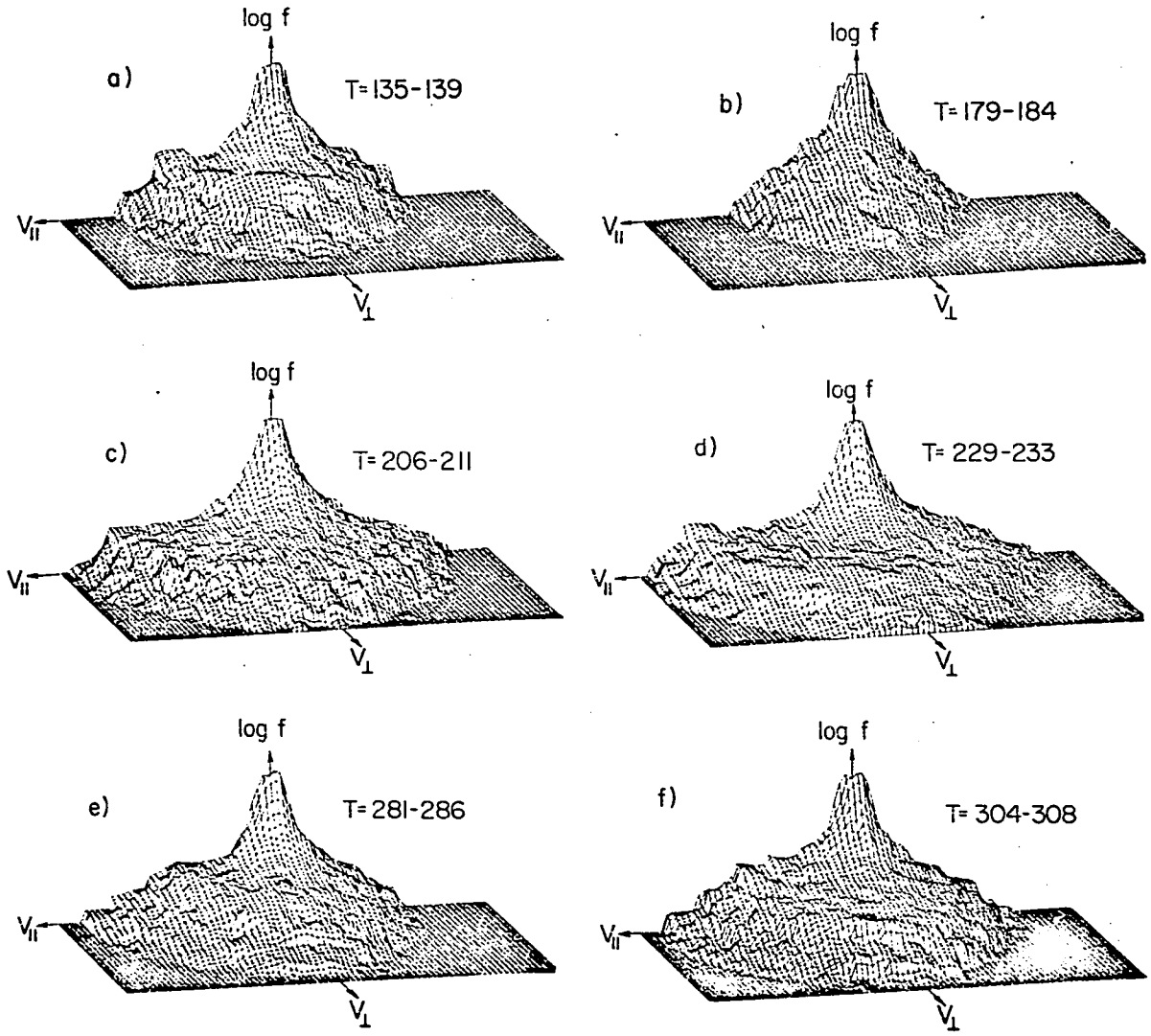
log f
a)
T=135-139
V_{II}
$V_{\perp}$
log f
b)
T=179-184
V_{II}
$V_{\perp}$
log f
c)
T=206-211
V_{II}
$V_{\perp}$
log f
d)
T=229-233
V_{II}
$V_{\perp}$
log f
e)
T=281-286
V_{II}
$V_{\perp}$
log f
f)
T=304-308
V_{II}
$V_{\perp}$

Figure 5.7

most striking feature of these contours is the plateau or very weak peak in the downcoming electron distribution between $v = 15 \times 10^8$ and 30×10^8 cm/s. In contrast, the upgoing part of the electron distribution decreases smoothly throughout this velocity interval. The plateau structure is clearly present at 90° pitch angle and is not present beyond 120°. Particles with pitch angles greater than 105° at the rocket location must all have been produced or backscattered below the rocket, and the sharp decrease in f^h_{eo} with increasing velocity results from the decreasing backscatter ratio. The period from T=150 to about 184s was the only interval during the flight when no plateau was present in the distribution function.

The bottom half of figure 5.2 and all of figures 5.3 and 5.4 show observations made as the rocket entered the southernmost bright arc that appears in the 1043 UT (T=180s) Fort Yukon all-sky camera photograph (figure 5.1). As can be clearly seen a plateau formed between T=188 and T=206s (see figure 5.7c). Fluxes of electrons with energies between 300 and 2000 eV reached some of the highest levels seen during the entire flight. Between T=202 and 220s the contours at $v = 35 \times 10^8$ cm/s are quite variable. The wavy appearance of these contours is produced by time changes which occurred during individual 4.5s sampling intervals. Each of the three detectors sweeps through a complete 50-point energy scan twice per second, but nine energy scans are required for all pitch angles to be observed at each energy. Rapid time variations in the electron flux produce quite different values of $f^h_{eo}(\underline{v})$ at any given energy and pitch angle during these nine energy sweeps. The wavy contours which characterize temporal changes are quite evident during these periods. The fact that smooth contours are produced during all other intervals shows

that $f^{h}_{ao}(\underline{v})$ was steady during the corresponding 4.5s sampling periods. Variations are present even in upgoing fluxes, as is expected if these upgoing electrons are backscattered primaries.

We believe that the rocket passed near or through a series of bright auroral rays. If so, these observations suggest that electron fluxes in the bright rays are not basically much different from fluxes between the rays. The low-energy flux and plateau appear to be the same throughout. The only difference between the two spectra is that the plateau apparently extends to higher energies when the rocket is in a ray than when it is between rays or in regions of less structured bright aurora.

Visual auroral activity became less intense near the rocket at 1044 UT (T = 244s). The rocket did not pass through any other unusually bright discrete arcs during the remainder of the flight.

A new distribution began to develop at T = 299s and is pronounced during the period T = 304 - 317s (figures 5.6 and 5.7f). Notice that the electron fluxes are field aligned throughout this period but that field alignment extends over a broad range of energies. We know of no other observation of field-aligned electrons extending over such a broad energy range. After T = 322 no significant changes were detected during the remainder of the flight.

Hall and Bryant (1974) and Bryant et al. (1977) analyzed very similar data from another rocket flight. They concluded that the observed electrons could have been accelerated in a parallel electric field but that either the field fluctuated or the electrons were unstable and diffused in velocity space above the rocket. Whalen and McDiarmid (1972) also detected similar field-aligned electrons which were discussed in

terms of a parallel electric field acceleration. Arnoldy (1974) has reviewed a number of other experiments that detected field-aligned electrons near auroras.

Reasoner and Chappell (1973) found electron distributions at altitudes of up to 800 kilometers that are similar to those we observed below 250 kilometers. They also noted that fluxes are nearly isotropic over 180° in pitch angle at energies of about 1 keV ($v = 20 \times 10^{8}$ cm/s) and less. Matthews et al. (1976) measured upgoing and downcoming electrons below 250 kilometers and reported that electrons are not quite isotropic at the lowest energy measured (500eV). Let us turn now to a study of the fluid properties of the measured distribution function.

5.3 The Fluid Properties of the Hot Electrons

Since complete measurements of $f_{eo}^{h}(\underline{v})$ are available in the energy range 25 eV < E < 15 keV, it is possible to evaluate the contribution of these electrons to the bulk properties of the auroral plasma. A knowledge of these bulk properties is needed if we are to determine the role that the observed electrons play in the coupling between the magnetosphere and ionosphere.

The functions which describe the bulk properties of any plasma are in general functions of space and time. However, in a spatially homogeneous plasma they are functions only of time. We saw in Chapter II that

$$\bar{N}_{\gamma} = \int \mathcal{N}_{\gamma}(\underline{X}, t)\, d\underline{X} \quad .$$

Because $\mathcal{N}_{\gamma}$ is a phase-space function we may average it over the $6\bar{N}$-dimensional probability density, $F_{\bar{N}}$ in Γ -space (Chapter II). The result, for the one-particle distribution, is

$$V = \int f_\gamma^{(1)} \, d\underline{x} \, d\underline{v} \quad .$$

We could just as easily have normalized our one-particle distribution to the total number of particles of type γ instead of the total volumn, V. That is,

$$\bar{N}_\gamma = \int f_\gamma^{(2)} \, d\underline{x} \, d\underline{v} \quad .$$

If our system is spatially homogeneous then from our study of the quasi-linear theory (see section 3.3), the average distribution function, $f_{\gamma o}$ is given as the spatial average of f_γ . Therefore,

5.1) $$\int f_{\gamma o}^{(1)} \, d\underline{v} = 1 \quad ,$$

5.2) $$\int f_{\gamma o}^{(2)} \, d\underline{v} = \bar{n}_\gamma \quad .$$

In Chapter III equation 3.18 was normalized according to equation 5.1. The measured distribution function however is normalized according to equation 5.2. This is the reason why we had to divide by n_e in equation 3.28 because the stability equations demanded the first normalization. We may now define a general fluid function, A(x,t) as follows:

$$A_i(\underline{x}, t) = \frac{\int \phi_i(\underline{v}) \, f_\gamma^{(2)}(\underline{x}, \underline{v}, t) \, d\underline{v}}{\int f_\gamma^{(2)}(\underline{x}, \underline{v}, t) \, d\underline{v}}$$

i.e.

$$A_i(\underline{x}, t) = \frac{1}{n_\gamma(\underline{x}, t)} \int \phi_i(\underline{v}) \, f_\gamma^{(2)}(\underline{x}, \underline{v}, t) \, d\underline{v}$$

where $\phi_i(\underline{v})$ is an arbitrary function of velocity. For a spatially homogeneous, slowly varying plasma $n_r(\underline{x},t) = \bar{n}_r$. Therefore the spatial average of A_i is

$$\bar{n}_r \langle A_i(\underline{x},t)\rangle = \frac{1}{V}\int \phi_i(\underline{v})\, f_r^{(2)}(\underline{x},\underline{v},t)\, d\underline{x}\, d\underline{v}$$

$$= \int \phi_i(\underline{v})\, f_{r0}^{(2)}(\underline{v},t)\, d\underline{v}\,.$$

We saw that in the linear theory (section 3.2) f_{r0} is independent of time and in the quasi-linear theory f_{r0} is only weakly dependent on time. Thus

$$\bar{n}_r \langle A_i(\underline{x})\rangle = \int \phi_i(\underline{v})\, f_{r0}^{(2)}(\underline{v})\, d\underline{v}\,. \tag{5.3}$$

The fluid functions defined by equation 5.3 carry no information about the interactions between the individual particles and between the particles and the waves present. We may therefore treat each species as a fluid. The modus operandi of fluid theory is a study of how these fluids interact. With this in mind, let us evaluate the following integrals.

Number density (el. cm^{-3})

$$\bar{n}_e^h = \int f_{e0}^h\, d\underline{v}$$

Drift velocity ($cm.\ s^{-1}$)

$$u_{\parallel} = \frac{1}{\bar{n}_e^h}\int v_{\parallel}\, f_{e0}^h\, dv_{\parallel}$$

Momentum flux (g cm^{-1} s^{-2})

$$\lambda_{\parallel} = \int | m_e v_{\parallel} | v_{\parallel} \, f_{eo}^{h} \, d\underline{v}$$

Energy flux (erg cm^{-2} s^{-1})

$$\Phi = \int | \tfrac{1}{2} m_e v^2 | v_{\parallel} \, f_{eo}^{h} \, d\underline{v}$$

Heat flux (erg cm^{-2} s^{-1})

$$q = \int \tfrac{1}{2} m_e | \underline{v} - \underline{u} |^2 (v_{\parallel} - u_{\parallel}) * \\ * f_{eo}^{h} \, d\underline{v}$$

Parallel temperture (eV)

$$K T_{\parallel} = \frac{1}{n_e^{h}} \int m_e | v_{\parallel} - u_{\parallel} |^2 f_{eo}^{h} \, d\underline{v}$$

Perpendicular temperature (eV)

$$K T_{\perp} = \frac{1}{n_e^{h}} \int m_e | v_{\perp} |^2 f_{eo}^{h} \, d\underline{v}$$

The results are listed for one typical data segment (T=277 - 281s) in Table 5.1. This analysis assumes that f_{eo}^{h} is azimuthally symmetric about the $v_{\parallel}$ axis. As a result, there are no net fluxes or net drifts across field lines, and all vector quantities evaluated above refer to components parallel to the magnetic field.

In interpreting the resulting bulk parameters in terms of magnetosphere-ionosphere coupling, it is important to keep in mind that the velocity integrals were only evaluated above a lower limit of 25eV. For example, the total number density of E > 25eV electrons listed in Table 5.1 is 11 el./cm^3. There are, of course, of the order of 10^5 el./cm^3 present in the background ionospheric plasma at rocket altitude (P.S. IV). Similarly, the average temperature of all electrons.

Number Density, Parallel Drift Velocity, Parallel Momentum Flux, Energy Flux, Current Density, Temperature[1], and Heat Flux[1].

Parameter	Upgoing	Downcoming	Net	Plateau[2]
$\frac{h}{n_e}$	4.8	6.6	11	2.2
$u_{\shortparallel}$	5.1×10^{8}	8.1×10^{8}	2.5×10^{8}	13×10^{8}
$\lambda_{\shortparallel}$	2.3×10^{-9}	8.7×10^{-9}	6.4×10^{-9}	6.5×10^{-9}
Θ	5.5	22	17	17
j	3.9	8.5	4.6	4.4

1. Here $KT_{\shortparallel} = 570$ eV, $KT_{\perp} = 680$ eV, $KT = 640$ eV, and $q = 9.9$ erg $\cdot$ cm^{-2} $\cdot$ S^{-1}.

2. The last column was obtained by fitting the measurements to the function $f_o(\underline{v}) = f_1 + f_2$ where $f_1 = 36.7\ E^{-1.45}\ e^{-E/1.94}$ models the low energy downcoming and all upgoing electrons at pitch angles 133° and $f_2 = (29.1 - 5.36\ \alpha^2)\ e^{(-|E-2.06|/E_o)}$ models the plateau. Here E is the electron energy in keV, α is the pitch angle in radians, $E_o = 0.695$ for $E < E_{peak} = 2.06$ keV, $E_o = 1.51$ keV for $E > E_{peak}$ and $f_2 = 0$ for $\alpha > 133°$.

TABLE 5.1

including this dense background plasma, is of the order of 0.1eV. The drift velocity and heat flux also depend sensitively upon the lowest velocity used in the integrals. All other parameters in Table 5.1 are almost independent of this lower velocity limit because kilovolt electrons are carrying most of the electric current, momentum and energy between the magnetosphere and the ionosphere.

Table 5.1 not only lists the total net fluxes carried by the electrons that we measure but also separates out the fluxes carried by upgoing and downcoming electrons. This separation is useful in placing requirements on the electron source region, since the energetic electron source must be able to supply or accelerate the full downward fluxes of energetic electrons rather than just the net (down minus up) fluxes.

Two techniques have been used to evaluate the integrals listed above. The contour diagrams in figures 5.2 - 5.7 were prepared by first using a weighted interpolation scheme to produce a matrix of values for f^{h}_{eo} that is uniformly spaced in $V_{\parallel}$, $V_{\perp}$ coordinates. The locations of the contour lines are then determined by a simple linear interpolation between points in this uniformly spaced matrix. The "up", "down" and "net" bulk parameters listed in Table 5.1 were obtained by numerical integration between points in this uniformly spaced matrix.

The second technique used was to perform a least squares fit to an analytical function using the roughly 1000 data points available each 4.5s. These analytical functions could then also be integrated to get estimates of the various fluxes. This second technique is not used much because measurements are available at nearly all pitch angles during flight 18:152. Unfortunately no other rocket flight had such complete pitch angle coverage, and we must use a fitting routine rather than

interpolation at some pitch angles for other flights. Both methods were used during flight 18:152 to check them for consistency. The two techniques generally agreed to within 5% on this flight. In addition, the fitting technique uses separate functions to fit the plateau electrons and the isotropic lower-energy electrons. The last column in Table 5.1 lists the contributions of just those electrons in the plateau.

The presence of plateaus in the downward hemisphere of so many of the electron distribution functions suggests that the electrons were accelerated and became unstable somewhere above the rocket. In the following section we will show that the measured distribution function is stable to ES waves propagating parallel and perpendicular to the earth's magnetic field.

5.4 Parallel and Perpendicular Stability

The stability of parallel-propagating waves is most easily studied by evaluating the following integral:

$$F_{\parallel}(v_{\parallel}) = 2\pi \int_0^{\infty} f_{eo}^{h}(v)\, v_{\perp}\, dv_{\perp} \qquad 5.4)$$

where we have assumed that f_{eo}^{h} is azimuthally symmetric in velocity-space. A plasma is stable to parallel-propagating waves if $F_{\parallel}$ has only a single peak (Krall and Trivelpiece, 1973). Figure 5.8 shows plots of $F_{\parallel}$ covering the entire time period discussed in the previous section (Kaufmann et al., 1977). Each curve corresponds to one of the 4.5s data sampling periods shown in figures 5.2 - 5.6. The integrations were performed in exactly the same manner as was done for the bulk parameters listed in Table 5.1.

At the beginning of the period studied (curves a to e in figure

Figure 5.8 The reduced distribution functions ($F_{\parallel}$, $F_{\perp}$) defined in equations 5.4 and 5.5 are plotted throughout flight 18:152. Each set of curves on a given panel, labeled by one lower-case letter, corresponds to data from one 4.5 second sampling period. For example, curves a in figure 5.8 correspond to T=125 - 130s. The absolute values of $F_{\parallel}$ and $F_{\perp}$ on the ordinate of each panel refer to the curves labeled by the letter a. Each succeeding curve has been moved down one order of magnitude. The tic marks on each $F_{\parallel}$ curve are at 10^{-10}sec/cm^4 and the tic marks on each $F_{\perp}$ curve are at 10^{-19}sec^2/cm^5; A) T=125 - 179s B) T= 179 - 229s C) T=229 - 281s D) T=281 - 326s.

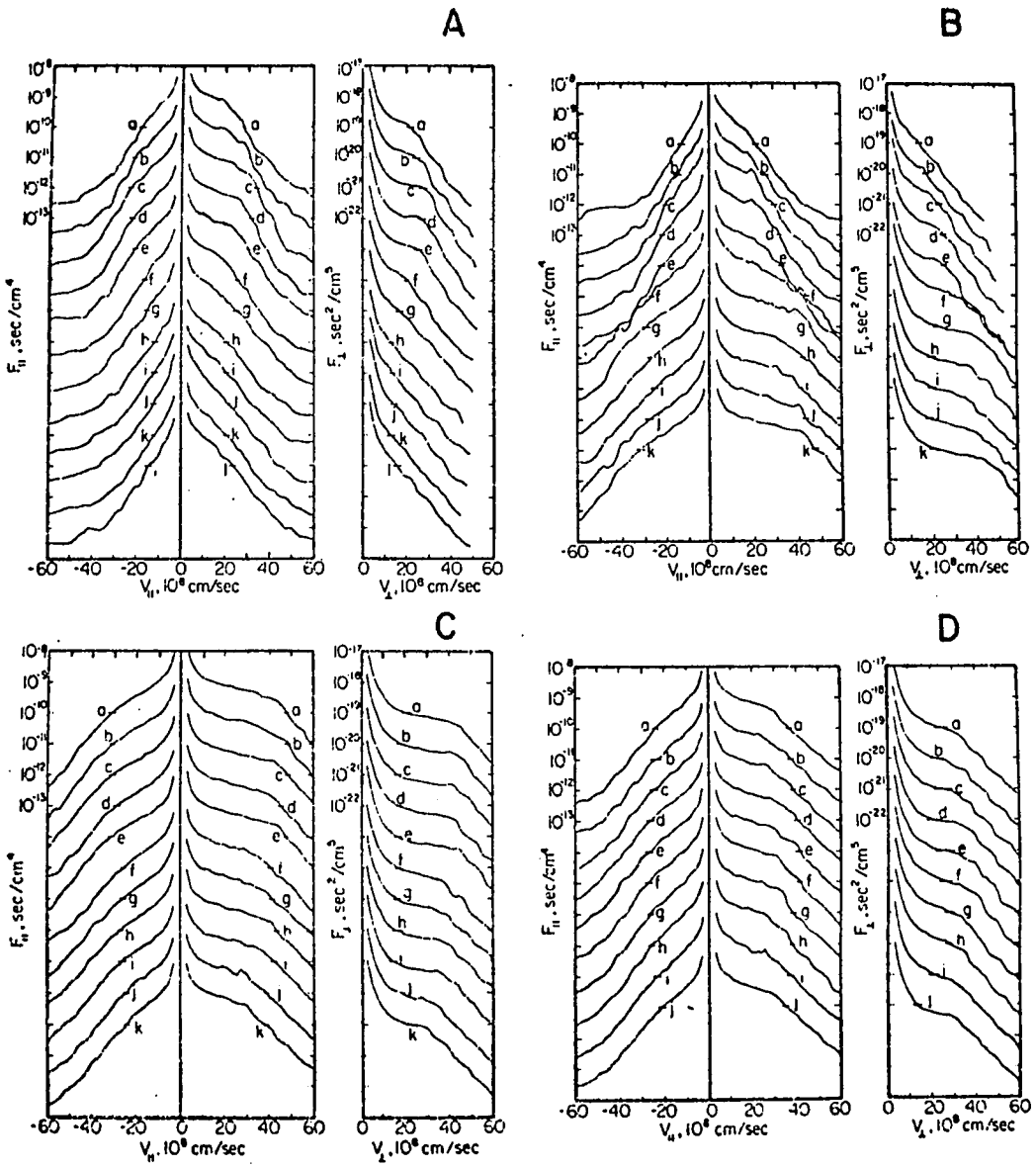
A
B
C
D
$F_{\parallel}$, sec/cm^4
$F_{\perp}$, sec^2/cm^5
$V_{\parallel}$, 10^8 cm/sec
$V_{\perp}$, 10^8 cm/sec

Figure 5.8

5.8A) the plateau and peak structure in the contour and three-dimensional plots fails to produce even a truly flat plateau in the one-dimensional distribution function, $F_{\parallel}$. The rocket encountered a high flux of low energy electrons at T=184-202 (curves b to e in figure 5.8B) just before entering a bright auroral arc. The very small bumps at $V_{\parallel} = 20 \times 10^{8}$ cm/s that appear in curves b, c and d of figure 5.8B are associated with these low energy electrons. This is the only time inteval during either flight 18:152 or flight 18:109 (Kaufmann et al., 1976) when we have found any possibility that parallel-propagating waves might be unstable. When the rocket entered the bright arc at T=202s even though f^{h}_{eo} contained a small peak in the very broad plateau, $F_{\parallel}$ once again declines monotonically from a single large peak at $V_{\parallel} = 0$ indicating parallel stability.

We conclude that the auroral plasma is stable to parallel-propagating ES waves, with the possible exception of a small region containing high fluxes of low energy electrons at the edge of a bright arc. The observation that plasma within the bright aurora is not even marginally unstable to parallel-propagating waves (flat plateaus in are not present) suggests that these waves were not the last ones to be unstable at higher altitudes.

A necessary condition for an ES flute instability ($k_{\parallel} = 0$) to exist is that the function

$$F_{\perp}(V_{\perp}) = \int_{-\infty}^{+\infty} f^{h}_{eo}(\underline{V})\, dV_{\parallel} \qquad 5.5)$$

be doubly peaked. Integrals for $F_\perp$ have been performed numerically and are presented in figure 5.8. No secondary peaks were seen, indicating that the auroral plasma at 200 - 250 kilometer altitude is stable to ES waves propagating exactly perpendicular to $\underline{B}_o$. The $F_\perp$ function did, however, exhibit nearly flat plateaus both within the weak aurora-like spectrum seen at the beginning of the flight (figure 5.8A curves b to e) and within much of the bright arc (most of figure 5.8C). The observation that $F_\perp$ tended to more nearly approximate a flat plateau than did $F_{||}$ suggests that the last waves to be unstable above the rocket may have been propagating at a large angle to $\underline{B}_o$. It is this possibility which we will explore in the following chapter, namely the possibility of exciting oblique ES instabilities in the auroral plasma.

5.5 Conclusion

We have been led in our kinetic theory to consider the importance of the measured distribution function, $f^h_{ao}(\underline{v})$, in exciting ES waves. The present chapter has been devoted to an understanding of the changes in this function as flight 18:152 passed through several active auroral forms. We then considered how these hot electrons couple the magnetosphere and ionosphere by looking at their fluid properties. We ended this chapter by considering the necessary conditions for parallel and perpendicular stability of ES waves. We found that indeed the measured distribution of electrons was ES stable for waves propagating in these two directions. The stage is now set for us to turn our attention to a study of oblique instabilities. Our model of the auroral plasma is now completely understood. The waves which must be excited at some arbitrary angle to $\underline{B}_o$ are known at every point in k-space (Chapter IV).

Therefore the two ingredients for a wave-particle interaction are known. In Chapter VI we shall put these two ingredients together to make an instability.

CHAPTER VI

WEAK WAVE-PARTICLE INTERACTIONS IN THE AURORA

6.1 An Introduction

In the previous chapters of this work, we have developed the requisite theory to understand weak ES turbulence in an auroral plasma. This theory requires accurate knowledge not only of the one-particle distributions making up the auroral plasma but also of the possible ES waves present that can resonantly interact with these distributions. We have studied both of the above criteria extensively. In this chapter we shall detail the exact steps one must follow in order to make an instability.

A complete study of this problem would have to specify every wave resonating at every harmonic. Each wave in such a study is treated independently as if it alone was the only one to be excited. This independence is a consequency of the weak turbulence approximation. In principle, the growth or damping rate ($\frac{I}{\omega_r}$) for every member of the excited wave spectrum may be computed. Such a spectrum would exist for every branch. Instead of looking at every frequency let us consider those frequencies in k-space which are in resonance with a particular feature in the particle distributions at a fixed harmonic. For instance, we may fix the perpendicular wave length of the wave, $k_\perp$ and demand that the wave be in resonance with all the particles with a parallel velocity of 20×10^8 cm/sec at the $n=-1$ harmonic. We will call such waves "principal harmonic waves". We are presently developing a program to calculate the dissipation of any normal oscillation that can occur in the

auroral plasma. To understand this interaction better, let us consider in more detail what we mean by a wave-particle resonance.

We shall refer to

$$6.1) \qquad v_{\parallel}^{r} = \frac{\omega_R + n|\omega_{ce}|}{k_{\parallel}}$$

as the resonance condition. For a given wave in k-space, equation 6.1 specifies which particles with a parallel velocity, $v_{\parallel}^{r}$ resonate with that wave. The reason for this is as follows. An observer in the rest frame of the plasma would measure the frequency of the excited wave to be ω_R. We see from figure 4.2 that the natural motion for a charged particle in a magnetic field is helical motion. The charged particles spiral about the magnetic field ($\underline{B}_o$) with a frequency we call the cyclotron frequency (ω_{cr}). Motion along the field is essentially free whereas motion perpendicular to the field is hindered greatly by the helical constraint put on the orbit of the charged particle. This freedom in the parallel direction allows the particles to resonantly interact with waves which either propagate along the field ($k_\perp = 0$) or which propagate obliquely to the field ($k_\perp \neq 0$).

In the former case the particles act as if there were no magnetic field present. Therefore, there can be no cyclotron resonance (i.e. $n=0$). Such waves were shown to be stable in the auroral plasma (see Chapter V). In the latter case, however, the wave sees particles executing a spiral motion. For a group of particles to resonate with an oblique wave those particles must see the wave at their cyclotron frequency or a harmonic thereof because this is the natural frequency of the particles. What we have therefore is a classical Doppler shift in the real frequency as seen

by particles with a parallel velocity, $V_{\parallel}^{r}$, given by equation 6.1. Because the electric field of the wave is in phase with the cyclotron motion of the resonant particles, a resonant transfer of energy between the particles and the wave becomes possible.

In this chapter we shall be concerned with developing a concise methodology for handling all linear ES wave-particle interactions in the auroral plasma. The particular plasma we shall choose as an example of this methodology will be a modified version of P.S. IV (see Chapter IV). Because there does not exist any low frequency ion waves except for the IC(n) waves we shall study the upper hybrid and Whistler branches only. Even if there did exist a low frequency branch as in P.S. II it is generally easier for the hot electrons to couple to the higher frequency waves. With this in mind, let us now develop a prescription to find ES instabilities.

6.2 The Method

In Chapter III we developed the requisite equations to calculate the linear dissipation of ES waves in the weak turbulent regime. For convenience we will list below our results from that chapter. The normal oscillations occur in the cool, Maxwellian background plasma of ionospheric origin. These oscillations must be in the kernel of ε_R^c where

$$6.2) \qquad \varepsilon_R^c = 1 + \sum_r \frac{1}{k^2 \lambda_{Dr}^2} \left\{ 1 + \sum_n \frac{\omega_R}{\omega_R - n\omega_{cr}} \left[W_R(x_r^n) - 1 \right] \Lambda_n(\lambda_r) \right\} .$$

From Appendix B we found that the slope of equation 6.2 must be positive

at a normal oscillation. Because we are interested in the high frequency branches of the ES mode we may use P.S. I(the cold plasma) to approximate P.S. IV (the auroral plasma at rocket altitude). Solving equation 6.2 for a cold plasma we find that

$$6.3) \quad \omega_R^2 = \frac{\omega_{uH}^2}{2} \pm \frac{1}{2}\sqrt{\omega_{uH}^4 - 4\omega_{pe}^2\omega_{ce}^2\cos^2\theta}\,.$$

The upper sign in equation 6.3 yields the upper hybrid branch while the lower sign yields the Whistler branch (note that the ions have been neglected in the calculation of equation 6.3).

We will find that we can simplify our analysis by reducing the number density in P.S. IV to $\bar{n}_e = 10^4$ cm^{-3}. We will refer to this modified model of the auroral plasma at rocket altitude ($\sim$ 250km) as P.S. V. The approximation of the dispersion of the upper hybrid and Whistler branches of either P.S. IV or P.S. V by the P.S. I dispersion relation embodied in equation 6.3 breaks down over some regions in k-space (see Section 4.5). In figure 6.1 we plot ω_R vs $k_{\parallel}$ for three different values of $k_\perp$ (.008, .01, .012 cm^{-1}) for P.S. IV and P.S. V. This figure shows not only the dramatic changes in the wave dispersion curves when only number density is changed, but also the fact that the continuous dispersion curves for a cold plasma may become discontinuous when temperature is added. We shall use equation 6.3 in our stability analysis for the auroral plasma but we must use it with caution.

The linear dissipation in the auroral plasma was given in Chapter III as

$$6.4) \quad \omega_I = -\beta_R(\varepsilon_I^c + \varepsilon_I^h) = \omega_I^c + \omega_I^h$$

Figure 6.1 ω_R vs $k_{//}$ for a) the WB of P.S. V, b) the WB of P.S. IV, c) the UHB of P.S. V and d) the UHB of P.S. IV.

α : $k_\perp = 0.008\text{cm}^{-1}$
β : $k_\perp = 0.01\text{cm}^{-1}$
γ : $k_\perp = 0.012\text{cm}^{-1}$

These curves again show the remarkable changes in the wave dispersion when only number density is changed.

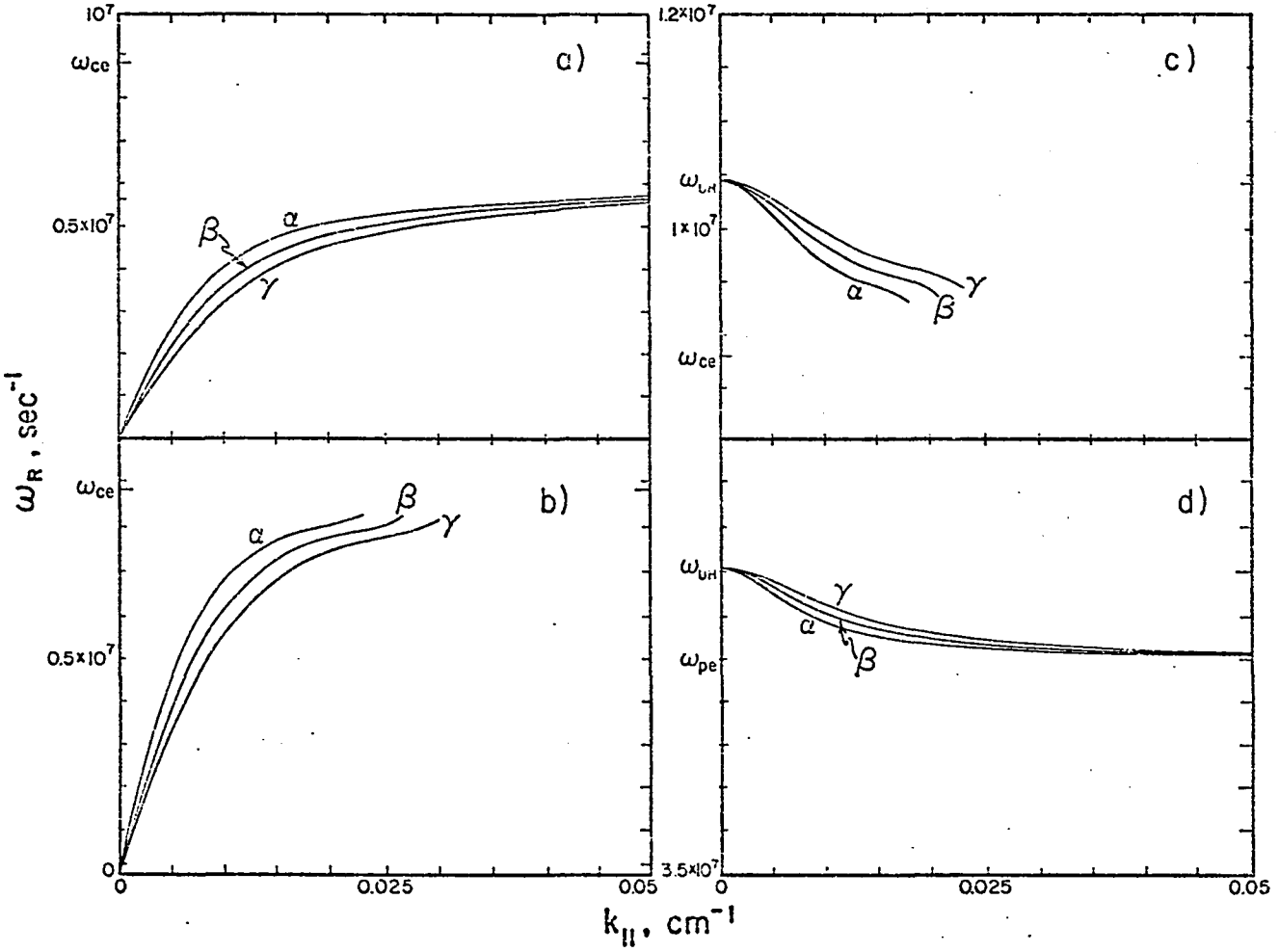
10^7
ω_{ce}
a)
0.5×10^7
β
α
γ
ω_R, sec^{-1}
ω_{ce}
b)
α
β
γ
0.5×10^7
0
0
0.025
0.05
1.2×10^7
c)
ω_{uH}
1×10^7
α
γ
β
ω_{ce}
d)
ω_{uH}
γ
α
β
ω_{pe}
3.5×10^7
0
0.025
0.05
$k_{\parallel}$, cm^{-1}

Figure 6.1

where $$\beta_R = \left(\frac{\partial \varepsilon_R^c}{\partial \omega_R}\right)^{-1} > 0 \quad ,$$

6.5) $$\varepsilon_I^c = \frac{1}{k^2 |k_{\parallel}|} \sum_{\gamma,n} \sqrt{\frac{\pi \alpha_\gamma}{2}} \frac{\omega_R}{\lambda_{D\gamma}^2} e^{-\frac{\alpha_\gamma}{2}\left(\frac{\omega_R - n\omega_{c\gamma}}{k_{\parallel}}\right)^2} \quad ,$$

6.6) $$\varepsilon_I^h = -\frac{\pi}{k^2 |k_{\parallel}|} \sum_n \frac{\omega_{pe}^2}{\bar{n}_e} \left(\mathcal{H}_{\perp e}^n + \mathcal{H}_{\parallel e}^n \right) \quad ,$$

6.7) $$\mathcal{H}_{\perp e}^n = -2\pi n |\omega_{ce}| \int_0^\infty dv_\perp \, J_n^2(a_e) \left.\frac{\partial f_{eo}^h}{\partial v_\perp}\right|_{v_\parallel^r} \quad ,$$

6.8) $$\mathcal{H}_{\parallel e}^n = k_\parallel \left.\frac{d G_\parallel^n}{d v_\parallel}\right|_{v_\parallel^r} \quad ,$$

6.9) $$G_\parallel^n = 2\pi \int_0^\infty dv_\perp \, v_\perp \, J_n^2(a_e) f_{eo}^h \quad .$$

The reaonant velocity, $v_\parallel^r$, is given by equation 6.1 For the upper hybrid and Whistler waves in the auroral plasma, equation 6.5 is found to be very nearly zero. We must therefore look at the measured electrons to find a source of free energy which can drive an ES instability ($\omega_I > 0$). This implies that

6.10) $$\sum_n \mathcal{H}_e^n > 0$$

where $$\mathcal{H}_e^n = \mathcal{H}_{\perp e}^n + \mathcal{H}_{\parallel e}^n$$

for an amplifying wave to exist in our plasma (see equation 6.4).

In Chapter V we noticed that during a few time intervals on flight 18:152 perpendicular peaking of f^h_{eo} was seen within the plateau region. The feature we wish to examine as a possible free energy source for our normal oscillations is this secondary bump in f^h_{eo}. We shall look at the hot electrons measured during T= 295 - 299 seconds of the rocket flight. In figure 6.2, for example, let us fix $v_{\parallel}$ at 20 x 10^8 cm/sec and plot $f^h_{eo}(v_{\parallel} = 20 \times 10^8, v_\perp)$ as a function of $v_\perp$. The resulting graph is shown in figure 6.3a and exhibits a clear peak at $v_\perp = 25 \times 10^8$ cm/sec. The bump produces a positive value of $\partial f^h_{eo} / \partial v_\perp$ near $v_\perp = 18 \times 10^8$ cm/sec. We wish to investigate whether this positive velocity gradient is large enough to make positive.

The positive slope in figure 6.3a makes $\mathcal{H}^n_{\perp e}$ positive over a range of perpendicular wave numbers for all negative harmonics. For example in figure 6.3c the $\mathcal{H}^{-1}_{\perp e}$ term is positive for $.008 < k_\perp < .0125$ cm^{-1}. The major problem we are faced with is in choosing the harmonic, n_o and the perpendicular wave number, $k_{\perp o}$ to make $\mathcal{H}^{n_o}_{\perp e}(k_{\perp o})$ a positive maximum. Once n_o and $k_{\perp o}$ have been chosen only one frequency is found from solving equations 6.1 and 6.3 simultaneously for the specific $v^b_{\parallel}$, n_o and $k_{\perp o}$. These oscillations are the principal harmonic waves we mentioned previously. Once such a wave is found for a particular branch it's resonant velocity with other groups of particles at all the other harmonics may be calculated from equation 6.1. Generally these other groups of particles will damp the wave. It is only by summing $\mathcal{H}^n_e$ for all harmonics that one is able to calculate whether a specific principal harmonic wave will be evanescent or amplifying. An

Figure 6.2 Contour and three dimensional plot of one representative measured electron distribution function (T = 295 - 299s). Similar to figures 5.2 and 5.7.

Figure 6.3

A. f^h_{eo} ($v_{\parallel} = 20 \times 10^8$ cm/sec, $v_\perp$) is plotted as a function of $v_\perp$.

B. The square of the n -1 Bessel function of the first kind, $J_n (k_\perp v_\perp / |\omega_{ce}|)$ is plotted as a function of $v_\perp$ for fixed values of $k_\perp = 0.01$ cm^{-1} and $|\omega_{ce}| = 8.8 \times 10^6$ sec^{-1}.

C. $\mathcal{H}^n_{\perp e}$ is plotted as a function of $k_\perp$. The $n = -1$ curve is evaluated at $v_{\parallel} = 20 \times 10^8$ cm/sec, and refers to both the principal harmonic waves on the UHB and WB. The $n = 2$, $n = 1$ and $n = -2$ curves are evaluated at $v_{\parallel} = -65 \times 10^8$ cm/sec, -40×10^8 cm/sec and 45×10^8 cm/sec respectively. These three curves refer to the principal harmonic wave on the WB only. The corresponding curves for the UH wave must be evaluated at much larger values of $v_{\parallel}$ (see Table 6.2) and are too close to zero to be shown on the scale used here.

D. $G^n_{\parallel}$ is plotted as a function of $v_{\parallel}$. The The ordinate scale refers to the $n = 0$ curve. The $n = \pm 1$ curve has been divided by 10 and the $n = \pm 2$ curve has been divided by 100 to make the figure readable. The tic marks on each curve are at 10^{-11} sec/cm^4.

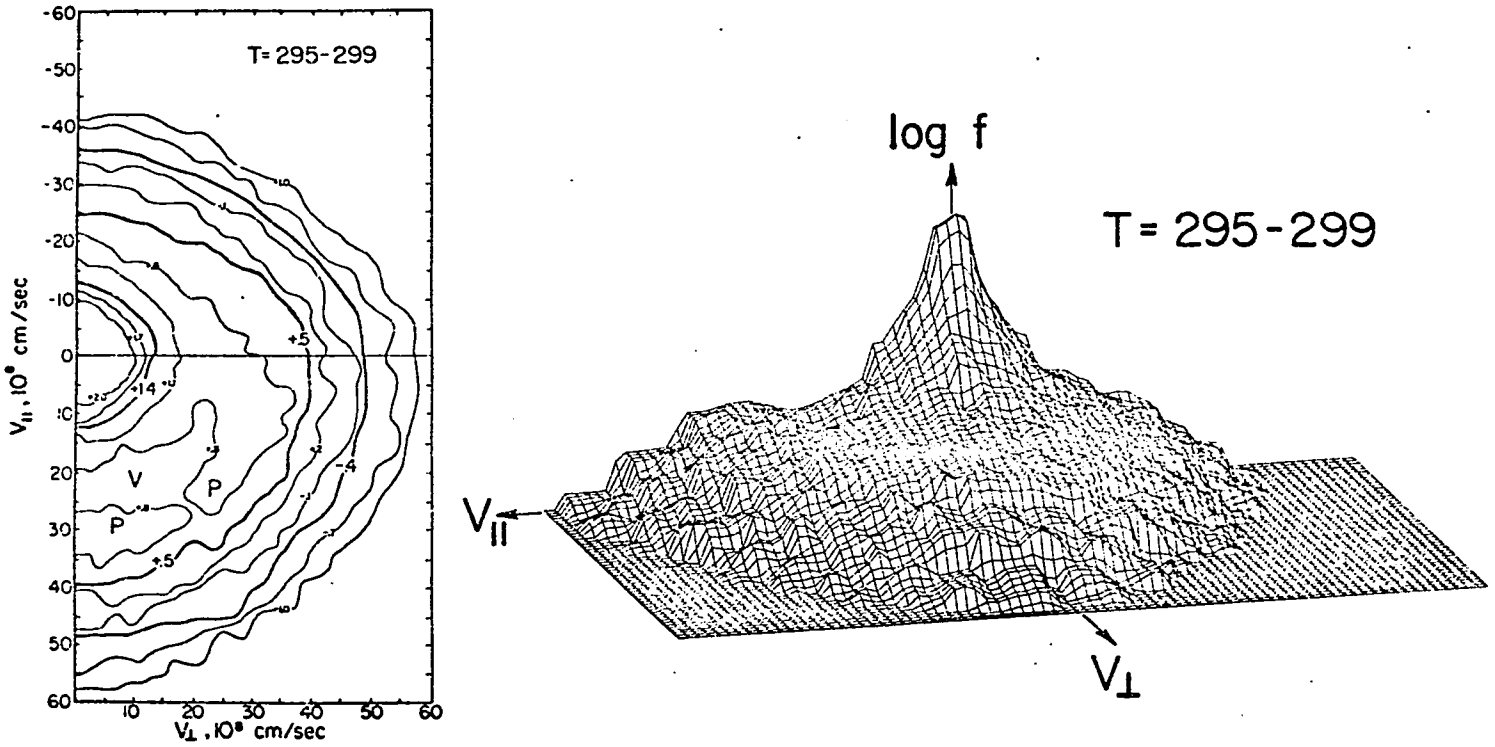
T= 295-299
V
P
P
+5
+14
+5
-4
-60
-50
-40
-30
-20
-10
0
10
20
30
40
50
60
10
20
30
40
50
60
$V_{\parallel}$, 10^8 cm/sec
$V_{\perp}$, 10^8 cm/sec
log f
T= 295-299
$V_{\parallel}$
$V_{\perp}$

Figure 6.2

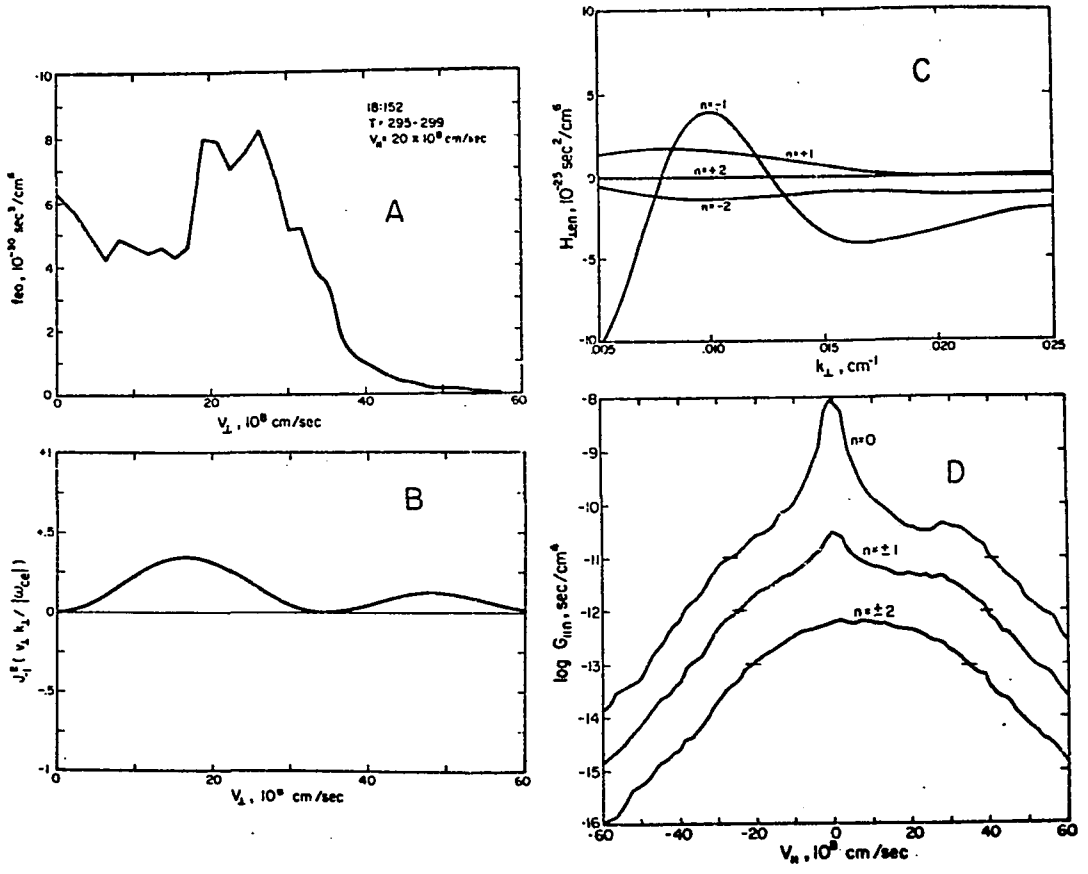
18:152
T = 295-299
V_n = 20 x 10^8 cm/sec
A
B
C
D
f_{eo}, 10^{-30} sec^3/cm^6
$V_\perp$, 10^8 cm/sec
$J_1^2(v_\perp k_\perp/|\omega_{ce}|)$
$H_{\perp en}$, 10^{-25} sec^2/cm^6
$k_\perp$, cm^{-1}
n=-1
n=+1
n=+2
n=-2
log G_{nn}, sec/cm^6
n=0
n=±1
n=±2
V_n, 10^8 cm/sec

Figure 6.3

alternative method, and one which is more general, would be to arbitrarily choose a frequency in k-space for a particular branch. The resonant velocities for all the harmonics may then be calculated from equation 6.1. It is our feeling that these waves are not as important as the principal harmonic waves. We are currently working on a program to find the imaginary frequencies of such waves in order to prove the above statement.

As an example of the method outlined above let us find the $n_o = -1$ harmonic wave which resonates at $v_{\parallel}^r = 20 \times 10^8$ cm/sec and has $k_{\perp o} = 0.01$ cm^{-1}. The frequency characteristics of this wave for the Whistler and upper hybrid branch in both P.S. IV and P.S. V are listed in Table 6.1. In Table 6.2 we list the corresponding resonant velocities, associated with the waves in Table 6.1. Looking at Table 6.2 we can clearly see why we have chosen to investigate ES stability in P.S. V rather than the more realistic P.S. IV. The reason is simply that the number of terms in equation 6.10 for the upper hybrid branch is far less in P.S. V than in P.S. IV. This frequency will in all probability be damped in P.S. IV. We will show shortly that it is growing in P.S. V. The dependence of these waves on number density is most remarkable (see figure 6.1). This dependence must certainly be a critical factor in the role ES waves play in determining the dissipation of any plasma state. We can also see from Table 6.2 while the upper hybrid branch seems to be number density dependent the Whistler branch does not, at least for $n_o = -1$. Such variations will have to be understood if we are to understand wave-particle interactions in the auroral plasma, because the number density can vary dramatically during an auroral substorm. Let us return now to our stability analysis of P.S. V where we shall consider

The Frequency Characteristics of the $n_o = -1$ Principal Harmonic Wave.

	W B		U H B	
	P. S. V	P. S. IV	P. S. V	P. S. IV
ω_R	1.62×10^{6} sec^{-1}	2.56×10^{6} sec^{-1}	1.04×10^{7} sec^{-1}	3.79×10^{7} sec^{-1}
$k_\perp$	1×10^{-2} cm^{-1}	1×10^{-2} cm^{-1}	1×10^{-2} cm^{-1}	1×10^{-2} cm^{-1}
$k_\parallel$	-3.59×10^{-3} cm^{-1}	-3.12×10^{-3} cm^{-1}	8.23×10^{-4} cm^{-1}	1.45×10^{-2} cm^{-1}
k	1.06×10^{-2} cm^{-1}	1.05×10^{-2} cm^{-1}	$\sim 1 \times 10^{-2}$ cm^{-1}	1.76×10^{-2} cm^{-1}
Θ	110°	107°	85°	35°

TABLE 6.1

TABLE 6.2

The Resonant Velocities ($\times 10^8$ cm/sec)

n	W B		U H B	
	P. S. V	P. S. IV	P. S. V	P. S. IV
-5	-	-	-	-4
-4	-	-	-	2
-3	-	-	-	8
-2	44.5	48	-90	14
-1	20	20	20	20
0	-4.5	-8	130	26
+1	-40	-36	-	32
+2	-	-	-	38
+3	-	-	-	44

first the upper hybrid branch.

The Upper Hybrid Branch

We may make $\mathcal{H}_{\perp e}^{-1}$ positive by choosing a $k_\perp$ such that $J_{-1}^2 (k_\perp v_\perp / |\omega_{ce}|)$ is large at values of $v_\perp$ where $\partial f_{eo}^h / \partial v_\perp$ has a positive slope and small where the slope is negative. In figure 6.3b we have plotted J_{-1}^2 for $k_\perp = 0.01$ cm^{-1}. Figure 6.3c shows the results of the integration indicated in equation 6.7. At $k_\perp = 0.01$ cm^{-1} $\mathcal{H}_{\perp e}^{-1}$ is 4×10^{-23} sec^2/cm^6. Because the other harmonics have such large resonant velocities, where there are very few particles, $\mathcal{H}_{\perp e}^{n}$ is very small for these harmonics. Note that the $\mathcal{H}_{\perp e}^{n}$ curves for $n \neq -1$ that are plotted in figure 6.3c do not refer to the UHB but only to the WB which will be discussed shortly.

We must now evaluate the $\mathcal{H}_{\parallel e}^{n}$ terms (see equation 6.8). The function $G_{\parallel}^{-1}$ is plotted in figure 6.3d. The slope of this function is small at $v_\parallel^r = 20 \times 10^8$ cm/sec so that $\mathcal{H}_{\parallel e}^{-1}$ is only -0.5×10^{-23} sec^2/cm^6 for the example we are considering (see Table 6.3). The other harmonics of $\mathcal{H}_{\parallel e}^{n}$ are negligible due to the large resonant velocities. Therefore,

$$\sum_n \mathcal{H}_e^n = 3.5 \times 10^{-23} \text{ sec}^2/\text{cm}^6 > 0 \ .$$

We are now in a position to calculate the imaginary frequency. From equation 6.4 we find that $\omega_I = 20$ sec^{-1}. The positive value of ω_I shows that the $n_o = -1$ harmonic wave of the UHB will grow with a characteristic e - folding time of $\tau = \frac{1}{|\omega_I|} = 0.05$ sec. A characteristic growth length may be defined once the group velocity of the wave is known.

The Stability Functions for the $n_o = -1$ Principal Harmonic Wave

n	U H B			W B		
	$v_{\parallel}^{r}$ ($\times 10^8 \frac{cm}{sec}$)	$H_{\perp}^{n}{}_{e}$ ($\frac{sec^2}{cm^6}$)	$H_{\parallel}^{n}{}_{e}$ ($\frac{sec^2}{cm^6}$)	$v_{\parallel}^{r}$ ($\times 10^8 \frac{cm}{sec}$)	$H_{\perp}^{n}{}_{e}$ ($\frac{sec^2}{cm^6}$)	$H_{\parallel}^{n}{}_{e}$ ($\frac{sec^2}{cm^6}$)
-2	-90	~ 0	~ 0	45	-1.2×10^{-23}	1.2×10^{-23}
-1	20	4×10^{-23}	-0.5×10^{-23}	20	4.0×10^{-23}	0.5×10^{-23}
0	130	0	~ 0	-5	0	-990×10^{-23}
+1	240	~ 0	~ 0	-30	1.6×10^{-23}	-3.8×10^{-23}
+2	-	~ 0	~ 0	-55	$.004 \times 10^{-23}$	$-.01 \times 10^{-23}$

TABLE 6.3

If the instability is not large then the group velocity, $\underline{V}_g$, is a meaningful concept.

6.11) $$\underline{V}_g = \frac{\underline{k}}{k} \frac{\partial \omega_R}{\partial k} + \frac{\hat{\theta}}{k} \frac{\partial \omega_R}{\partial \theta}$$

Substituting equation 6.3 into equation 6.11 gives

$$\underline{V}_g = -2.0 \times 10^7 \hat{\theta} \text{ cm/sec.}$$

It should be noted that the group velocity is normal to $\underline{k}$ and in the $\hat{\theta}$ direction for ES waves in the cold plasma approximation. This is not true for a warm plasma and is another important instance where approximating a warm plasma by P.S. I breaks down. Since $\underline{k}$ is 85° from $\underline{B}_o$, the group velocity is nearly parallel to $\underline{B}_o$. The amplifying wave we just found will grow over a characteristic length $D = \tau |V_g| = 10$km. Because an auroral arc can be many 10's of km long, one could conclude that this wave might grow substantially before propagating out of the auroral arc. Such a conclusion would be premature for the following reasons.

I must emphasize strongly that the purpose of this work is to develop a methodology for understanding wave-particle interactions which may be present in the auroral plasma. The distinction is important for such predictions can only come after detailed models of the auroral arc are developed as to composition, spatial homogeneity and temporal homogeneity. Even if we assume that the morphology of the arc satisfies our assumptions which were made in the kinetic theory we must still understand a great deal more about the wave-particle interaction. For instance in which regions of k-space do the ES waves lose their

electrostatic nature (see Appendix A)? Which waves grow the fastest? Does the non-zero value of ε_I^h calculated in equation 6.6 change the real frequency calculated in equation 6.3 (see Appendix B)? We are presently working on answering these and other questions pertaining to the wave. It is, however, certain that varying the background plasma density and the introduction of finite temperature effects in the real part of the longitudinal dielectric function will change our numerical results. A definite conclusion concerning the growth rate of these waves must be delayed until we can carry out more extensive numerical calculations over a wide range of plasma parameters.

The Whistler Branch

Once again, we will start by evaluating $\mathcal{H}_{\perp e}^{n}$. We use the same value of $k_\perp$ ($0.01 cm^{-1}$) as was used for the UHB wave to once again make $\mathcal{H}_{\perp e}^{\prime}$ large and positive (see figure 6.3c). The oscillation characteristics for the $n_0 = -1$ harmonic wave of the WB are listed in Table 6.1. The negative value of $k_{\parallel}$ ($\theta > 90^\circ$) shows that this whistler wave, which resonates with downcoming electrons, is going up the magnetic field line. Table 6.2 shows the corresponding resonant velocities for this wave. It is interesting to note the similarity between the whistler waves in P.S. IV and P.S. V. This is in marked contrast to the upper hybrid wave we considered in the preceeding subsection. Figure 6.3c shows plots of all the significant $\mathcal{H}_{\perp e}^{n}$ terms. For $k_\perp = 0.01\ cm^{-1}$ these terms are listed in Table 6.3. We may use figure 6.3d to evaluate the $\mathcal{H}_{\parallel e}^{n}$ terms. Table 6.3 shows the the n=0 term, $\mathcal{H}_{\parallel e}^{0}$, dominates all other terms indicating the wave is Landau damped by those particles with

$v_{\parallel}^{r} = -5 \times 10^{8}$ cm/sec. Damping by these electrons completely dominates over any growth that could be produced by the small secondary peak at $v_{\parallel}^{r} = 20 \times 10^{8}$ cm/sec. Summing the terms in Table 6.3 gives $\omega_{i} = -5.1 \times 10^{3}$ sec^{-1} or $\tau = 2 \times 10^{-4}$ sec. for the damping time for this whistler wave. The group velocity of this wave is 48×10^{7} cm/sec so that damping length is 1 km.

6.3 A Summary

In this chapter we have used the kinetic equations which detail weak wave-particle interactions in an auroral plasma to investigate the dissipation of high frequency principal harmonic waves in P.S. V. We noticed that P.S. V is probably a poor approximation to P.S. IV, a rather good model of the auroral plasma at rocket altitude, at least for waves on the UHB. We chose P.S. V because it simplified our stability calculations without losing any essential steps in the method we wanted to develop to find ES instabilities. Along the way toward an understanding of this method we mentioned various pitfalls which have to be understood if we are to make detailed predictions about the wave-particle event. Even though this work represents one of the most complete calculations of ES stability in an auroral plasma much work still remains to be done if we are ever to understand how the magnetosphere and ionosphere couple. In the last chapter of this thesis we shall tie together what we have done and indicate the directions we must turn to if we are to gain this understanding.

CHAPTER VII

CONCLUSIONS

7.1 An Overall Summary

The purpose of this work has been to understand wave-particle interactions in an auroral plasma. An understanding of such interactions will eventually aid us in the understanding of the coupling between the magnetosphere and ionosphere. The particular piece of this complex puzzle we chose to investigate was a detailed analysis of the possible ES waves present in the auroral plasma and their linear characteristics (i.e. ω_R, ω_I, k, θ, ω_R/k, V_g etc.) We were aided in our study by having access to a measured, highly non-Maxwellian electron distribution function.

In order to make use of the measured distribution function we had to develop a kinetic theory which incorporated wave-particle interactions. We did this from first principles because a truly comprehensive treatment of these very important interactions has not been formulated in a single text. The kinetic equations were derived in Chapter II. Once various assumptions on the homogeneity of the plasma were made in both space and time we could solve the wave equation to find the normal oscillations in terms of the one-particle distribution function. By modeling the auroral plasma in terms of a background plasma of ionospheric origin which was represented by a MB distribution function for each species and using the measured distribution for the hot electrons of magnetospheric origin, we found the specific normal oscillations of this plasma. This work was

developed in Chapters III and IV.

We found, in the weak turbulent regime, that only velocity space anisotropies (e.g. positive velocity gradients) in the one-particle distribution could excite ES instabilities in a spatially homogeneous plasma. Because we modeled the background plasma by a thermal equilibrium distribution we were led to look closely at the measured distribution to see whether any anisotropies were present. We studied this distribution throughly in Chapter V. We even turned aside from the microscopic treatment we had been developing to look at the fluid characteristics of these hot electrons. Because we showed that this hot plasma is stable for waves propagating exactly parallel and perpendicular to the earth's magnetic field, the stage was set for looking at the stability of oblique ES waves. We used the linear stability equations formulated in Chapter III to develop a methodology (Chapter VI) for understanding the linear wave-particle interactions of any normal ES oscillation existing in k-space. An example of this method was used on the $n_0 = -1$ principal harmonic wave of the Whistler and upper hybrid branches. In this chapter we mentioned various problem areas which had to be overcome if we were to understand completely the effect these waves have in dissipating free energy in the plasma.

With this work as a foundation we shall briefly describe those areas which must be investigated if we are truly to understand the wave-particle interactions in any plasma including the auroral plasma.

7.2 Future Investigations

1. It hardly seems appropriate to look at the effect of ES waves in a plasma when the wave is not ES. We have assumed that the waves we

discussed in Chapter IV are completely ES but as we saw in Appendix A this is only an approximation. We must therefore look at how much EM behavior our "ES" waves have. This requires knowing the kernel of the dispersion tensor, $\underline{\underline{\Delta}}\ (\underline{k}, \omega)$.

2. In our work we have assumed that ω_R and ω_I are uncoupled because $\kappa \ll 1$ (see Appendix B). We may do this because the auroral plasma at 250 km is only weakly turbulent. Such an assumption would probably be wrong near the so-called "acceleration region" ($\sim$5,000 km). We must therefore understand this coupling better. The plasma does not necessarily have to be turbulent for even at 250 km a wave may be so heavily damped that it affects the real frequency.

3. With areas 1. and 2. understood, a complete stability analysis for any given normal oscillation could be undertaken. The question which we must now answer is which of these waves would effect the plasma the most?

4. Obviously only those waves with an $\omega_I > 0$ would have to be included in the set of waves which cause the plasma to be dissipative. What is not obvious is the fact that even if a wave is unstable it may convect out of the plasma before it has had time to do any real interacting. In a warm plasma, most ES waves are convective. We must therefore find those waves which have a small group velocity and/or a small growth time. This implies that D, the growth length, must be small ($D \ll L$, the scale length of the plasma - see Table 2.1).

5. The reader must have noticed our omission of the stability of the low frequency ion waves. To fill in this gap we should look at how these waves couple to the hot electrons. Because the background ions and electrons are approximately isothermal there cannot be any ion

acoustic waves or Alfvén-like waves supported in the plasma. Therefore, the only ion waves are the IC(n) which propagate nearly perpendicular to the magnetic field. We may consider an even better model of the auroral plasma by including multiple ions (e.g. O^+ , N_2^+ , NO^+ at 250 km). In this case the IC(n) waves are much more complicated as one would expect. The stability of these waves however can still be calculated.

6. Once the frequency and wave vectors of the unstable or marginally stable waves are known for every branch of the ES mode, a comparison with experimental observations of wave turbulence must be undertaken. From such a comparison we may ascertain to what extent the real auroral plasma approximates the infinite and spatially homogeneous plasma we have assumed in our theory. This would be a very important test of the validity of linear plasma theory because no other plasma to date has been so well modeled as the one we have considered.

7. It would be satisfying to understand more about the accelaration process which brings the solar wind particles that enter the magnetosphere, with an average energy of 50eV, to the keV energies of the hot electrons that are measured at 250 km. The journey these particles must have taken is obviously very complicated. There is much supporting evidence for this acceleration region to be situated somewhere in the top-side ionosphere (see Chapter I concerning this process). In fact, an important wave-particle interaction is often advanced in order to explain the occurence of what may be a parallel electric field. The problem of an electric field along the magnetic field is the lack of collisions (between 5 - 10,000 km). Without collisions there can be no resistance and without resistance there can be no electric field. However if we treat our excited plasmons as particles which carry momentum ($\hbar \underline{k}$).

then an effective collision frequency may be formulated from simple conservation laws (Hasegawa, 1974). It may be shown that this collision frequency is proportional to $\epsilon_I(\underline{k}, \omega)$. The imaginary longitudinal dielectric function for a plasma which is passing through an electric field induced by anisotropics in some portion of the plasma may be far different from the one we have considered. This is a type of bootstrap process which must clearly be better understood. It may only be a small portion of the plasma on the high energy tail of the distribution which is actually accelerated. Such electrons are commonly referred to as run-away electrons. We bring up this important process not because our work has a direct bearing on it but rather to indicate that we must understand the properties of the functions which describe the various interactions within a plasma to a fuller degree than has been attained up to the present. It is my feeling that the knowledge these functions embody will lead us to a deeper understanding of the complex interactions which occur in the plasma we call the magnetosphere.

Bibliography

1. Akasofu, S. -I., A Review of Magnetospheric Studies.

2. Alfvén, H. and P. Carlqvist, Currents in the Solar Atmosphere and a Theory of Solar Flares, Solar Phys., 220, 1967.

3. Arnoldy, R. L., P. B. Lewis and P. O. Isaacson, Field Aligned Auroral Electron Fluxes, J. Geophys. Res. 79, 4208, 1974.

4. Arnoldy, R. L., Auroral Particle Precipitation and Birkeland Currents, Rev. Geophys. Space Phys., 12, 217, 1974.

5. Block, L. P., Potential Double Layers in the Ionosphere, Cosmic Electrodyn., 3, 349, 1972.

6. Bogoliubov, N. N., Studies in Statistical Mechanics (E. K. Gora, transl.; J. de Boer and G. E. Uhlenbeck, eds.) (North Holland, Amsterdam), Vol. 1, 1962.

7. de Boor, C. Cadre: An Algorithm for Numerical Guadrature, Mathematical Software (John R. Rice, ed.) (Academic Press), 1971.

8. Bryant, D. A., D. S. Hall and D. R. Lepine, Electron Acceleration in an Array of Auroral Arcs, Planet. Space Sci., in press, 1977.

9. Carlqvist, P., On the Formation of Double Layers in Plasmas, Cosmic Electrodyn., 3, 377, 1972.

10. Chen, F. F., Introduction to Plasma Physics (Plenum Press), 1974.

11. Davidson, R. C., Methods in Nonlinear Plasma Theory (Academic Press, Inc.), 1972.

12. Dennery, P., and A. Krzywicki, Mathematics for Physicists (F. Seitz, ed.) (Harper and Row), 1967.

13. Fried, B. D., S. D. Conte, The Plasma Dispersion Function (Academic Press), 1961.

14. Gold, T., Rotating Neutron Stars and the Nature of Pulsars, Nature, 221, 25, 1969.

15. Hall, D. S., and D. A. Bryant, Collimation of Auroral Particles by Time-Varying Acceleration, Nature, 251, 402, 1974.

16. Hasegawa, A., Plasma Instabilities and Nonlinear Effects (Springer-Verlag), 1975.

17. Ichimaru, S., Basic Principles of Plasma Physics (W. A. Benjamin, Inc.), 1973.

18. Kan, J.R. and S.-I. Akasofu, A Mechanism for Current Interruption in a Collisionless Plasma, J. Geophys. Res., (submitted), 1977.

19. Kaufmann, R. L., D. N. Walker, and R. L. Arnoldy, Acceleration of Auroral Electrons in Parallel Electric Fields, J. Geophys. Res., 81, 1673, 1976.

20. Kaufmann, R. L., P. B. Dusenbery, B. J. Thomas and R. L. Arnoldy, Auroral Electron Distribution Functions, J. Geophys. Res., (in press), 1978.

21. Kaufmann, R. L, P. B. Dusenbery, B. J. Thomas, Stability of the Auroral Plasma: Parallel and Perpendicular Propagation of Electrostatic Waves, J. Geophys. Res. (submitted).

22. Kennel, C. F. and H. E. Petschek, Limit on Stably Trapped Particle Fluxes, J. Geophys. Res., 71, 1966.

23. Kindel, J. M., and C. F. Kennel, Topside Current Instabilities, J. Geophys. Res., 76, 3055, 1971.

24. Kintner, P. M., L. J. Cahill, Jr. and R. L. Arnoldy, Current System in an Auroral Substorm, J. Geophys. Res., 79, 4326, 1974.

25. Klimontovich, Yw. L., The Statistical Theory of Non-Equilibrium Processes in a Plasma (H. S. H. Massey and O. M. Blunn, transl.; D. ter Haar, ed.) (M. I. T. Press), 1967.

26. Krall, N. A., and A. W. Trivelpiece, Principles of Plasma Physics (McGraw-Hill, Inc.), 1973.

27. Landau, L., J. Phys. (U.S.S.R.) 10, 25, 1946.

28. Maehlum, B. N. and H. Moestue, High Temporal and Spatial Resolution Observations of Low Energy Electrons by a Mother-Daughter Rocket in the Vicinity of Two Quiescent Auroral Arcs, Planet. Space Sci., 21, 1957, 1973.

29. Matthews, D. L., M. Pongratz, and K. Papadopoulos, Nonlinear production of Suprathermal Tails in Auroral Electrons, J. Geophys. Res., 81, 123, 1976.

30. Mayer, J. E. and M. G. Mayer, Statistical Mechanics (Wiley, New York), 1940.

31. Mizera, P. F., D. R. Croley, Jr. and J. F. Fennel, Electron Pitch-Angle Distributions in an Inverted 'V' Structure, Geophys. Res. Letters, 3, 149, 1976.

32. Montgomery, D. C. and D. A. Tidman, Plasma Kinetic Theory (McGraw-Hill, Inc.), 1964.

33. Papadopoulos, K., A Review of Anamlous Resistivity for the Ionosphere, Rev. Geophys. Space Phys., 15, 113, 1977.

34. Reasoner, D. L. and C. R. Chappell, Twin Payload Observations of Incident and Backscattered Auroral Electrons, J. Geophys. Res., 78, 2176, 1973.

35. Swift, D. W., A Mechanism for Energizing Electrons in the Magnetosphere, J. Geophys. Res., 70, 3061, 1965.

36. Watson, G. N., A Treatise on the Theory of Bessel Functions (Cambridge University Press), 1966.

37. Whalen, B. A. and I. B. McDiarmid, Observations of Magnetic-field-aligned Auroral Electron Precipitation, J. Geophys. Res., 77, 191, 1972.

38. Whipple, E. C., Jr., The Signature of Parallel Electric Fields in a Collisionless Plasma, J. Geophys. Res., 82, 1525, 1977.

Appendix A

The Nature of Waves in a Vlasov Plasma

Let us consider the following question. If an electric field is induced in a plasma with an angular frequency, ω and wave number, $\underline{k}$ what mode (either ES or EM) or combination of modes is this field in? If $\underline{k} \cdot \underline{E}_i$ and $\underline{k} \times \underline{E}_i$ are non zero, we have a very complicated problem on our hands. The dispersion for such a wave in k-space is not a trivial problem to solve, especially for the warm, magnetized plasma we are presently studying. In this work we are interested in those waves which are primarily electrostatic. We would like then to be able to find under what conditions a given frequency and wave vector will be in such a mode. The answer to this question will shed light not only on ES waves but on the EM waves as well.

We will begin our study by looking at the classical wave equation of Maxwell. In Chapter II we showed that

$$\text{A.1)} \qquad \underline{k} \times (\underline{k} \times \underline{E}) + \frac{\omega^2}{c^2} \underline{\underline{\varepsilon}} \cdot \underline{E} = 0$$

where

$$\underline{\varepsilon} = \underline{E}_i .$$

Because a vacuum can only support transverse waves (i.e. $\underline{k} \cdot \underline{E} = 0$), equation A.1 implies that $\omega^2 = k^2 c^2$ which is the familiar dispersion relation for a light wave ($\underline{\underline{\varepsilon}} = \underline{\underline{1}}$). It is much more difficult to find a similar relationship for a plasma because the structure of the dielectric tensor, $\underline{\underline{\varepsilon}}(\underline{k}, \omega)$ is much more complicated. This complicated nature

of $\underline{\underline{\varepsilon}}$ gives rise to a rich variety of possible oscillations so long as collisions do not randomize these collective motions appreciably (the Vlasov plasma approximation - see Chapter II). Let us begin our search for the condition that assures that our waves will be ES by representing $\underline{E}$ in a Cartessian basis. That is

$$\underline{E} = \underline{E}_1 e^{i} = \begin{bmatrix} E_x \\ E_y \\ E_z \end{bmatrix} \quad , \quad \underline{k} = \begin{bmatrix} k_\perp \\ 0 \\ k_\parallel \end{bmatrix}$$

$$n^2 = k^2 c^2 / \omega^2 \text{ (the index of refraction).}$$

For a general plasma let

$$\underline{\underline{\varepsilon}} = \begin{bmatrix} \varepsilon_{xx} & \varepsilon_{xy} & \varepsilon_{xz} \\ \varepsilon_{yx} & \varepsilon_{yy} & \varepsilon_{yz} \\ \varepsilon_{zx} & \varepsilon_{zy} & \varepsilon_{zz} \end{bmatrix} .$$

Substituting the above expressions into equation A.1 gives

A.2) $$\underline{\underline{\Delta}} \cdot \underline{E} = \underline{0}$$

where,

$$\underline{\underline{\Delta}} = \begin{bmatrix} -n^2 c_\parallel^2 + \varepsilon_{xx} & \varepsilon_{xy} & \varepsilon_{xz} + n^2 c_\parallel s \\ \varepsilon_{yx} & \varepsilon_{yy} - n^2 & \varepsilon_{yz} \\ \varepsilon_{zx} + n^2 c_\parallel s & \varepsilon_{zy} & \varepsilon_{zz} - n^2 s^2 \end{bmatrix}$$

$$c_\parallel = \cos\theta \quad , \quad s = \sin\theta \quad .$$

For equation A.2 to have a nontrivial solution the determinant of the coefficient matrix must be zero, i.e.

$$A.3)\quad (\varepsilon_{xx} - n^2\cos^2\theta)\left[(\varepsilon_{yy}-n^2)(\varepsilon_{zz}-n^2\sin^2\theta) - \varepsilon_{zy}\varepsilon_{yz}\right] - \varepsilon_{xy}\left[\varepsilon_{yx}(\varepsilon_{zz}-n^2\sin^2\theta) - \varepsilon_{yz}(\varepsilon_{zx}+n^2\cos\theta\sin\theta)\right] + (\varepsilon_{xz} + n^2\cos\theta\sin\theta)\left[\varepsilon_{yx}\varepsilon_{zy} - (\varepsilon_{yy}-n^2)(\varepsilon_{zx}+n^2\cos\theta\sin\theta)\right] = 0 .$$

θ is the angle of propagation (see figure 3.1). When one refers back to Chapter III where $\underline{\underline{\varepsilon}}$ was found for the simple case of a plasma immersed in a constant magnetic field the overwhelming complexity of equation A.3 seems insurmountable. The situation is not all that bad as we shall see. We may rewrite equation A.3 as follows

$$A.4)\qquad A + \frac{B}{n^2} + \frac{C}{n^4} = 0$$

where,

$$A = \varepsilon_{xx}S^2 + (\varepsilon_{xz}+\varepsilon_{zx})C_1S + \varepsilon_{zz}C_1^2,$$

$$B = -\varepsilon_{zz}\varepsilon_{xx} - \varepsilon_{yy}\varepsilon_{xx}S^2 - \varepsilon_{yy}\varepsilon_{zz}C_1^2 - \varepsilon_{zy}\varepsilon_{yz}C_1^2 + \varepsilon_{xy}\varepsilon_{yx}S^2 + \varepsilon_{xy}\varepsilon_{yz}C_1S - \varepsilon_{yy}\varepsilon_{xz}C_1S + \varepsilon_{zx}\varepsilon_{xz} + \varepsilon_{yx}\varepsilon_{zy}C_1S - \varepsilon_{yy}\varepsilon_{zx}C_1S ,$$

and,

$$C = \varepsilon_{yy}\varepsilon_{zz}\varepsilon_{xx} - \varepsilon_{xx}\varepsilon_{zy}\varepsilon_{yz} - \varepsilon_{xy}\varepsilon_{yx}\varepsilon_{zz} + \varepsilon_{xy}\varepsilon_{yz}\varepsilon_{zx} + \varepsilon_{xz}\varepsilon_{yx}\varepsilon_{zy} \quad .$$

We can see a simplification of the determinant of the dispersion tensor when it is written as in equation A.4, namely if $n^2 \to \infty$ (B, C remaining finite) then

$$A = 0 \quad .$$

Therefore the above equation would give the dispersion of those waves which have zero phase velocity ($\frac{\omega}{k} = 0$). Such a limit in a warm plasma is not feasible, however $n^2 >> 1$ is. If

A.5) $$n^2 >> |\varepsilon_{ij}| \qquad \forall i,j$$

then $\frac{B}{n^2}$ and $\frac{C}{n^4}$

are very small. This implies that

$$A \approx 0 \quad .$$

What mode does the above expression correspond to, if any?

To answer the above question we must return to equation A.1. Let us rewrite it in terms of n.

A.6) $$\underline{n} \times (\underline{n} \times \underline{E}) + \underline{\underline{\varepsilon}} \cdot \underline{E} = \underline{0} \quad .$$

For an arbitrary vector field we may expand the field into components along and transverse to any arbitrary vector. Let our vector field be $\underline{E}$ and the arbitrary vector be $\underline{k}$.

$$\underline{E} = \underline{E}_L + \underline{E}_T$$

where

$$\underline{E}_L = \frac{\underline{k}\,(\underline{k}\cdot\underline{E})}{k^2} = \begin{bmatrix} s^2 E_x + s c_1 E_z \\ 0 \\ s c_1 E_x + c_1^2 E_z \end{bmatrix}$$

$$\underline{E}_T = -\frac{\underline{k}\times(\underline{k}\times\underline{E})}{k^2} = \begin{bmatrix} c_1^2 E_x - c_1 s E_z \\ E_y \\ s^2 E_z - c_1 s E_x \end{bmatrix}$$

Therefore equation A.6 reads

$$-n^2 \underline{E}_T + \underline{\underline{\varepsilon}}\cdot(\underline{E}_L + \underline{E}_T) = 0$$

i.e.

A.7) $$\underline{E}_T - \frac{\underline{\underline{\varepsilon}}}{n^2}\cdot\underline{E}_T = \frac{\underline{\underline{\varepsilon}}}{n^2}\cdot\underline{E}_L$$

The condition

$$n^2 \gg |\varepsilon_{ij}| \quad \forall\, i,j$$

implies that

$$|\underline{E}_T| \ll |\underline{E}_L| \quad .$$

Therefore the wave associated with equation A.5 has a small phase velocity with respect to light and one whose longitudinal field is much

larger than its transverse field. In other words the plasma is oscillating in the ES mode. If we let $\underline{E}_T \to \underline{0}$ in equation A.7 we see that

$$\underline{\underline{\varepsilon}} \cdot \underline{E}_L = \underline{0}$$

or

A.8) $$\underline{k} \cdot \underline{\underline{\varepsilon}} \cdot \underline{E}_L = 0 \quad .$$

Because $\underline{E}_L$ is longitudinal it may be expressed in terms of a scalar potential,

i.e. $$\underline{E}_L = -i \underline{k} \phi(\underline{k}, \omega) \quad .$$

Therefore equation A.8 reduces to

$$\varepsilon_L(\underline{k}, \omega) \phi(\underline{k}, \omega) = 0$$

where ε_L is the longitudinal dielectric function (l.d.f.) given by

$$\varepsilon_L = \frac{\underline{k} \cdot \underline{\underline{\varepsilon}} \cdot \underline{k}}{k^2} \quad .$$

To find the frequencies and wavelengths which the ES field oscillates at, we must look at the kernel of the l.d.f., i.e.

A.9) $$\varepsilon_L(\underline{k}, \omega) = 0 \quad .$$

We can easily show that

$$\varepsilon_L = A \quad .$$

Therefore a wave which satisfies equation A.5 is in the ES mode. It's dispersion in k-space may then be found from equation A.9. Our analysis to this point has said nothing about the coupling between the ES mode and

the EM mode.

Let us look at an isotropic plasma without any external fields present in order to understand this cpupling better. In such a plasma the only direction is in terms of the wave vector, $\underline{k}$. We are free to choose $\underline{k}$ to be along the z direction. The only tensors of second rank that can be constructed from $\underline{k}$ and are independent are the following projection dyads:

$$\hat{\underline{\underline{L}}} = \frac{\underline{k}\,\underline{k}}{k^2} = \hat{z}\,\hat{z}$$

$$\hat{\underline{\underline{T}}} = \underline{\underline{1}} - \hat{\underline{\underline{L}}} = \hat{x}\,\hat{x} + \hat{y}\,\hat{y}$$

where

$$\hat{\underline{\underline{L}}} \cdot \underline{k} = \underline{k} \quad ,$$

$$\hat{\underline{\underline{T}}} \cdot \underline{k} = \underline{0} \quad .$$

The dispersion tensor must be a linear combination of $\hat{\underline{\underline{L}}}$ and $\hat{\underline{\underline{T}}}$, i.e.

A.10) $$\underline{\underline{\Delta}} = \varepsilon_L \hat{\underline{\underline{L}}} + (\varepsilon_T - n^2)\hat{\underline{\underline{T}}}$$

$$= \begin{bmatrix} -n^2 + \varepsilon_T & 0 & 0 \\ 0 & -n^2 + \varepsilon_T & 0 \\ 0 & 0 & \varepsilon_L \end{bmatrix} .$$

For an isotropic plasma in velocity space, the off diagonal elements vanish. In such a plasma the EM and ES modes are completely decoupled. When an external field is present the motion of particles along the field is very different from those which travel perpendicular to the field. For such a plasma we cannot expand its' dispersion tensor into the unit dyads we have considered above. For now there are not just two independent functions (i.e. ε_L and ε_T) but rather six. We can see in what sense these off diagonal terms contribute to the coupling of the EM and ES modes by rotating our xyz coordinate system about the y axis by the angle θ so that the z axis lines up along the $\underline{k}$ direction. There are six independent elements of $\underline{\underline{\varepsilon}}$ because the dielectric tensor satisfies the following symmetry relations.

$$\varepsilon_{yx} = -\varepsilon_{xy} \quad , \quad \varepsilon_{zx} = \varepsilon_{xz} \quad , \quad \varepsilon_{zy} = -\varepsilon_{yz} .$$

The rotation matrix, $\underline{\underline{R}}$, is given by

$$\underline{\underline{R}} = \begin{bmatrix} c_1 & 0 & -s \\ 0 & 1 & 0 \\ s & 0 & c_1 \end{bmatrix} .$$

$$\underline{E}' = \underline{\underline{R}} \cdot \underline{E} = \begin{bmatrix} c_1 E_x - s E_y \\ E_y \\ s E_x + c_1 E_z \end{bmatrix} .$$

In this new basis what is the dispersion tensor?

$$\underline{\underline{\Delta}} \cdot \underline{E} = \underline{0}$$

$$\underline{\underline{\Delta}} \cdot \underline{\underline{R}}^{-1} \cdot \underline{E}' = \underline{0}$$

$$(\underline{\underline{R}} \cdot \underline{\underline{\Delta}} \cdot \underline{\underline{R}}^{-1}) \cdot \underline{E}' = \underline{0}$$

Or

$$\underline{\underline{\Delta}}' \cdot \underline{E}' = \underline{0}$$

where

A.11) $$\underline{\underline{\Delta}}' = \underline{\underline{R}} \cdot \underline{\underline{\Delta}} \cdot \underline{\underline{R}}^{-1} \quad .$$

We call the above transformation a similarity transformation. Performing the indicated matrix multiplications in equation A.11 we find that

A.12) $$\underline{\underline{\Delta}}' = \begin{bmatrix} -n^2 + d_{11} & d_{12} & d_{13} \\ -d_{12} & -n^2 + d_{22} & d_{23} \\ d_{13} & -d_{23} & \varepsilon_\perp \end{bmatrix}$$

where

$$\underline{\underline{d}} = \begin{bmatrix} \varepsilon_{xx} c_1^2 - 2\varepsilon_{xz} s c_1 + \varepsilon_{zz} s^2 & \varepsilon_{xy} c_1 + \varepsilon_{yz} s & c_1 s(\varepsilon_{xx} - \varepsilon_{zz}) \\ -\varepsilon_{xy} c_1 - \varepsilon_{yz} s & \varepsilon_{yy} & -\varepsilon_{xy} s + \varepsilon_{yz} c_1 \\ c_1 s(\varepsilon_{xx} - \varepsilon_{zz}) + \varepsilon_{xz}(c_1^2 - s^2) & \varepsilon_{xy} s - \varepsilon_{yz} c_1 & \varepsilon_\perp \end{bmatrix}$$

In this new representation can we find a condition which assures that the EM mode is decoupled from the ES mode? If d_{13} and d_{23} approach zero for some $\omega(k)$ which satisfies $\det | \underline{\underline{\Delta}}' | = 0$ then

A.13) $$\underline{\underline{\Delta}}' = \begin{bmatrix} -n^2 + d_{11} & d_{12} & 0 \\ -d_{12} & -n^2 + d_{22} & 0 \\ 0 & 0 & \varepsilon_L \end{bmatrix}$$

Therefore $\det | \underline{\underline{\Delta}}' | = 0$ implies that

A.14) $$\begin{cases} \varepsilon_L = 0 & \text{:ES} \\ \det \begin{vmatrix} -n^2 + d_{11} & d_{12} \\ -d_{12} & -n^2 + d_{22} \end{vmatrix} = 0 & \text{:EM} \end{cases}$$

The wave is therefore either ES or EM but not a hybrid. We have begun to look at this very important coupling problem for an auroral plasma. The magnitude of d_{13} and d_{23} should give a sensitive test as to which mode a particular wave is actually in.

In this appendix we considered the nature of waves in a Vlasov plasma (one in which we neglect collisions). After finding an important condition which our ES waves must satisfy (equation A.5) we were led to consider the coupling between the EM and ES mode. For these modes to be uncoupled we found that d_{13} and d_{23} must approach zero.

Appendix B

The Taylor Series Expansion of ε_L^f

Because we are looking at ES oscillations of a magnetized plasma in the weak turbulent regime, it seems natural to expand ε_L^f, the longitudinal dielectric function, about the real frequency. However apart from our natural inclination, from a mathematical point of view it is essential that we do so. This is because we can find the real and imaginary parts of ε_L^f exactly at all points along the real frequency axis in ω-space. We discussed this fact in section 3.4. What a Taylor series expansion does for us is to allow us to step away from the ω_R axis, anywhere within a circle of radius R, where R is the radius of convergence of the Taylor series. Beyond this point the expansion becomes invalid. In this appendix we are not interested in the actual value of this radius but rather in how many terms we must keep to insure the weak turbulent approximation, i.e.

$$\mathcal{R} = \frac{|\omega_I|}{\omega_R} << 1 \quad .$$

In Chapter IV we noticed that there are zero crossings of $\varepsilon_R^f(\omega_R)$ with a negative slope. Are these zeros normal oscillations? If they are, then it would imply that an equilibrium plasma is ES unstable. We would like to determine how much error is introduced in ω_R by simply obtaining ω_R from $\varepsilon_R^f(\omega_R) = 0$. Let us begin our analysis by describing what we mean by a Taylor series in a complex plane (Dennery and Krzywicki, 1967).

Theorem. Let $\varepsilon_L^f(\omega)$ be a function, analytic within and on a circle Γ centered at $\omega=\omega_0$. The value of this function at any point ω within Γ is given by the uniformly convergent power series

B.1) $$\varepsilon_L^f(\omega) = \sum_{n=0}^{\infty} a_n (\omega - \omega_0)^n$$

where

$$a_n = \frac{1}{n!} \left. \frac{d^n \varepsilon_L^f(\omega)}{d\omega^n} \right|_{\omega=\omega_0}$$

$$= \frac{1}{2\pi i} \int_\Gamma \frac{\varepsilon_L^f(\omega')}{(\omega' - \omega_0)^{n+1}} d\omega' \quad .$$

The radius of convergence, R, for which the above power series is a well defined representation of $\varepsilon_L^f(\omega)$ cannot be greater than the distance from the point $\omega=\omega_0$ to the nearest singularity of $\varepsilon_L^f(\omega)$.

Figure B.1a shows the real part of the longitudinal dielectric function, $\varepsilon_R^f(\omega)$ when $\omega = \omega_R + i\omega_I$ is purely real, $\omega_I=0$, for the range $10^{-7} < \frac{\omega_R}{|\omega_{ce}|} < 10^2$ and figure B.2a is an expanded view of the fine structure that appears when $\omega_R \sim |\omega_{ce}|$. Similarly, figures B.1b and B.2b show the imaginary part of the l.d.f., $\varepsilon_I^f(\omega)$ when ω is purely real. In this appendix we are looking at ES waves in P.S. III.

In Appendix A we saw that the normal branches of the ES mode are given by those frequencies which satisfy

$$\varepsilon_L(\underline{k}, \omega) = 0$$

i.e.

$$\varepsilon_R(\omega) = \varepsilon_I(\omega) = 0$$

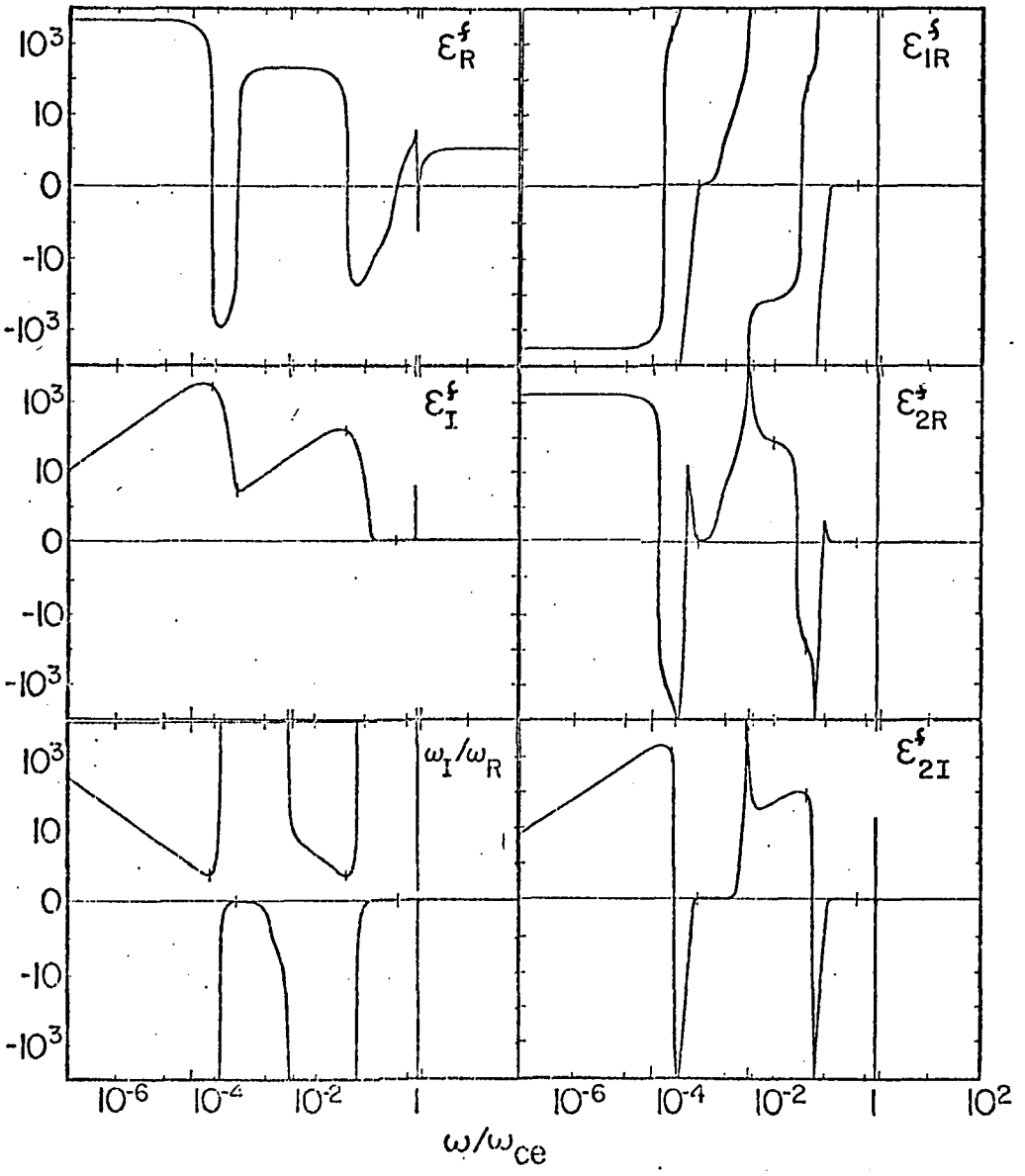

Figure B.1

The Taylor series functions for $10^{-7} < \frac{\omega_R}{|\omega_{ce}|} < 10^2$. The curve is derived by setting the first two terms in equation B.5 equal to zero. ε_{1R}^f is the first order term in equation B.4 and ε_{2R}^f is the second order term in equation B.4. ε_{2I}^f is the second order term in equation B.5.

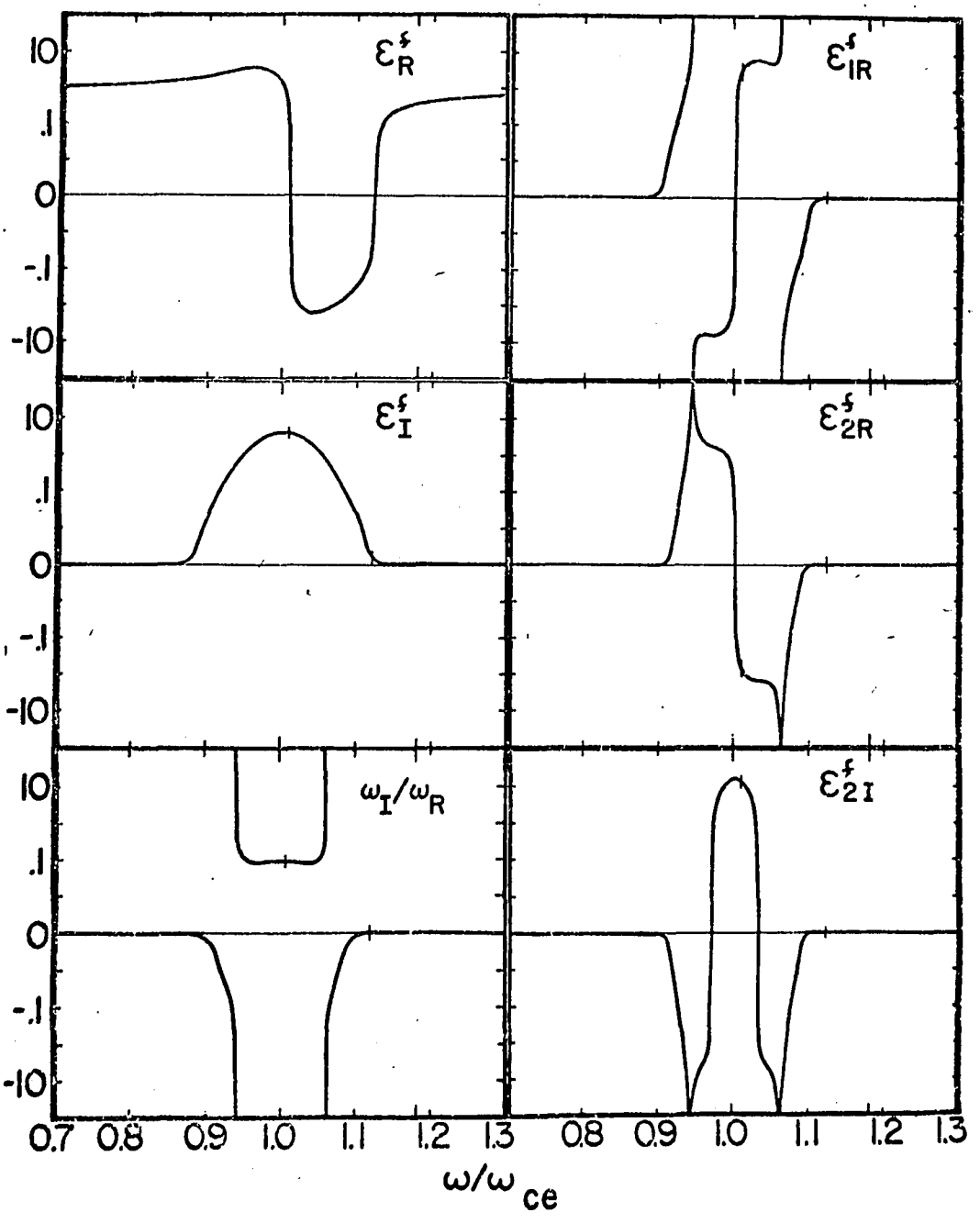

Figure B.2

Similar to figure B.1 except for $0.7 < \frac{\omega_R}{|\omega_{ce}|} < 1.3$. This figure shows the detail which exists close to the electron cyclotron frequency.

where $\omega = \omega_R + i\omega_I$ is not necessarily real. The usual procedure is to assume that $\kappa << 1$ and to approximate ω_R by solving the equation

$$\varepsilon_R(\omega_R) = 0 \quad .$$

This is the approach we took in Chapter IV. In general, $\varepsilon_I(\omega_R)$ is non-zero at this point. A small ω_I is then added so that $\varepsilon_I(\omega) = 0$ to first order in a Taylor series expansion i.e., (letting $\omega_o = \omega_R$ in equation B.1)

B.2) $$\varepsilon_I(\omega_R + i\omega_I) \approx \varepsilon_I(\omega_R) + \omega_I \frac{\partial \varepsilon_R(\omega_R)}{\partial \omega_R},$$

It is assumed that the addition of a small ω_I does not make a significant change in ε_R, so that the resulting $\omega_R + i\omega_I$ represents a normal oscillation of our plasma.

Figure B.1a shows six values of ω_R for which $\varepsilon_R^f(\omega_R) = 0$. Since $\varepsilon_R^f(\omega_R)$ is always positive in figure B.1a, a positive value of ω_I would be required to make $\varepsilon_I^f(\omega) = 0$ in equation B.2 whenever $\partial \varepsilon_R^f(\omega_R)/\partial\omega_R$. It is however easy to show (e.g., using the procedure on page 446 of Krall and Trivelpiece 1973) that the l.d.f. allows only damped ($\omega_I < 0$) oscillations in a plasma in thermodynamic equilibrium. For this reason only the three solutions to $\varepsilon_R^f(\omega_R) = 0$ with $\partial \varepsilon_R^f / \partial \omega_R > 0$ can be retained. In P.S. III these ES waves are on the upper hybrid, whistler and acoustic branches.

The purpose of this appendix is to investigate a few of the problems encountered in finding the normal oscillations of any plasma. In particular we will be concerned with answering the following questions: 1) Why doesn't the Taylor series approximation work when $\partial \varepsilon_R^f / \partial \omega_R < 0$ with a Maxwellian plasma? This question must be answered carefully

because we cannot simply discard all growing waves ($\omega_I > 0$) in a real plasma (see Chapter VI).

2) How large can ω_I be for the Taylor series approximation to work? This question is important because we will be dealing with the measured ionospheric plasma rather than a pure Maxwellian plasma. And as we mentioned earlier,

3) How much error is introduced by simply obtaining ω_R from $\varepsilon_R(\omega_R)=0$?

First, we will expand $\varepsilon_L(\omega)$ in a Taylor series about the point ω_0 ω_R and keep one more term than is usual.

$$\text{B.3)} \quad \varepsilon_L(\omega) = \varepsilon_L(\omega_R) + i\omega_I \left.\frac{\partial \varepsilon_L}{\partial \omega}\right|_{\omega=\omega_R} - \frac{1}{2}\omega_I^2 \left.\frac{\partial^2 \varepsilon_L}{\partial \omega^2}\right|_{\omega=\omega_R} + \cdots$$

Because it is easy to evaluate $\varepsilon_R^f(\omega_R)$, $\varepsilon_I^f(\omega_R)$ and the derivatives of these functions numerically, the Taylor series defined by equation B.3 is rewritten as follows. The first order term in equation B.3 is rewritten in terms of easily evaluated derivatives.

$$i\omega_I \frac{\partial \varepsilon_L}{\partial \omega_R} = i\omega_I \frac{\partial \varepsilon_R}{\partial \omega_R} - \omega_I \frac{\partial \varepsilon_I}{\partial \omega_R}$$

where

$$\varepsilon_L = \varepsilon_R + i\varepsilon_I \quad .$$

Similarly, expanding the second order term in equation B.3 into real and imaginary parts we find that equation B.3 can be expressed as

$$\text{B.4)} \quad \varepsilon_R(\omega) = \varepsilon_R(\omega_R) - \omega_I \frac{\partial \varepsilon_I}{\partial \omega_R} - \frac{\omega_I^2}{2} \frac{\partial^2 \varepsilon_R}{\partial \omega_R^2} + \cdots$$

and

$$\text{B.5)} \quad \varepsilon_I(\omega) = \varepsilon_I(\omega_R) + \omega_I \frac{\partial \varepsilon_R}{\partial \omega_R} - \frac{\omega_I^2}{2} \frac{\partial^2 \varepsilon_I}{\partial \omega_R^2} + \cdots$$

Equations B.4 and B.5 can be used to answer the first two questions posed above. The usual method of determining ω_I is to set equation B.2 equal to zero. Note that equation B.2 includes just the first two terms of the Taylor series for ε_I (equation B.5). The resulting ω_I is plotted in figures B.1c and B.2c. These values of are just large enough so that the first order term of the ε_I^f expansion is equal to minus the zero order term (figures B.1b and B.2b). The tick marks on the curves in figures B.1 and B.2 show the frequencies at which $\varepsilon_R^f(\omega_R) = 0$, which is the usual approximation to find the real frequency of the normal oscillations.

We would like to find some simple criterion to separate the normal oscillations (associated with $\omega_I < 0$ for the Maxwellian plasma) from the three spurious roots of $\varepsilon_R^f(\omega_R) = 0$ that do not correspond to the normal oscillations (associated with $\omega_I > 0$ for the Maxwellian plasma). The sign of ω_I itself could, of course, be used for the Maxwellian case, but is not useful in a real plasma for which $\omega_I > 0$ solutions are allowed (e.g. see Chapter VI). We first note that $\varepsilon_I^f(\omega_R)$ is much larger at the roots which are associated with positive ω_I than at roots associated with a negative ω_I . The absolute value of ε_I^f , however, does not provide a good means of distinguishing between the normal oscillations and the three spurious roots. As an example, $\varepsilon_I^f = 3$ for the acoustic wave that is one of the normal oscillations in P.S. III in figure B.1b and $\varepsilon_I^f = 5$ at the spurious root in figure

B.2b that does not correspond to a normal oscillation.

Since the Taylor series expansion is in terms of ω_I , it is usually stated that ω_I must be much less than ω_R ($\varkappa \ll 1$) for any normal oscillation obtained from the Taylor series method. This statement is certainly true but does not provide a simple test for distinguishing between real and unreal oscillations because it is not clear how small $\varkappa$ must be. In the example shown here, $\varkappa < 1$ for all three spurious roots and $\varkappa < 0.1$ for the spurious root near $\omega_R \sim |\omega_{ce}|$ (figure B.2c). Clearly a value of 0.1 is not small enough for the expansion parameter in this case. The values of $\varkappa$ are all much smaller than 0.1 for the three actual normal modes shown in figures B.1 and B.2. The largest value of $\varkappa$ for any real mode is 4.5×10^{-3} for the acoustic wave in P.S. III.

Figures B.1d - B.1f and B.2d - B.2f show a clear test that can distinguish between real and spurious roots. These figures also demonstrate why the Taylor series expansion breaks down at the three roots for which $\partial \varepsilon_R^f / \partial \omega_R < 0$. We have already seen that ω_I is adjusted so that the first two terms in the Taylor series expansion for ε_I^f (equation B.5) are exactly equal and of opposite signs so they cancel. The third term (second order in the derivative) must be much smaller than the first two if the Taylor series is to converge. The third term is shown in figures B.1f and B.2f as ε_{aI}^f . We note that ε_{aI}^f is much smaller than ε_I^f at the three roots which correspond to the normal oscillations and that ε_{aI}^f is comparable to ε_I^f at the three spurious roots. For example, $\varepsilon_I^f = 5.8 \times 10^{-3}$ and $\varepsilon_{aI} = 8.75 \times 10^{-6}$ at the normal oscillation in figure B.2 while $\varepsilon_I^f = 3.76$ and $\varepsilon_{aI}^f = 3.13$ at the spurious root. The Taylor series is not converging at the spurious root,

and the usual technique for evaluating ω_I from equation B.2 breaks down. It is not possible to make both $\epsilon_R^f(\omega)$ and $\epsilon_I^f(\omega)$ simultaneously zero by introducing a small ω_I given by setting equation B.2 to zero.

Similarly, figures B.1d, B.1e, B.2d and B.2e show that the Taylor series for $\epsilon_R^f(\omega)$ in equation B.4 converges at the normal oscillations and diverges at the spurious roots, even though $\kappa < 1$ at all roots. The function ϵ_{1R}^f in figures B.1d and B.2d is the first order term in equation B.2 and the function ϵ_{2R}^f in figures B.1e and B.2e is the second order term. Each of these terms is small compared to typical values of ϵ_R^f in the vicinity of the normal oscillations and comparable to typical ϵ_R^f's near the spurious roots. This observation qualitatively answers the last question posed at the start of this appendix. It is not completely correct to use the root, ω_R, derived by setting $\epsilon_R^f(\omega_R) = 0$ (as we did in Chapter IV). The actual value of ω_R that will make the sum of the Taylor series terms, $\epsilon_R^f(\omega)$, equal to zero, with ω_I given in figures B.1c and B.2c, is slightly different from the usual value of ω_R described in Chapter IV. The figures show that ϵ_{1R}^f and ϵ_{2R}^f are very small at a normal oscillation so a very slight shift in ω_R will adjust ϵ_R^f enough to cancel the rest of the Taylor series and make $\epsilon_R^f(\omega) = 0$.

Appendix C

The W Function

In Chapter III we expanded $\varepsilon_L = \varepsilon_L^f$ into MB form where f was defined in equation 3.18. In deriving equation 3.19 we defined a function called the W function (Ichimaru, 1973). In this appendix we shall analyze the important properties of this function.

The W function, as a function of a complex argument, is defined as

C.1) $$W(\zeta) = \int_{-\infty}^{+\infty} \frac{x\, e^{-x^2/2}}{x - \zeta}\, dx \quad .$$

The only problem we face in solving equation C.1 is in knowing how to deal with the pole at $x = \zeta$. To find W, the above expression implies that we integrate along the real x axis from $-\infty$ to $+\infty$. What happens when the imaginary part of ζ , ζ_I is positive, negative or even zero? Do we have to modify our contour when considering these problems? Landau addressed himself to a similar question (Landau, 1946) when dealing with ES oscillations in a field-free, homogeneous plasma. In such a system there is no perferred direction defined by the field. In Appendix A we saw that we could arbitrarily rotate our space coordinates so as to line up the z axis parallel to $\underline{k}$. The dispersion tensor in such a plasma decouples into pure ES and pure EM modes. Because $\underline{k}$ defines our perferred direction it is taken to be a positive quantity. Therefore, when Landau discussed the actual solution of velocity integrals with complex

poles he implicitely assumed $k_{\parallel} > 0$. For a plasma immersed in a magnetic field such an assumption on $k_{\parallel}$, namely $k_{\parallel} > 0$, is incorrect. This is because in a magnetized plasma both forward and back propagating waves are physically possible.

Figure C.1 summarizes the contours we shall use to describe all possible states our plasma is in when a weak turbulent oscillation is excited. These contours are referred to as the generalized Landau contours. Figure C.1a represents the contour we would naturally choose to solve equation C.1. Note that figure C.1 defines contours in the complex $V_{\parallel}$-plane while equation C.1 must be solved in the complex x-plane. It is easy to show that the contours $L_1 - L_6$ are identical in both planes because the $V_{\parallel}$-plane can be transformed into the x-plane by simple dilation i.e. $x = \sqrt{\alpha_s}\, V_{\parallel}$.

As the state of our system goes from amplifying to evanescent the generalized Landau contours go from L_1 to L_3 for $k_{\parallel} > 0$ and L_4 to L_6 for $k_{\parallel} < 0$. From our work in Appendix B we know that we need to find ε_L only at $\omega = \omega_R\ (\omega_I = 0)$. We therefore need to make use of L_2 and L_5 in the actual solution of W. Let us begin solving equation C.1 by letting $t = x - \zeta$. (note that t is a complex number). Under this translation $W(\zeta)$ must now be solved in the complex t-plane. Under such a transformation the contours L_i $(i=1,\ldots,6)$ are transformed into L_1' and L_2' only (see figure C.2).

Therefore

$$W(\zeta) = \frac{1}{\sqrt{2\pi}} \int_{-\infty-\zeta,\, L'}^{+\infty-\zeta} dt\, \frac{(t+\zeta)}{t} e^{-(t+\zeta)^2/2} \qquad \text{C.2)}$$

Figure C.1 The generalized Landau contours in the complex $v_{\parallel}$ -plane:

a) $k_{\parallel} > 0, \omega_I > 0$
b) $k_{\parallel} > 0, \omega_I = 0$
c) $k_{\parallel} > 0, \omega_I < 0$
d) $k_{\parallel} < 0, \omega_I > 0$
e) $k_{\parallel} < 0, \omega_I = 0$
f) $k_{\parallel} < 0, \omega_I < 0$

Figure C.2 The generalized Landau contours in the complex t-plane:

a) $k_{\parallel} > 0$
b) $k_{\parallel} < 0$

The shape of these contours is independent of the sign of ω_I .

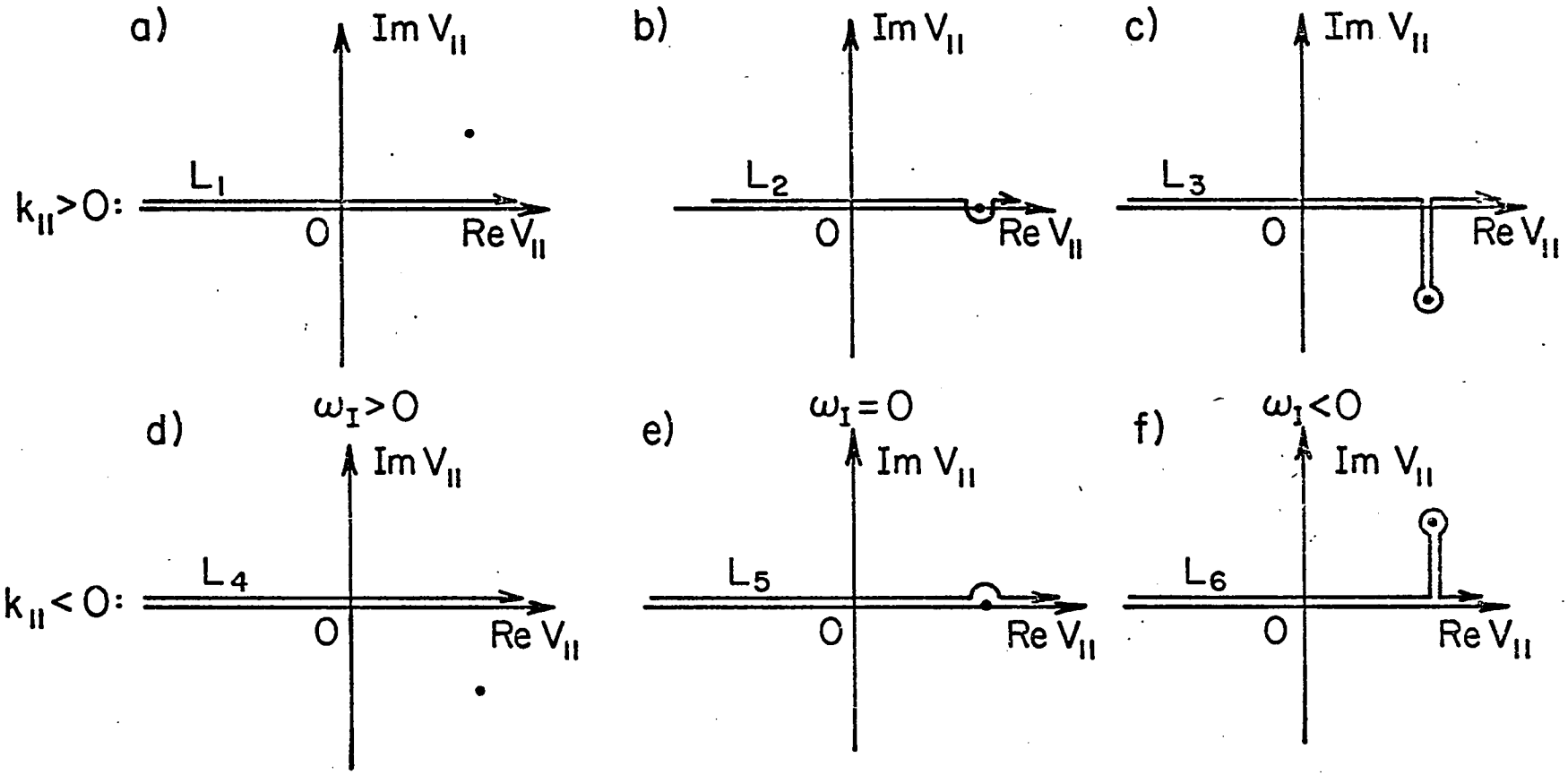
a)
Im $V_{||}$
$k_{||}>0$:
L_1
0
Re $V_{||}$
b)
Im $V_{||}$
L_2
0
Re $V_{||}$
c)
Im $V_{||}$
L_3
0
Re $V_{||}$
d)
$\omega_I>0$
Im $V_{||}$
$k_{||}<0$:
L_4
0
Re $V_{||}$
e)
$\omega_I=0$
Im $V_{||}$
L_5
0
Re $V_{||}$
f)
$\omega_I<0$
Im $V_{||}$
L_6
0
Re $V_{||}$

Figure C.1

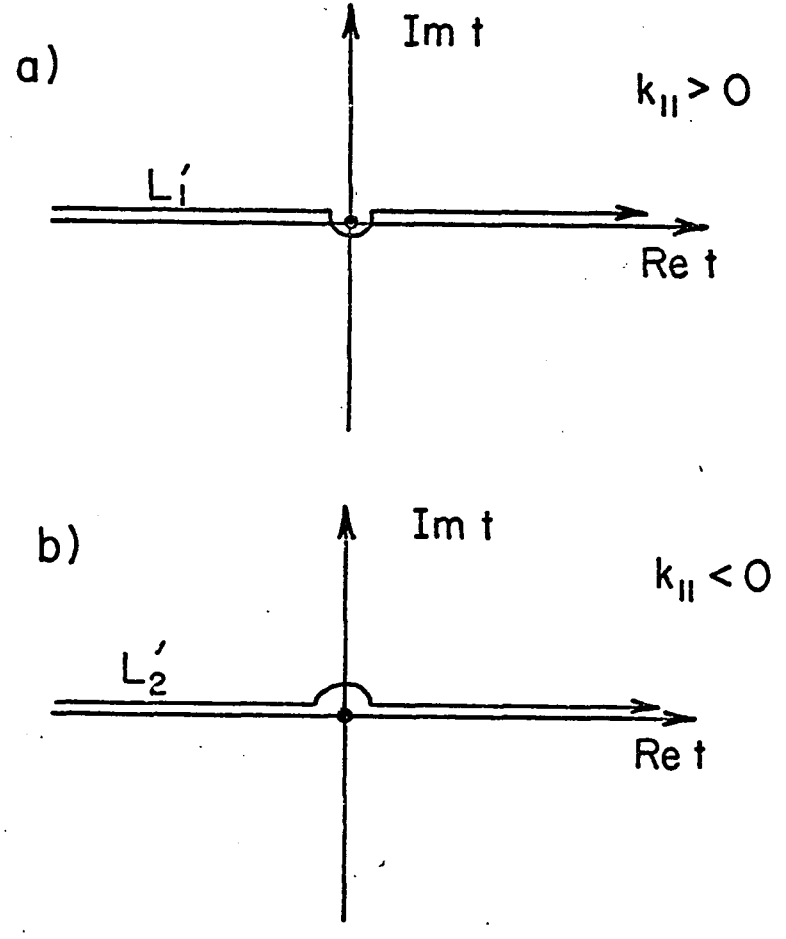

Figure C.2

where $L' \in \{L_1', L_2'\}$.

i.e.

$$W(\xi) = \frac{1}{\sqrt{2\pi}} \int_{-\infty-\xi}^{+\infty-\xi} dt\, e^{-(t+\xi)^2/2} + \frac{1}{\sqrt{2\pi}} \int_{-\infty-\xi}^{+\infty-\xi} dt\, \frac{\xi}{t} * e^{-(t+\xi)^2/2}$$

$$= I_1 + I_2 .$$

In I_1, let $x = t + \xi$ this implies that $I_1 = 1$. That is

C.3) $$W(\xi) = 1 + \frac{\xi e^{-\xi^2/2}}{\sqrt{2\pi}} \int_{-\infty-\xi}^{+\infty-\xi} dt\, \frac{e^{-t^2/2 - \xi t}}{t} .$$

To solve equation C.3 let

$$J(\xi) = \frac{1}{\sqrt{2\pi}} \lim_{R\to\infty} \int_{-R-\xi=\phi_1}^{R-\xi=\phi_2} F(t,\xi)\, dt$$

where

$$F(t,\xi) = \frac{e^{-t^2/2 - \xi t}}{t} .$$

Therefore

$$\frac{dJ(\xi)}{d\xi} = \frac{1}{\sqrt{2\pi}} \lim_{R\to\infty} \left\{ \int_{\phi_1}^{\phi_2} \frac{\partial F}{\partial \xi}\, dt + F(\phi_2, \xi)\frac{d\phi_2}{d\xi} - F(\phi_1, \xi)\frac{d\phi_1}{d\xi} \right\}$$

$$= \frac{1}{\sqrt{2\pi}} \lim_{R\to\infty} \left\{ \int_{-R-\xi}^{R-\xi} -e^{-t^2/2 - \xi t}\, dt - \frac{2R}{R^2-\xi^2} e^{-\frac{1}{2}(R^2-\xi^2)} \right\}$$

$$= -\frac{1}{\sqrt{2\pi}} \int_{-\infty-\xi, L'}^{+\infty-\xi} dt\, e^{-t^2/2 - \xi t} .$$

Completing the square in the above expression gives

$$e^{-\xi^2/2}\frac{dJ}{d\xi} = -\frac{1}{\sqrt{2\pi}} \int_{-\infty-\xi}^{\infty-\xi} dt\, e^{-(t+\xi)^2/2}$$

$$= -1 .$$

That is

$$\frac{dJ}{d\xi} = -e^{\xi^2/2} .$$

Integrating the above, first order differential equation, from "0" to ξ gives

$$J(\xi) = J(0) - \int_0^{\xi} e^{y^2/2}\, dy$$

where

$$J(0) = \frac{1}{\sqrt{2\pi}} \int_{-\infty, L'}^{+\infty} dt \; \frac{e^{-t^2/2}}{t}$$

$$= \frac{1}{\sqrt{2\pi}} \begin{cases} \oint_{-\infty}^{+\infty} F(t,0)\,dt + \pi i, & L' = L_1' \\ \oint_{-\infty}^{+\infty} F(t,0)\,dt - \pi i, & L' = L_2' \end{cases}.$$

Because F(t,o) is an odd function of t, the principal value integrals vanish in the above expression. Therefore equation C.3 is

C.4) $$W(\xi) = 1 - \xi\, e^{-\xi^2/2} \int_0^{\xi} e^{y^2/2}\, dy + \begin{cases} i\sqrt{\frac{\pi}{2}}\, \xi\, e^{-\xi^2/2}, & k_{11} > 0 \\ -i\sqrt{\frac{\pi}{2}}\, \xi\, e^{-\xi^2/2}, & k_{11} < 0 \end{cases}.$$

Differentiating equation C.4 we find that

C.5) $$\frac{dW(\xi)}{d\xi} = \left(\frac{1}{\xi} - \xi\right) W(\xi) - \frac{1}{\xi}$$

where

W(0)=1.

So far in our analysis of the W function we have made no restrictions on the size of the imaginary part of ζ , ζ_I .

We will soon see that the W function is closely related to the error function of a complex argument. It is also closely related to the plasma dispersion function, Z, which Fried and Conte (1960) numerically integrated to produce a series of tables that are still widely used. Let us now explore the relationship between the plasma dispersion function and the W function.

In equation C.1 let $x=(x-\zeta)+\zeta$,

Therefore ($L''=L$)

$$W(\zeta)=1+\frac{\zeta}{\sqrt{2\pi}}\int_{-\infty,L''}^{+\infty}\frac{e^{-x^2/2}}{x-\zeta}\,dx \quad .$$

Let $\alpha=\frac{x}{\sqrt{2}}$,

$$W(\zeta)=1+\frac{\zeta}{\sqrt{2\pi}}\int_{-\infty,L}^{+\infty}\frac{e^{-\alpha^2}}{\alpha-\zeta/\sqrt{2}}\,d\alpha .$$

Fried and Conte defined Z as

C.6) $$Z(\beta)=\frac{1}{\sqrt{\pi}}\int_{-\infty,L}^{+\infty}\frac{e^{-x^2}}{x-\beta}\,dx \quad .$$

Therefore

C.7) $$W(\zeta) = 1 + \frac{\zeta}{\sqrt{2}} Z\left(\frac{\zeta}{\sqrt{2}}\right) .$$

Let us find the differential equation satisfied by Z. Substituting equation C.7 into equation C.5 we see that

$$\frac{1}{\sqrt{2}} Z + \frac{\zeta}{\sqrt{2}} Z' = \left(\frac{1}{\zeta} - \zeta\right)\left(1 + \frac{\zeta}{\sqrt{2}} Z\right) - \frac{1}{\zeta}$$

i.e.

$$\frac{dZ(\zeta/\sqrt{2})}{d\zeta} = -\zeta Z\left(\frac{\zeta}{\sqrt{2}}\right) - \sqrt{2} .$$

Let $$\alpha = \frac{\zeta}{\sqrt{2}}$$

Therefore

C.8) $$\frac{dZ(\alpha)}{d\alpha} = -2\left(1 + \alpha Z(\alpha)\right) .$$

We shall now turn to look at a few of the more important properties of the W function.

I. The Real Argument.

In the kinetic theory we have developed, we need to know the W

function when $\omega_I = 0$ ($\zeta_I = 0$). When $\zeta = \zeta_R$ equation C.4 reduces to

$$W(\zeta_R) = 1 - \zeta_R e^{-\zeta_R^2/2} \int_0^{\zeta_R} e^{y^2/2}\, dy + \sqrt{\frac{\pi}{2}} \begin{cases} +i\zeta_R e^{-\zeta_R^2/2}, & k_{\parallel} > 0 \\ -i\zeta_R e^{-\zeta_R^2/2}, & k_{\parallel} < 0 \end{cases} \tag{C.9}$$

II. The Imaginary Argument.

If $\zeta_R = 0$ then $\zeta = i\zeta_I$, i.e. equation C.4 is

$$W(i\zeta_I) = 1 - i\zeta_I e^{\zeta_I^2/2} \int_0^{i\zeta_I} e^{y^2/2}\, dy \mp \sqrt{\frac{\pi}{2}}\, \zeta_I e^{\zeta_I^2/2}$$

where the upper sign will always refer to $k_{\parallel} > 0$ and the lower sign to $k_{\parallel} < 0$. Let $I = \int_0^{i\zeta_I} e^{y^2/2}\, dy$.

If $y = i\sqrt{2}\,u$ then

$$I = \sqrt{2} \int_0^{\xi_I/\sqrt{2}} e^{-u^2}\, du$$

$$= i\sqrt{\frac{\pi}{2}}\, \mathrm{erf}\left(\frac{\xi_I}{\sqrt{2}}\right)$$

where $\mathrm{erf}(x) = \frac{2}{\pi} \int_0^x e^{-u^2}\, du$.

Therefore

C.10) $$W(i\,\xi_I) = 1 \mp \xi_I \sqrt{\frac{\pi}{2}}\, e^{\xi_I^2/2} * \left[1 \mp \mathrm{erf}\left(\frac{\xi_I}{\sqrt{2}}\right)\right] .$$

III. Expansions.

We are often interested in the power series and asymptotic series of the W function of a real argument (see figure 3.3). We may rewrite equation C.9 in terms of the error function as

C.11) $$W(\xi_R) = 1 \pm \xi_R\, e^{-\xi_R^2/2} * \left[1 \mp \mathrm{erf}\left(-i\,\frac{\xi_R}{\sqrt{2}}\right)\right] .$$

a. The Power Series.

The power series expansion of erf(x) is

$$erf(x) = \frac{2}{\pi}\left(x - \frac{x^3}{3 \cdot 1!} + \frac{x^5}{5 \cdot 2!} - \frac{x^7}{7 \cdot 3!} + \cdots \right)$$

Let

$$I = \int_0^{\xi_R} e^{y^2/2}\, dy$$

$$= i\sqrt{\frac{\pi}{2}}\, erf\left(-i\,\frac{\xi_R}{\sqrt{2}}\right) .$$

Therefore

$$I = \xi_R + \frac{\xi_R^3}{6} + \frac{\xi_R^5}{40} + \cdots .$$

$$W(\xi_R) = 1 \pm i\sqrt{\frac{\pi}{2}}\,\xi_R\, e^{-\xi_R^2/2} - \xi_R\, e^{-\xi_R^2/2}\left(\xi_R + \frac{\xi_R^3}{6} + \frac{\xi_R^5}{40} + \cdots\right) .$$

Because

$$e^{-\xi_R^2/2} = 1 - \frac{\xi_R^2}{2} + \frac{\xi_R^4}{8} - \cdots ,$$

$$W(\xi_R) = 1 \pm i\sqrt{\frac{\pi}{2}}\,\xi_R\, e^{-\xi_R^2/2} - \left(1 - \frac{\xi_R^2}{2} + \frac{\xi_R^4}{8} - \cdots\right)\left(\xi_R^2 + \frac{\xi_R^4}{6} + \frac{\xi_R^6}{40} + \cdots\right)$$

C.12) $$= i\sqrt{\frac{\pi}{2}}\,\xi_R\, e^{-\xi_R^2/2} + 1 - \xi_R^2 + \frac{\xi_R^4}{3} - \cdots \frac{(-1)^{n+1}\xi_R^{2n+2}}{(2n+1)!!} .$$

b. The Asymptotic Series.

The asymptotic series expansion of erf(x) is

$$\operatorname{erf}(x>>1) \sim 1 - \frac{e^{-x^2}}{x\sqrt{\pi}}\left\{1 - \frac{1}{2x^2} + \frac{1\cdot 3}{(2x^2)^2} - \cdots\right\}.$$

Therefore,

$$I = i\sqrt{\frac{\pi}{2}} + \frac{e^{\xi_R^2/2}}{\xi_R}\left\{1 + \frac{1}{\xi_R^2} + \frac{3}{\xi_R^4} + \cdots\right\}.$$

This implies that

C.13) $$W(\xi_R >> 1) \sim -\frac{1}{\xi_R^2} - \frac{3}{\xi_R^4} - \cdots - \frac{(2n-1)!!}{\xi_R^{2n}}.$$

Appendix D

Definitions and a List of Symbols

q_γ the charge of the $\gamma^{\pm h}$ species

m_γ the mass of the species

χ_γ the Klimontovich function

ρ, $\underline{j}$ the charge and current densities

$\underline{E}^m$, $\underline{B}^m$ the electric and magnetic microfields

$F_{\bar{N}}$ the $\bar{N}$-body probability density defined in Γ-space (a $6\bar{N}$-dimensional phase space)

$\underline{\underline{\sigma}}(\underline{k},\omega)$ the transformed conductivity tensor

$\underline{\underline{\varepsilon}}(\underline{k},\omega)$ the dielectric tensor

$\underline{\underline{\Delta}}(\underline{k},\omega)$ the dispersion tensor

$\varepsilon_L(\underline{k},\omega)$ the longitudinal dielectric function (l.d.f.)

$\omega_{c\gamma} = q_\gamma B_0 / m_\gamma c$ cyclotron frequency of $\gamma^{\pm h}$ species

α pitch angle in velocity space

θ wave propagation angle

$a_\gamma = k_\perp v_\perp / \omega_{c\gamma}$

J_n, I_n the Bessel functions of the 1st and 2nd kind of order n

$\mu = i\omega_I/\omega_R$ the Taylor series expansion parameter

$\mathcal{E}(\underline{k},t)$ spectral wave energy density

$\omega_{p\gamma} = (4\pi n_\gamma e^2/m_\gamma)^{1/2}$ plasma frequency of the $\gamma^{\pm h}$ species

$\lambda_{D\gamma} = (K T_{\|,\gamma}/4\pi n_\gamma e^2)^{1/2}$ Debye length

$$\lambda_\gamma = \frac{K T_{\perp\gamma}}{m_\gamma \omega_{c\gamma}^2} k_\perp^2$$

$$\alpha_\gamma = \frac{m_\gamma}{K T_{\|,\gamma}}$$

$K = 1.3807 \times 10^{-16}$ erg/°K, Boltzmanns constant

$\underline{k}$; $k_{\parallel}, k_{\perp}$ wave vector; parallel and perpendicular components respectively

ω_R real frequency

ω_I imaginary frequency

$W(z)$ the W-function (see Appendix C)

$v_{\parallel}^{r}$ the resonant velocity

A Summary of the Classification of Waves

A wave is in either an ES or EM or a hybrid mode. It is a member of a specific branch (e.g. the UHB). Associated with any wave is a real and imaginary frequency (ω_R, ω_I) and a real and imaginary wave vector ($\underline{k}_R, \underline{k}_I$). By assuming the wave vector to be real we may find an explicit expression for ω_R and ω_I and vice versa. Because we are interested in temporal effects in our plasma this is the approach we have adopted in this work. In the weak turbulent regime ($\mu \ll 1$) the expressions one uses to find ω_R and ω_I decouple. A wave which has $\omega_I < 0$ is called evanescent (damped) while one which has $\omega_I > 0$ is called amplifying (growing, unstable). A wave which has $\omega_I = 0$ is called normal. A wave is convective if its' group velocity is non-zero. If a wave grows at every point in a system then it is termed an absolute instability.